Improvements to Constitutive Material Model for Fabrics

by

Mihai I. Morea

A Thesis Presented in Partial Fulfillment
of the Requirements for the Degree
Master of Science

Approved April 2011 by the
Graduate Supervisory Committee:

Subramaniam Rajan, Chair
Apostolos Fafitis
Barzin Mobasher

ARIZONA STATE UNIVERSITY

May 2011

ABSTRACT

The high strength to weight ratio of woven fabric offers a cost effective solution to be used in a containment system for aircraft propulsion engines. Currently, Kevlar is the only Federal Aviation Administration (FAA) approved fabric for usage in systems intended to mitigate fan blade-out events. This research builds on an earlier constitutive model of Kevlar 49 fabric developed at Arizona State University (ASU) with the addition of new and improved modeling details. Latest stress strain experiments provided new and valuable data used to modify the material model post peak behavior. These changes reveal an overall improvement of the Finite Element (FE) model's ability to predict experimental results. First, the steel projectile is modeled using Johnson-Cook material model and provides a more realistic behavior in the FE ballistic models. This is particularly noticeable when comparing FE models with laboratory tests where large deformations in projectiles are observed. Second, follow-up analysis of the results obtained through the new picture frame tests conducted at ASU provides new values for the shear moduli and corresponding strains. The new approach for analysis of data from picture frame tests combines digital image analysis and a two-level factorial optimization formulation. Finally, an additional improvement in the material model for Kevlar involves checking the convergence at variation of mesh density of fabrics. The study performed and described herein shows the converging trend, therefore validating the FE model.

DEDICATION

To my son and my brother …

ACKNOWLEDGMENTS

I would like to thank my advisor and committee chair, Dr. Subramaniam Rajan, for giving me the opportunity to work on this project. He has been a tutor, mentor, and role model for me and without his guidance and support I would not have been able to accomplish this work. I would also like to thank my committee members for taking the time to serve on my committee. I am grateful for the comments and suggestions they have made in support of my research. I could not have achieved this without the time and effort put forth by the other graduate students that worked on this project including both current and past students. I am appreciative of Dr. Jeff Simons (SRI International) for sharing his knowledge and experience with LS-DYNA. I would also like to thank the other members of the research team which include members from Honeywell and NASA-GRC for their technical insight and experimental contributions. Last but not least, I would like to thank Don Altobelli and Bill Emmerling of the Federal Aviation Administration for providing funding for this research.

TABLE OF CONTENTS

Page

LIST OF FIGURES

Figure Page

Figure Page

LIST OF TABLES

Table Page

1. INTRODUCTION

1.1. Motivation for Research and Overview

High strength woven fabrics are ideal materials for use in structural systems where large deformations and high energy absorption are required. Their high strength per weight ratio and ability to resist high speed impacts enable them to be more efficient than metals. One of the most widely used applications for woven fabrics is in propulsion engine containment systems that are designed to mitigate the effects from a fan blade-out event. This event occurs when an object causes fan blades or portions of the fan blades to be ejected from the rotor. The containment system is designed so that the fan blade fragments do not cause any additional damage to the engine that would compromise the pilot's ability to safely navigate the aircraft. Woven fabrics are ideal materials for this use because of their light weight and ability to absorb high amounts of energy. Currently the only woven fabric that has been approved by the Federal Aviation Administration (FAA) for use in engine containment systems is Kevlar®49 developed by DuPont in the 1970s. It was the first organic fiber with sufficient tensile strength and modulus to be used in advanced composites. Originally developed as a replacement for steel in radial tires, Kevlar is now used in a wide range of applications. Kevlar is an aramid, an abbreviation for aromatic polyamide. The chemical composition of Kevlar is poly para-phenyleneterephthalamide, and it is more properly known as a para-aramid. Aramids belong to the family of nylons. Like nylons, Kevlar filaments are made by extruding the precursor through a spinneret. The rod form of the para-aramid molecules and the extrusion process

make Kevlar fibers anisotropic – they are stronger and stiffer in the axial direction than in the transverse direction. In this research, the Kevlar woven fabric that is used is shown in Fig.1. The main longitudinal direction of the fabric is typically referred to as the warp direction and perpendicular to the warp direction is typically referred to as the fill direction. Each yarn is constructed by bundling together hundreds of filaments . The fabric has 17 yarns per inch in both the warp and fill directions.

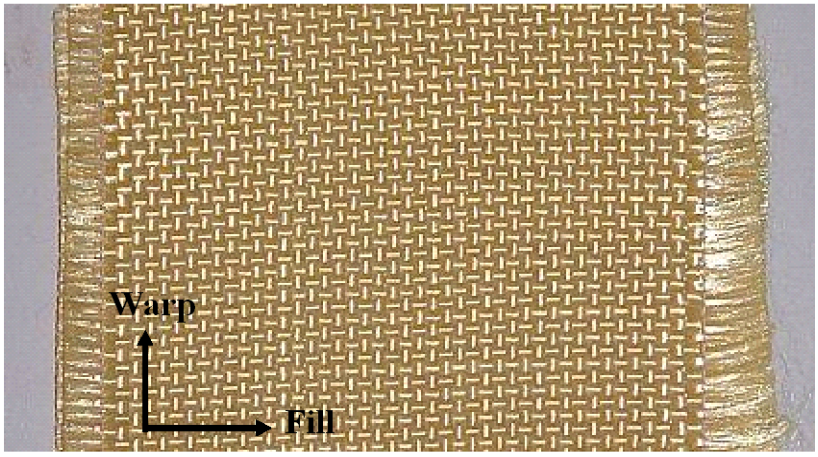

Fig.1. Kevlar® 49 sample

This fabric works well in propulsion engine containment systems not only because of its high strength to weight ratio and large deformation capabilities but also because of its high temperature and chemical resistance. The containment system is typically constructed by wrapping multiple layers of Kevlar®49 around a thin aluminum encasement. The fabric is then covered with a protective layer. A propulsion engine with a containment system is shown in Fig.2.

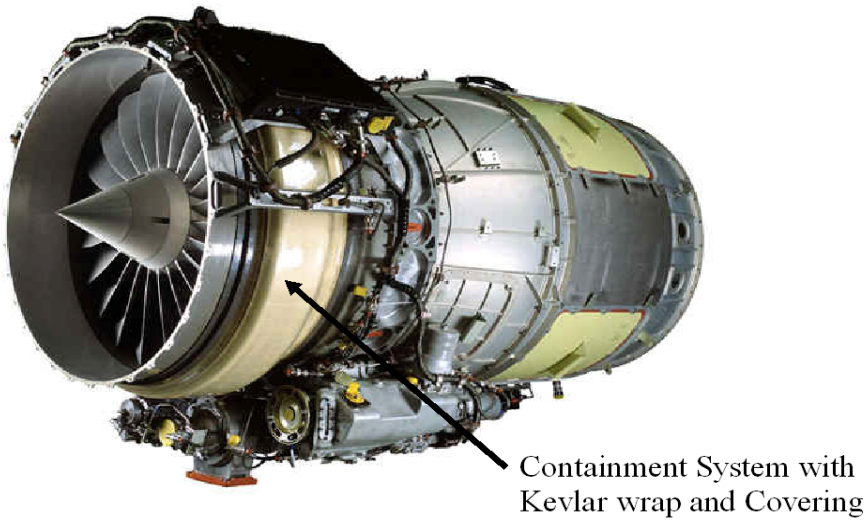

Fig.2. Propulsion engine with containment system [courtesy, Honeywell Engines, Phoenix, AZ]

Part of the design of the containment system consists of determining the number of fabric layers and fabric width required. Currently the FAA's design standards require that a certain number of experimental tests must be completed to determine these design variables. The tests include launching projectiles into a running engine, which causes a fan blade-out event. If all fan blade fragments are contained by the fabric then the number of fabric layers and fabric width are determined to be acceptable for the containment system. These tests are very expensive so the ability to perform numerical simulations of the experimental tests to either reduce or eliminate the number of experimental tests required is attractive to the FAA. With today's advanced numerical techniques, modeling a propulsion engine and simulating a fan blade-out event can be accomplished using finite elements and explicit finite element analysis. There are proven constitutive models that can simulate the behavior of most of the materials that compose a propulsion engine and containment system. The difficulty lies in fact

that there is no publicly available mechanistic based constitutive model for Kevlar®49, or essentially any woven fabric, especially a model that can be used to predict the behavior of the fabric when it is subjected to impact loads.

1.2. Literature Review of Current Fabric Modeling Procedures

In recent years at Arizona State University extensive research has been conducted to develop a reliable model to capture fabric behavior as a structural system. Initial steps in the research geared towards understanding fabric material behavior as well as determining parameters to be used in the finite element model were experiments. The first sequence of experiments, conducted by Sharda [1], were followed by supplementary experiments conducted at ASU by Naik and Sankaran and described in [2]. The finite element modeling at ASU was set off by the development of the continuum model (macro-scale) made by Stahlecker [3] and [4]. This initially developed material model has produces good results, allowing great computational efficiency and was easily integrated into a multicomponent system model.

The above described experimental work has been conducted to determine the effective material properties of fabric composites and fabrics to be used in the elastic analysis. The main techniques employed are analytical methods including the method of cells (MOC) [5] and classical lamination theory (CLT) [6], as well as numerical methods using finite element modeling with virtual testing [7]. There has been recent success in the development of non-linear material models for simulating simple structural events such as uniaxial tension tests and for simulating complex structural events such as those involving ballistic impacts [8].

For both cases the majority of the material models were developed for use with finite element solutions. However, there have been some models developed for use with finite difference solutions as well [9]. Research has also been conducted in the area of strain rate effects on fabric composites and fabrics [10], [11]. Since most of these materials are used in areas where ballistic events occur, an accurate prediction of strain rate effects is necessary.

Additional research was performed at Arizona State University to further improve and analyze the behavior of fabrics. Observing that the continuum model may leave out potentially important behaviors, Bansal analyses the fabric failure to capture interaction of the yarns families [12] and [13]. The three main interactions are: 1) crimp interchange, a mechanism in which the fabric elongates along the direction of one yarn family with negligible yarn stretching, as the yarns of that family become less crimped (i.e. the yarn waves decrease in amplitude and increase in wavelength), while the fabric contracts along the direction of the other yarn family, as the yarns of that family become more crimped; 2) locking, a mechanism in which the fabric resists deformations as the interwoven yarns jam against each other and 3) resistance to relative yarn rotation, which is the dominant mechanism for the response of fabric to inplane shear. Based on those observations Bansal developed a finite element model of dry fabrics [12]. This model includes yarn geometry details (meso-scale) for use in the analysis. Because the usage of such a model may not be practical in a multicomponent system model, the information obtained by observing fabric behavior under different loading conditions can be essential in improving the continuum model.

1.2.1. Modeling Techniques for Fabrics and Fabric Composites

Determining the equivalent continuum model (macro-scale) properties or macromechanical properties of a woven fabric can be a challenging task. Experimental testing can be conducted to ascertain some or all of the effective material properties. However, this approach is expensive since new tests must be conducted if the effective properties are needed for different weaves and weave geometries. Small changes in the fabric architecture alter the fabric's behavior and a model that can simulate the effect of these changes is a valuable tool. The difficulty in developing a model to simulate the effective properties lies in (1) determining accurately the yarn geometry in the fabric, and (2) simulating the yarn-yarn interaction and the yarn-matrix interaction (for composites). More recently very accurate descriptions of the yarn geometry have been made through the use of photomicrographs or scanning electron microscope (SEM) images. In the absence of these high resolution images, researchers have made reasonable assumptions for the fabric geometry. Currently there are several approaches being used in computing the effective properties - the MOC, variations of the MOC, finite element modeling with virtual testing, and classical lamination theory. With each method only a representative unit of material is considered due to the repetitive pattern in the composite material. The terms "representative unit cell (RUC)", "unit cell", or "representative volume element (RVE)" will be used interchangeably. An example of a repetitive unit cell for a plain weave fabric [5] is shown in Fig. 3. Symmetric conditions are used to improve the computational efficiency - one quarter of the unit cell model is shown in the same figure.

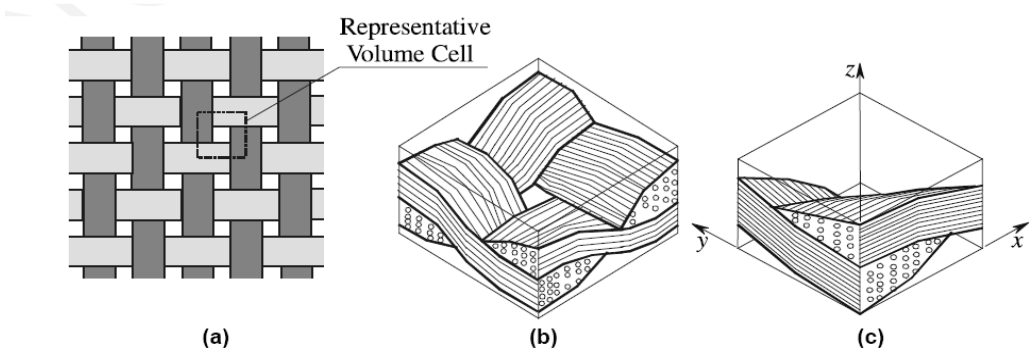

Fig. 3. (a) Weave architecture (b) RVE (c) quarter of the RVE

Analytical methods including CLT and MOC have been successful in determining effective material properties. Some of the earliest CLT models that have been used to determine the elastic modulus of woven fabric composites include those by Ishikawa and Chou [14], [15], [16] and [17]. One of the more recent CLT models referred to as Mesotex [18] is general enough to capture the 3D elastic properties and the ultimate failure strengths of several types of fabric composites and is very computationally efficient. Models using the method of cells have shown good correlation with experimental results [19], [20] and [21]. One of the approaches used is referred to as a four-cell model in which the quarter cell RVE is divided into four subcells as shown in Fig. 4 [5].

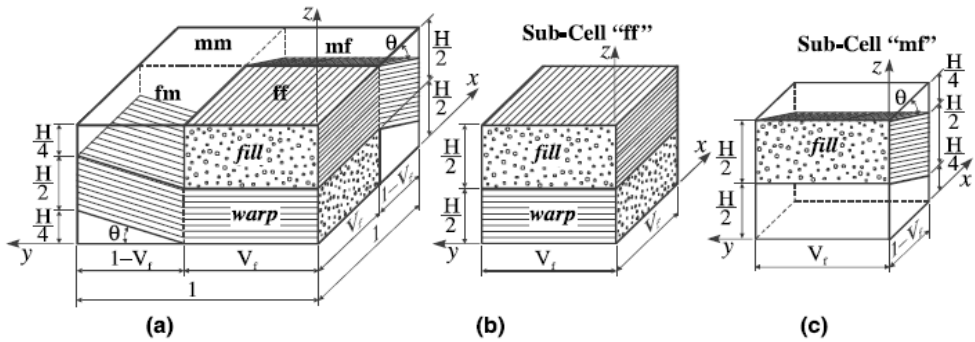

Fig. 4. Division of quarter RVE into subcells using the four-cell method

Using four subcells allows the model to be computationally efficient compared to its similar counterparts. In these MOC models, iso-strain and iso-stress conditions are assumed and the constitutive equations are averaged through the thickness of the RVE. The unit cell is then divided into many subcells and an averaging procedure is then performed again by assuming uniform state of stress in the subcells. The stress-strain relations of each subcell can then be obtained and related to the effective stress-strain behavior of the unit cell. Tabiei and Yi [5] developed a simplified method of cells model and compared it to the previously developed methods of cells models, the four-cell model, and finite element solutions. They concluded that their simplified method could be used as a fast tool for predicting the material properties of fabric composites but they recommended the four-cell model for most structural analysis problems. Another model utilizing the method of cells technique was developed by Naik and Ganesh [22], [23] and [24] and showed good correlation with experimental results. Vandeurzen and co-workers [25] and [26] developed what they refer to as a combi-cell model where the complementary variational principle was used to obtain the stiffness matrix of the unit cell.

Another method for determining the effective material properties of the unit cell is through numerical, or finite element, solutions. Typically this procedure involves modeling the actual yarn and matrix geometry of the unit cell with many elements. Then virtual tests are conducted by varying the loading and boundary conditions on the unit cell and the results are used to establish the

effective material properties. An example of a finite element mesh of a woven fabric unit cell is shown in Fig. 5 taken from [27].

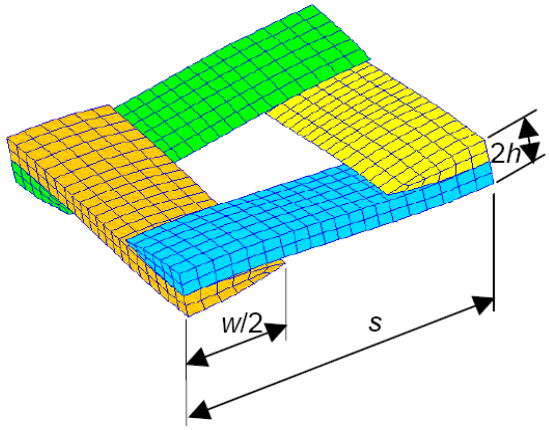

Fig. 5. Example of FE mesh of a plain woven fabric unit cell

Using finite elements is more computationally expensive than using closed form methods. However using finite elements provides detailed stress-strain distributions. The most challenging aspect of this technique is obtaining the appropriate weave architecture of the fabric. Using high resolution images such as photomicrograph or SEM images provides a microscopic view of the yarn geometry. Researchers have been able to fit mathematical functions to these images to accurately model the weave pattern in three dimensions. An example of a photomicrograph image of a fabric similar to Kevlar is shown in Fig. 6 [28] and [29].

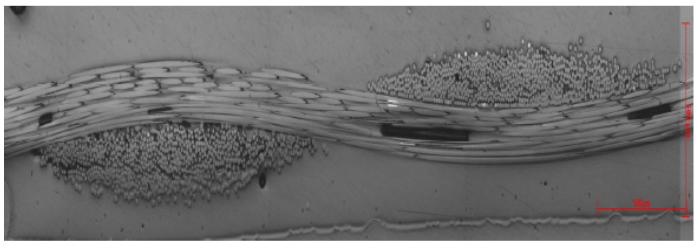

Fig. 6. Photomicrograph image of a fabric similar to Kevlar in cross section

Barbero and co-workers created a 2D model of the RVE geometry by fitting a sinusoidal curve to the image. To create a 3D model, the researchers used the 2D fit along with the capabilities of an advanced commercial modeling program. The yarns were modeled with transversely isotropic solid elements and the effective elastic material constants were obtained by varying the boundary conditions and loading on the unit cell. The researchers reported good correlation with experimental values and with values predicted from analytical methods. Peng and Chao [27] used a similar approach by conducting virtual tests on a finite element model of the unit cell. However, they also took into account the non-linearity of the material and fit the results to a shell element equal in size to the unit cell. They developed equations for the elastic modulus, shear modulus, and Poisson ratio as a function of strain. Srirengan and co-workers [30] proposed a global/local method that required two stages. First a macroscopic finite element model using a small number of elements and homogenized material properties is created. The results from the global analysis are then used in a more detailed local analysis in which a finite element model taking into account the weave geometry is used.

1.2.2. Nonlinear Material Models

In the previous subsection, various techniques were examined to determine the effective elastic properties of the fabric and fabric composites. These properties are generally useful for modeling structural systems that are designed for the elastic regime with simple failure criteria. Simulating the

performance of the fabric or fabric composite during much more complicated loading, such as in impact events, is necessary when the material is used under these loading conditions. In these situations, a non-linear material model is needed not only to capture the non-linear material behavior but also to capture damage growth and failure. Researchers have had varying success using analytical solutions, finite difference solutions, and finite element solutions to model impact events.

Several researchers have developed material models to predict the damage evolution and failure strengths fabrics and fabric composites. Kollegal and Sridharan [31] developed a 3D finite element model to compute the effective elastic properties of a fabric composite. The researchers then added non-linearity to the model by including damage and failure of the matrix material and yarns (once failure is reached the stiffness is reduced to a very small value). The ultimate strength of the composite was approximated and showed good agreement with experimental results. Kollegal and co-workers [32] conducted a failure analysis of plain weave fabrics by first obtaining the effective elastic material properties using classical lamination theory. Their model assumed that damage was a function of the dissipated energy density that yields a power law type stress-strain relation beyond the elastic limit. Tensile behavior and in plane shear behavior using this material model compared well with experimental results. Barbero and co-workers [28] added to the research work discussed in the previous subsection by adding damage considerations into the material model. In the nonlinear model, damage occurred when the thermodynamic force tensor reached

the damage surface in the yarn material. The matrix was assumed to be elastic. Their method used many damage factors that are a function of the yarn material properties. A system of equations is solved to determine these factors. One model that takes into account the non-orthogonality of the principal material directions was developed by Xue [33]. In the model, shell elements are used to represent the fabric and unlike many of the aforementioned models the elements are not limited to the unit cell size. The non-orthogonality of the fabric is based on a material matrix that needs to be obtained from matching load versus displacement results from either tensile or biaxial and pure shear experimental tests. The researchers use a picture frame test for the pure shear test and found good correlation with numerical results.

Analytical solutions have been developed for idealized forms of impact with fabrics and fabric composites. By assuming that the fabric deforms as a tetrahedron, Gu [34] developed a method for computing the decrease in a projectile's kinetic energy after penetration. His model is able to account for multiple fabric layers and changes in the mechanical material properties due to strain rate. The model showed good agreement with experimental results. However, it is not robust enough to handle various boundary conditions and projectile geometries.

Several researchers have used finite difference solution techniques to predict fabric behavior during impact events. Roylance and co-workers [35] used finite difference techniques and modeled the fabric as a series of pin-jointed massless fiber elements. The nodes were assigned a mass value so that the model

density was equivalent to the actual fabric density. Velocity boundary conditions were applied at the point of impact and at the end of each time increment, the projectile velocity was computed based on the tension exerted on the projectile by the fibers. The model was however, not verified using experimental results. A similar technique was used by Shim et al. [36]. They also modeled the fabric using pin-jointed massless fiber elements. However, they took into account the strain rate effects by using a 3-element viscoelastic model. The authors conducted experimental ballistic tests using a spherical steel projectile on Twaron® fabric and compared their results with numerical simulations. They reported good correlation between the two for both the projectile residual velocity and absorbed energy of the fabric. The researchers noted that the accuracy of the model is significantly dependent on the rate-sensitivity.

Although the use of finite difference techniques has proven to produce accurate results for simulating impact events, the use of finite elements can provide solutions to much wider classes of problems. Lim [37] conducted a similar analysis to Shim and co-workers by simulating the ballistic impact of a spherical steel projectile with Twaron® fabric. However, instead of using 1D massless elements to model the fabric, the authors used membrane elements and the explicit finite element software DYNA3D for the solution technique. They used the predefined Material Type 19 in DYNA3D that is a strain-dependent isotropic elastic-plastic model. The model offers strain rate dependence of the elastic modulus, failure stress, yield stress, and tangent modulus by specifying user defined load curves. The load curves were based off of observed results from

experimental strain rate tests that had previously been conducted on Twaron® fabric. The researchers reported good correlation between experimental and numerical results. However, they noted that improvements and corrections to the model could be made with regards to yarn frictional effects and strain rate effects. Innucci and Willows [38] used LS-DYNA and a damage growth model to simulate the behavior of woven carbon composites when subjected to impact loads. They used plane stress shell elements to represent the composite and consider damage of the fabric fibers and matrix by reducing the effective stiffness values with damage growth until failure. Johnson and Simon [39] conducted a similar analysis using damage mechanics model with shell elements and the explicit finite element software PAM-CRASH. They also use a predefined material behavior listed as Material Type 131 that is a partial elastic damage model. Tabiei and Ivanov [8] developed a model for woven fabrics that used a method of cells approach to homogenize the unit cell and considered yarn re-orientation or non-orthogonality of the material directions. They implemented the model into LS-DYNA through a user defined material definition and simulated the impact of a cylindrical projectile with one layer of Kevlar®129 fabric using membrane shell elements to represent the fabric. Damage and failure of the fabric were not considered in the model. Only the deformation of the fabric and projectile displacement versus time could be compared between the simulation and experiment. A good correlation was observed.

A detailed study that compares the method of cells and finite-element based virtual testing for multi-physics linear and nonlinear problems is discussed by Krishnan [40].

1.2.3. Strain Rate Effect

The challenges of including load rate effects in a fabric material model are twofold. First, there is difficulty in obtaining accurate experimental results especially at very high strain rates. Second, there is difficulty in choosing a strain rate model. One of the more successful techniques for conducting experimental strain rate testing is the Split Hopkinson bar (SHB) test. Wang and Xia [10] and [11] conducted strain rate tests on Kevlar® 49 yarns using the SHB test up to 1350 s^{-1} and found that the fabric had both temperature and rate dependence. The yarn's elastic modulus, peak stress, strain to peak stress, and failure strain each increased with an increase in strain rate. The same properties were shown to decrease with an increase in temperature as well. After conducting strain rate tests on Kevlar® KM2 yarns using the SHB, Cheng and co-workers [41] concluded that the yarns were not rate dependent up to a strain rate of approximately $2450s^{-1}$. Rodriquez et al. [42] conducted strain rate tests using the SHB on aramid and polyethylene fabrics up to a strain rate of about 1000 s^{-1}. They observed that both types of fabrics were rate sensitive with an increase in peak stress and a decrease in failure strain as the strain rate increased. Shim et al. [43] conducted strain rate tests using the SHB on Twaron® fabric up to a rate of approximately 500 s^{-1}. The authors observed that Twaron® fabric was very sensitive to loading rate with significant

increases in the elastic modulus and peak stress values and a large decrease in the failure strain with an increase in strain rate. It should be noted that the test results are one of the few published where fabric samples not yarns were used in the test. The samples were 5 mm wide with a 30 mm gauge length. The authors noted that Twaron® fabric is very similar to Kevlar®29 in both microstructure and mechanical properties.

As mentioned there is difficulty in choosing an accurate model which captures rate effects. One model which has previously been noted is the three element linear viscoelastic model or three spring model. A representation of this model is shown in Fig. 7.

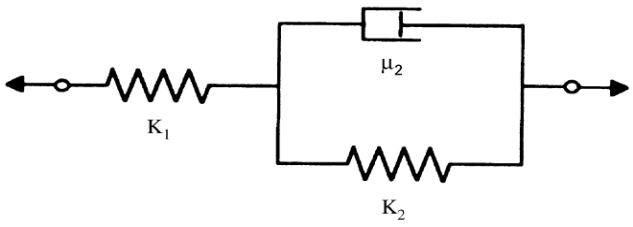

Fig. 7. Three element linear viscoelastic model

The primary and secondary bond of the material are represented by stiffness K_1 and K_2, respectively. Viscous effects caused by polymer chains slipping and sliding relative to each other are accounted for in the viscosity constant μ_2. The stress-strain relationship associated with the three element model is described by

$$\left(1+\frac{K_2}{K_1}\right)\sigma+\left(\frac{\mu_2}{K_1}\right)\dot{\sigma}=K_2\varepsilon+\mu_2\dot{\varepsilon} \qquad (1)$$

The three element linear viscoelastic model has shown to have good correlation with the dynamic experimental results for Twaron® fabric. Other strain rate models that are popular include the Cowper-Symonds model that accounts for rate effects on the yield stress by

$$\bar{\sigma} = \bar{\sigma}_0 \left[1 + \left(\frac{\dot{\varepsilon}}{C} \right) \right]^{\frac{1}{P}} \tag{2}$$

where $\bar{\sigma}_0$ is the yield stress at zero strain rate and C and P are determined from experiments. Yet another model is the Johnson-Cook model expressed as

$$\bar{\sigma} = \bar{\sigma}_0 \left[1 + C \ln \left(\frac{\dot{\varepsilon}_p}{\dot{\varepsilon}_0} \right) \right] \tag{3}$$

where C and $\dot{\varepsilon}_0$ are determined from experiments. Söderberg and Sellgren [44] conducted a study on the influence of using various forms of the Johnson-Cook and the Cowper-Symonds equations in finite element simulations of high speed crash events with metals. They concluded that the choice of strain rate model did have an influence on the simulation results. They noted that for the metals tested Cowper-Symonds model fit the experimental results well at both high and low strain rates.

1.3. Thesis Objectives and Overview

The major objectives if the theses are outlined below.

(1) Improvement to current continuum model for the single and multi FE layer models to simulate ballistic test conducted at NASA-GRC.

(2) Mesh convergence study and energy checks to validate results for single layer and multi layer ballistic test models.

(3) Picture frame test model for determination of shear behavior of fabric and comparison with experimental results.

2. THEORETICAL BACKGROUND

2.1. Overview of Explicit Finite Element Analysis

The type of solution technique used to analyze the problem depends on the type of phenomena that is of interest in the study. Structures and solids problems can be categorized into two classes – those for which the stress wave propagation is of engineering importance and those for which the duration of the load is large relative to the time required for a wave to propagate through the structure. Both types of problems are governed by the same set of physical equations but have solutions obtained using different numerical techniques. The first type of problem, also known as transient analysis (explicit dynamics), uses a solution technique which is described as explicit time integration where differential equations are solved explicitly in time. The second type of problem, also known as static analysis, uses a solution technique which is described as implicit integration where differential equations are solved implicitly in time. In general, explicit integration refers to the solution at any step, $N^{t+\Delta t}$ being solved by using information from the previous step's solution, N whereas implicit integration refers to the solution at any step, $N^{t+\Delta t}$ being obtained by solving a system of equations and iterating many times within that step.

Some of the advantages of an explicit technique over an implicit technique are as follows.

(1) Explicit technique is suitable for modeling brief, transient dynamic events, such as impact and blast problems, and is also very efficient for highly nonlinear problems involving changing contact conditions, such

as forming simulations [45]. Material degradation and failure often lead to severe convergence difficulties in implicit analysis programs (because the material stiffness can become negative) but can be solved by explicit technique.

(2) Relatively, much fewer computations and computer memory storage are required per time step since the system equations are not stored, assembled and solved.

(3) The algorithm is simple. For example, the most striking feature of the explicit method is the lack of a global tangent stiffness matrix, which is required with implicit methods. Since the state of the model is advanced explicitly, iterations and tolerances are not required [45].

The only disadvantage is to the explicit technique is that the solution is only conditionally stable. The time step must often be very small to ensure stability and the total number of time steps may be many to obtain the solution. The stability of the explicit integration procedure is dependent on the highest eigenvalue of the system [45]. For an undamped system, the stable time step is determined by

$$\Delta t = \frac{2}{\omega_{\max}} \tag{4}$$

where $\omega_{\max}$ is the highest frequency of the system. With damping the stable time step is determined by

$$\Delta t = \frac{2}{\omega_{\max}} \sqrt{1+\xi^2} - \xi \tag{5}$$

where ξ is the fraction of critical damping in the highest mode. In finite elements the stability equation expressed in (12) can be rewritten as

$$\Delta t = \min\left(\frac{L_{(e)}}{c_d}\right) \tag{6}$$

where $L_{(e)}$ is the characteristic element dimension and c_d is the dilatational wave speed of the material. The critical time step is the equivalent to the smallest value of time for the dilatational wave to travel through an element. The characteristic element length is a function of the element type and element dimensions and the dilatational wave speed is a function of the material properties [45].

The governing equations for explicit finite element analysis are the equivalent to those used for all non-linear finite element problems [46]:

(1) Conservation of mass.

(2) Conservation of energy.

(3) Conservation of momentum.

(4) A measure of deformation which relates strain to displacement.

(5) A constitutive equation which relates the measure of deformation to stress.

The conservation of mass is stated as

$$\rho J = \rho_0 \tag{7}$$

where ρ_0 is the density in the reference configuration, ρ is the density in the current configuration, and J is the determinant of the deformation matrix. Conservation of energy states

$$\rho \dot{U} = \sigma : \mathbf{D} - \frac{\partial \mathbf{q}}{\partial x} + \rho s \tag{8}$$

where $\dot{U}$ is the rate of internal work, $\mathbf{D}$ is the symmetric part of the velocity gradient or rate of deformation, $\mathbf{q}$ is the heat flux, and s is the power supplied by a heat source. In a purely mechanical process this equation reduces to

$$\dot{U} = \sigma : \mathbf{D} \tag{9}$$

which states that the internal rate of work or power is equivalent to the outer product of the Cauchy stress and the rate of deformation [45]. From this it is determined that the Cauchy stress is conjugated in power to $\mathbf{D}$ and thus any measure of stress must be conjugated to a specific measure of strain. Conservation of momentum produces the momentum equation which is expressed as

$$\frac{\partial \sigma}{\partial x} + \rho \mathbf{b} = \rho \ddot{\mathbf{u}} \tag{10}$$

where σ is the Cauchy stress, $\mathbf{b}$ is the body force per unit mass, and $\ddot{\mathbf{u}}$ is the body acceleration. A weak form solution to the momentum equation is the principle of virtual work. After discretizing the domain into a number of elements the discrete approximation to this solution can be written as

$$\mathbf{M}\ddot{\mathbf{u}} = \mathbf{f}^{ext} - \mathbf{f}^{\text{int}} \tag{11}$$

where $\mathbf{M}$ is the mass matrix of the system, $\mathbf{f}^{ext}$ is a vector of external nodal forces, and $\mathbf{f}^{\text{int}}$ is a vector of internal nodal forces. These equations are a system of N^{DOF} ordinary differential equations where N^{DOF} represents the number of degrees of freedom or the number of nodal acceleration/velocity components.

After nodal accelerations are obtained, the nodal velocities, the rate of deformation and finally stresses are computed in that order [47].

2.2. General Solution and Algorithm for Explicit Analysis

The explicit solution to (11) generally uses the central difference technique [47]. Recognizing that the time step Δt changes as the continuum deforms the time increments are defined as shown in Fig. 8.

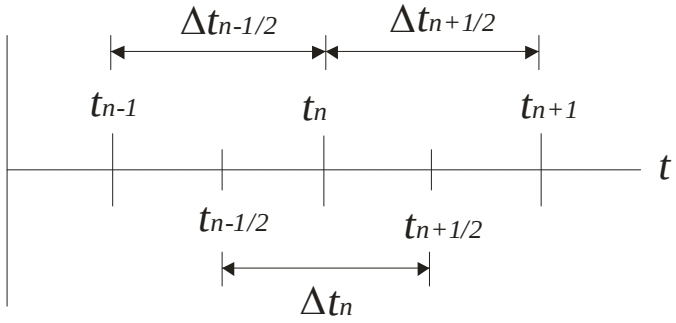

Fig. 8. Time increments using the central difference method

Thus the time increment at step *n* can be written as

$$\Delta t^{n} = t^{n+1/2} - t^{n-1/2} \tag{12}$$

where

$$t^{n+1/2} = \frac{1}{2}\left(t^{n+1} + t^{n}\right) \tag{13}$$

And the partial time increment can be written as

$$\Delta t^{n+1/2} = t^{n+1} - t^{n} \tag{14}$$

The central difference formula for the acceleration is written as

$$\ddot{u}^{n} = \left(\frac{\dot{u}^{n+1/2} - \dot{u}^{n-1/2}}{t^{n+1/2} - t^{n-1/2}}\right) \tag{15}$$

Rearranging and recognizing that $t^{n+1/2} - t^{n-1/2} = \Delta t^n$ gives the following expression for velocity at the partial step.

$$\dot{\mathbf{u}}^{n+1/2} = \dot{\mathbf{u}}^{n-1/2} + \Delta t^n \ddot{\mathbf{u}}^n \tag{16}$$

which can be rewritten by braking into two substeps by

$$\dot{\mathbf{u}}^{n+1/2} = \dot{\mathbf{u}}^n + \left(t^{n+1/2} - t^n\right)\ddot{\mathbf{u}}^n \tag{17}$$

where

$$\dot{\mathbf{u}}^n = \dot{\mathbf{u}}^{n-1/2} + \left(t^n - t^{n-1/2}\right)\ddot{\mathbf{u}}^n \tag{18}$$

The central difference formula for the velocity at the half step is written as

$$\dot{\mathbf{u}}^{n+1/2} = \left(\frac{\mathbf{u}^{n+1} - \mathbf{u}^n}{t^{n+1} - t^n}\right) \tag{19}$$

Rearranging and recognizing that $t^{n+1} - t^{n-1} = \Delta t^{n+1/2}$ gives the following expression for the displacement at the next step.

$$\mathbf{u}^{n+1} = \mathbf{u}^n + \Delta t^{n+1/2}\dot{\mathbf{u}}^{n+1/2} \tag{20}$$

Using these equations the solution to (11) for the nodal velocities can be expressed as

$$\dot{\mathbf{u}}^{n+1/2} = \dot{\mathbf{u}}^{n-1/2} + \Delta t^n \mathbf{M}^{-1}\left(\mathbf{f}^{ext} - \mathbf{f}^{\text{int}}\right) \tag{21}$$

where $\left(\mathbf{f}^{ext} - \mathbf{f}^{\text{int}}\right)$ can be computed using the strain-displacement equations. If $\mathbf{M}$ is a diagonal matrix, often referred to as the lumped mass matrix, then the above expression does not require the solution of any equations. Determining the nodal velocities only requires a single computation hence, the efficiency of the explicit integration technique [47].

The following is a general algorithm for the solution of non-linear finite element problems using the explicit integration technique. The algorithm is based on the algorithm presented by [47].

Step 1. Set the initial conditions

Set n=0, t=0, $\mathbf{u}^{n=0} = 0$.

Set initial velocities, $\dot{\mathbf{u}}^{n=0}$.

Set initial stresses, $\sigma^{n=0}$.

Set $\dot{\mathbf{u}}^{n-1/2} = \dot{\mathbf{u}}^{n=0}$.

Step 2. Compute the diagonal lumped mass matrix $\mathbf{M}$.

Step 3. Compute nodal forces (*COMPUTE_FORCE Procedure).*

Step 4. Compute initial nodal accelerations

$$\ddot{\mathbf{u}}^{n} = \mathbf{M}^{-1}\left(\mathbf{f}^{n}\right)$$

Step 5. Update time

$$t^{n+1} = t^{n} + \Delta t^{n+1/2},\ t^{n+1/2} = \frac{1}{2}\left(t^{n} + t^{n+1}\right)$$

Step 6. Update nodal velocities at half step

$$\dot{\mathbf{u}}^{n+1/2} = \dot{\mathbf{u}}^{n-1/2} + \left(t^{n+1/2} - t^{n}\right)\ddot{\mathbf{u}}^{n}$$

Step 7. Enforce velocity boundary conditions.

Step 8. Update nodal displacements

$$\mathbf{u}^{n+1} = \mathbf{u}^{n} + \Delta t^{n+1/2}\dot{\mathbf{u}}^{n+1/2}$$

Step 9. Compute nodal forces (*COMPUTE_FORCE Procedure).*

Step 10. Compute $\ddot{\mathbf{u}}^{n+1}$

$$\ddot{\mathbf{u}}^{n+1} = \mathbf{M}^{-1}\left(\mathbf{f}^{n+1}\right)$$

Step 11. Update nodal velocities at next step

$$\dot{\mathbf{u}}^{n+1} = \dot{\mathbf{u}}^{n+1/2} + \left(t^{n+1} - t^{n+1/2}\right)\ddot{\mathbf{u}}^{n+1}$$

Step 12. Check energy balance at time step n+1

Step 13. Update step counter

$$n = n + 1$$

Step 14. Create output. If $t^{n+1} < t^f$ go to step 5.

COMPUTE_FORCE Procedure

Step 1. Initialize $\mathbf{f}^n = \left(\mathbf{f}^{ext} - \mathbf{f}^{\text{int}}\right) = 0$, $\Delta t_{crit} = \infty$.

Step 2. Compute global external nodal forces, $\mathbf{f}_n^{ext,n}$.

Step 3. Loop over all elements.

Step 3.1. Get element nodal displacements $\mathbf{u}_e^n$ and velocities $\dot{\mathbf{u}}_e^n$

.

Step 3.2. Set the internal nodal forces for the element $\mathbf{f}_e^{\text{int},n} = 0$.

Step 3.3. Loop over all integration points.

Step 3.3.1. If n = 0, go to step 3.3.4

Step 3.3.2. Compute measure(s) of deformation

$\mathbf{D}^{n-1/2}$ - Rate of deformation tensor

$\mathbf{F}^n$ - Deformation gradient

$\mathbf{E}^n$ - Lagrangian/Green strain

Step 3.3.3. Relate deformation to stress σ^n through constitutive equation.

Step 3.3.4. Relate stress to internal forces and add to sum $\mathbf{f}_e^{\text{int},n}$

Step 3.3.5. End integration point loop.

Step 3.4. Compute external forces on element, $\mathbf{f}_e^{ext,n}$.

Step 3.5. Compute, $\mathbf{f}_e^{\,n} = \left(\mathbf{f}_e^{\,ext} - \mathbf{f}_e^{\,\text{int}}\right)$.

Step 3.6. Compute new critical time step for element, Δt_{crit}^e

If $\Delta t_{crit}^e < \Delta t_{crit}$ then set $\Delta t_{crit} = \Delta t_{crit}^e$.

Step 3.7. Construct element forces $\mathbf{f}_e^{\,n}$ into global nodal forces $\mathbf{f}^{\,n}$.

Step 3.8. End loop over elements.

Step 4. Set $\Delta t^{n+1/2} = \beta \Delta t_{crit}$, where β is a reduction factor that is typically used to prevent instabilities.

There are also many additional topics related to explicit finite element analysis that were not covered in this section but are typically considered by most commercial codes. These include contact/impact algorithms, damping forces, hourglass resistance, inclusion of artificial bulk viscosity etc.

3. CONTINUUM MODEL

3.1. Introduction

In prior studies at ASU constitutive material model for Kevlar®49 were developed based on the results from static and dynamic experimental tests. These models are referred to as ASUumatv1.0 [3] and ASUumatv1.1 [12]. They include non-linearity in the stress-strain response, strain rate effects as well as failure criteria that allow elements to be deleted from the model. The models were incorporated into the LS-DYNA finite element program through a user defined material definition (subroutine) and were validated by comparing the results against experimental ballistic tests conducted at NASA Glenn Research Center. In the first version of this model (ASUumatv1.0) all fabric layers were represented by a single FE layer. The thickness of the FE layer was assumed to be equivalent to the thickness of the total number of layers in the experiment. Although, the simulation results were shown to match closely with the experimental tests for most of the test cases however, the results for the very low or very high projectile velocity test cases did not match closely with the experiments. Furthermore, this model did not capture friction between the fabric layers that exists in the experiments. To overcome these shortfalls a second generation constitutive model was developed [12]. In this version both single and multi-layers were used to model the Kevlar fabric. For single layers the same methodology as previously presented was used while for the multi-layer model four fabric layers were models into a FE layer with the equivalent four layers thickness.

3.2. ASU Continuum model - Improvements in current model

3.2.1. New stress-strain experimental data

As shown through tests conducted at ASU [48] the primary mode of failure of Kevlar®49 is the breakage of the warp or fill direction yarns. Initially based on the tension tests conducted at ASU and described in [48] it was assumed the failure strain was simply the strain reported at the end of the tension tests as shown in Fig. 9.

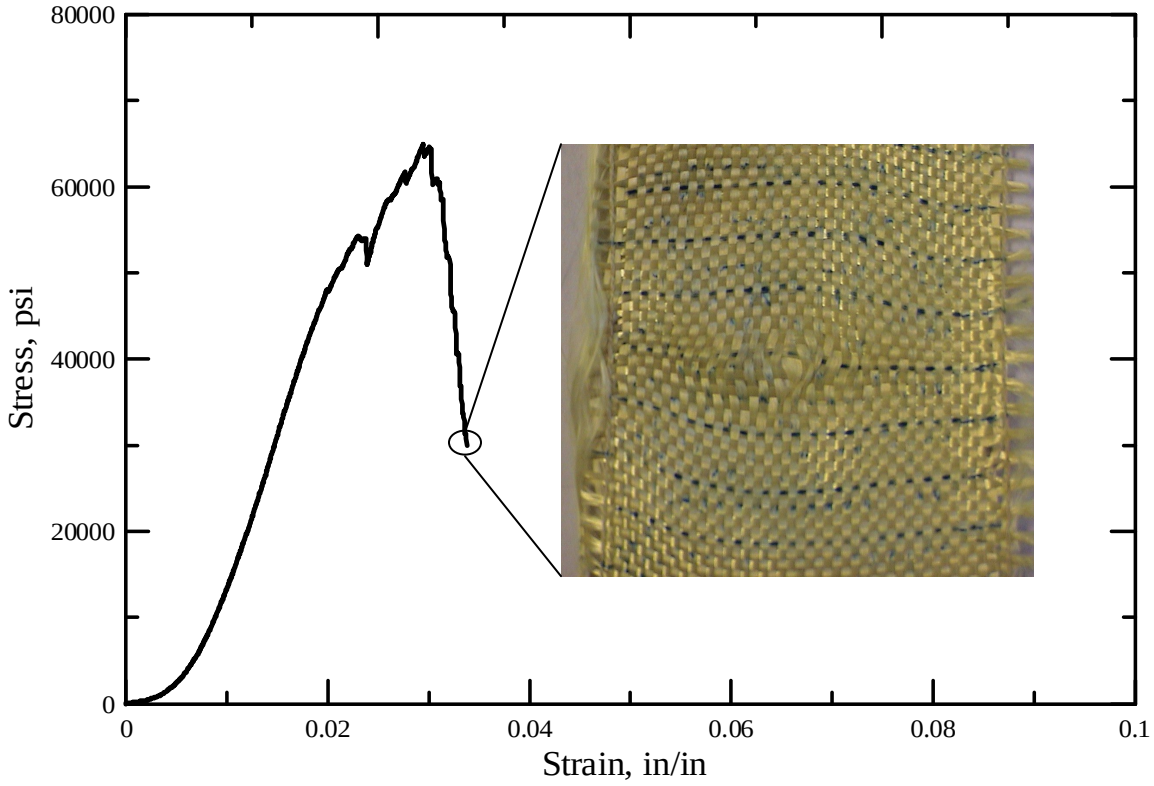

Fig. 9. Stress strain curve and fabric at the end of tension test (warp direction)

After analyzing the deformed fabric samples it was determined that much larger strains are required to fully fail the fabric yarns [12]. To account for this behavior in the material model, the post-peak region was approximated with a

linear region followed by a non-linear region up until fabric failure. The fill and the warp directions resulting stress strain behavior are shown in Figures 10(a) and 10(b).

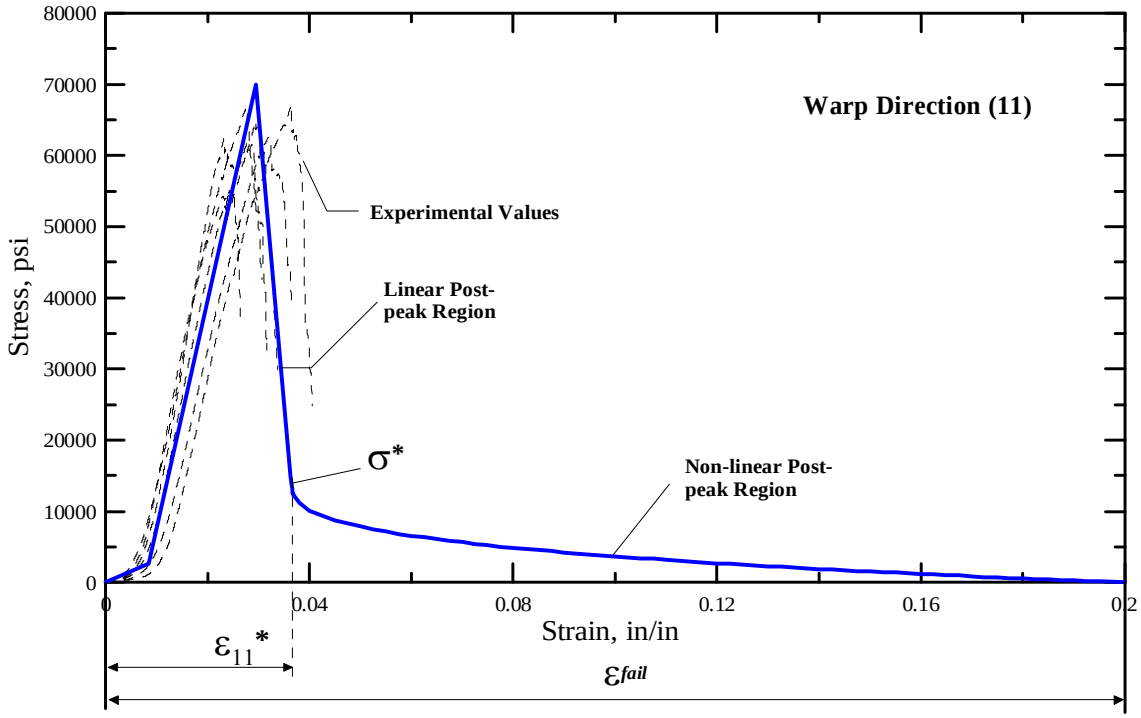

Fig. 10(a). Kevlar® 49 warp (11) direction uniaxial stress-strain results with approximation for pre-peak and post-peak behavior

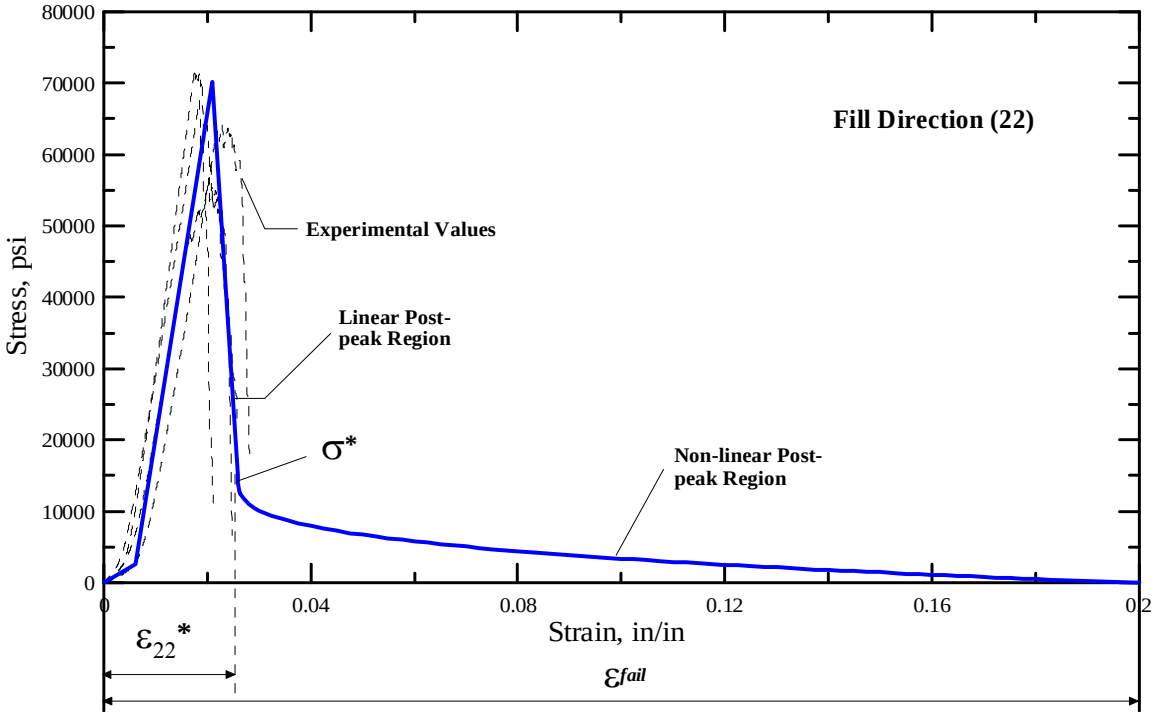

Fig. 10(b). Kevlar® 49 fill (22) direction uniaxial stress-strain results with approximation for pre-peak and post-peak behavior

A comparison of the ASUumatv1.0 and ASUumatv1.1 for warp and fill directions is shown in Figures 11(a) and 11(b) respectively.

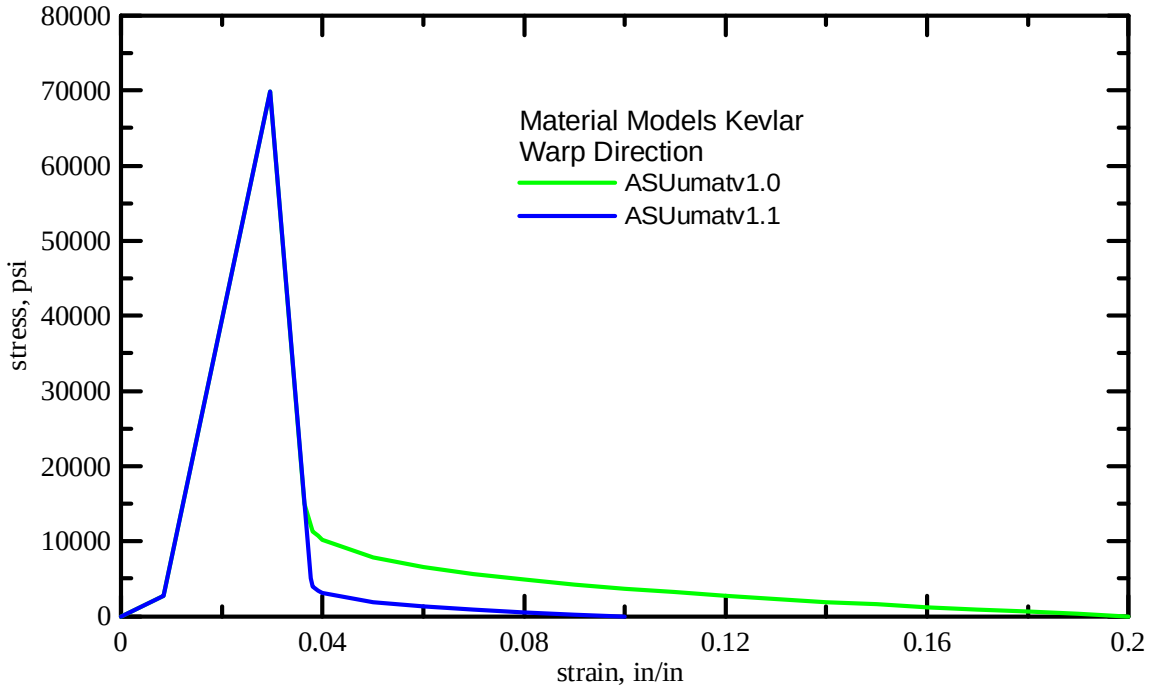

Fig. 11(a). Kevlar® 49 warp (11) direction load curves used in ASU material model v1.0 and v1.1

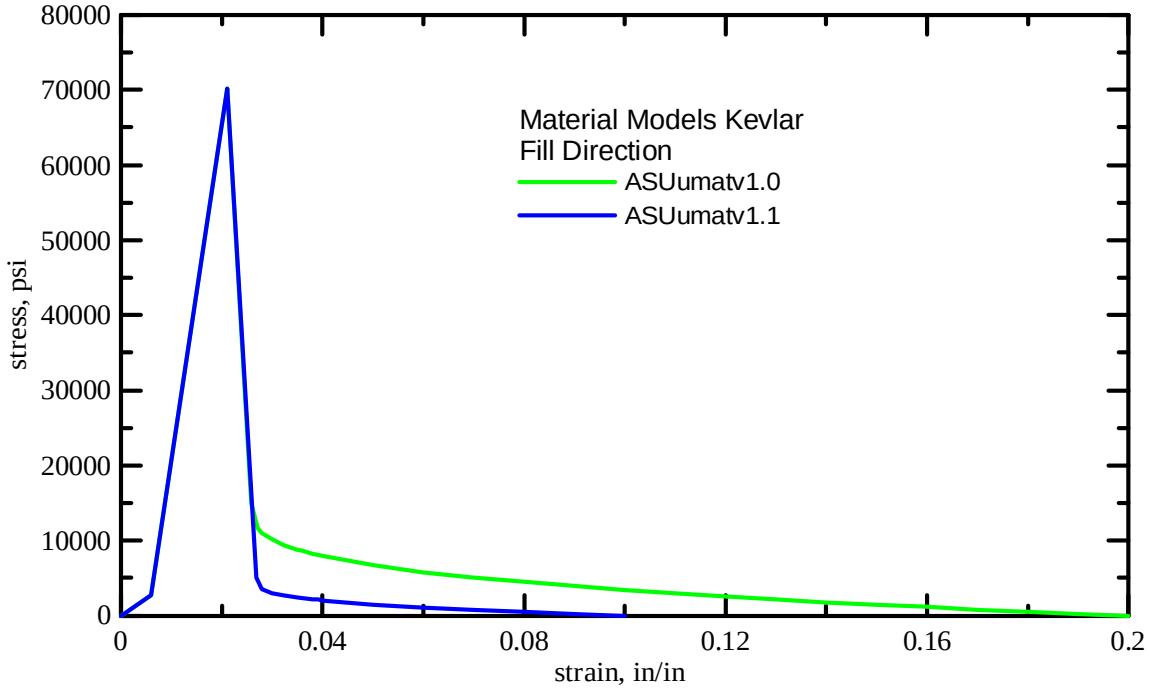

Fig. 11(b). Kevlar® 49 warp (11) direction load curves used in ASU material model v1.0 and v1.1

In the finite element model, the fabric is represented by the shell elements and local coordinate system of shell element is used to define material directions. In ASUumatv1.0 when the normal strain reached the failure strain (in either the warp or fill direction), the element is deleted from the model. To account for the fact that fill yarns may still have load carrying capacity even if warp yarns may have failed and vice versa, the erosion criterion was modified in ASUumatv1.1. An element was deleted only when the strain in both principal directions reached the failure strain value (i.e. 0.16), or if the strain either in the warp or in the fill direction reached a peak value of 0.35. A second change that was introduced with ASUumatv1.1 was that the stress at which the post peak non-linear curve begins was changed from 15000 psi to 5000 psi to match more closely the new experimental results especially in the post-peak region [49]. The complete stress strain curves obtained with the most recent experiments are shown in Fig. 12.

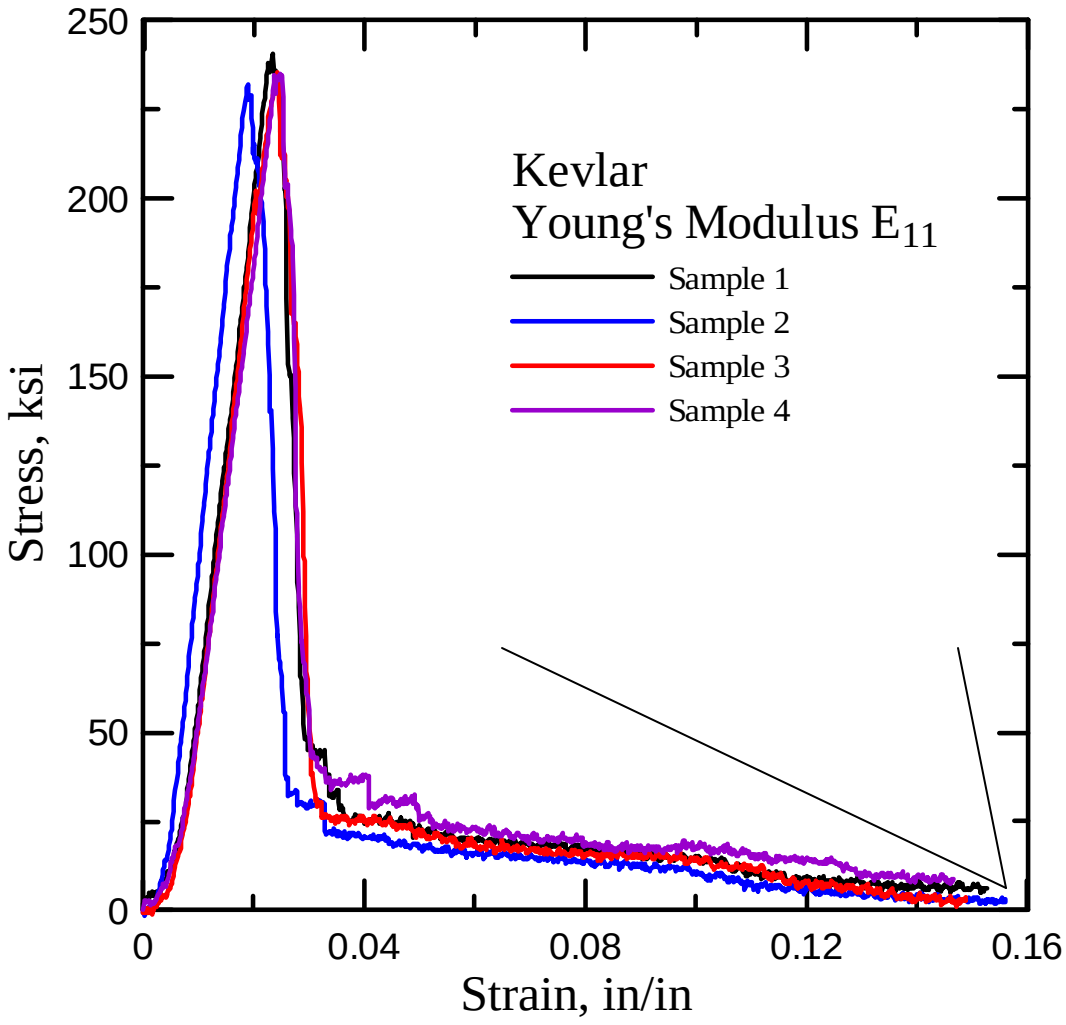

Fig. 12. Stress strain curve and fabric at the end of tension test (warp direction)

A comparison of the fabric used in the tension test at failure is presented in Fig. 13(a) and 13(b) showing the almost complete damage in the fabric achieved in the latest tests.

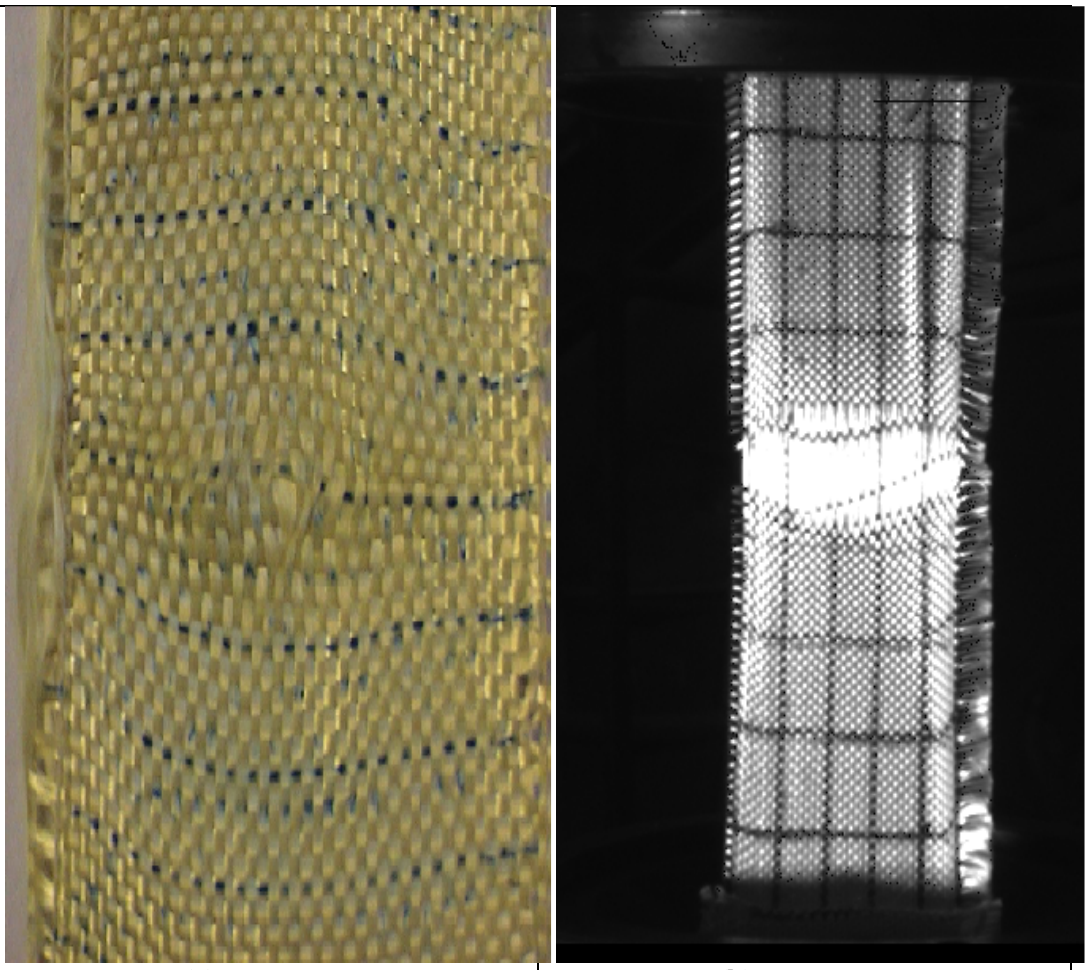

(a) 2002 test (b) 2009 tests

Fig. 13. Fabric specimens at the end of the tensile test

3.2.2. Projectile elasto-plastic material model

Analysis of the video recordings of the experimental ballistic tests conducted at NASA Glenn Research Center indicates a large deformation of the projectile after contact with the fabric. The material used in the ballistic test is a 304L stainless steel with similar properties as determined by Blandford and co-workers [50]. The typical stress-strain curves at different temperatures are shown in Fig. 14.

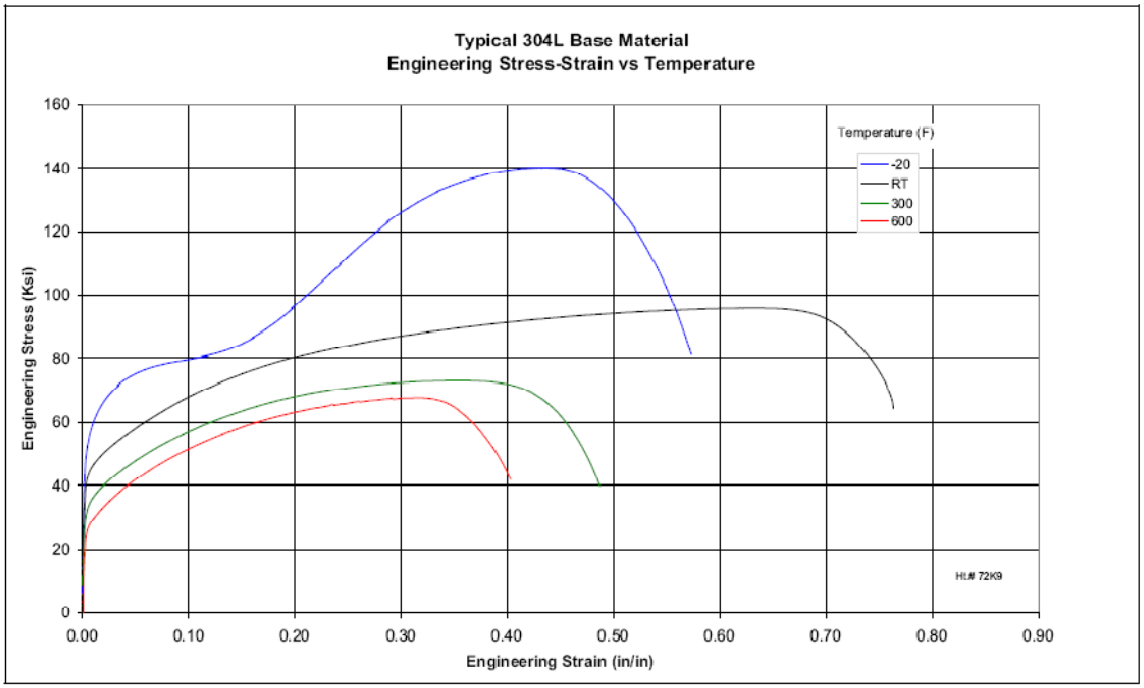

Fig. 14. Stress strain curves for stainless steel 304L

The current material model used for projectile is perfectly elastic. The material card used to model the material can be seen in Fig. 15.

```
*MAT_ELASTIC
$#     mid        ro         e        pr        da        db
         2  7.290E-4      30.0       0.3
```

Fig. 15. Mat_Elastic input card

For an improved and more realistic simulation of the ballistic experiments, a new material card was used. This provides a much closer match for the stainless steel 304L material behavior. The LS-DYNA *MAT_JOHNSON_COOK (Mat ID 15) was utilized. A typical card used for input is listed in Fig. 16.

```
*MAT_JOHNSON_COOK
$ ---------------------------------------
$  MAT#    RHO      G
$#     mid        ro         g         e        pr       dtf        vp
        11  7.290E-4      11.5
$#      a         b         n         c         m        tm        tr      epso
  0.050000  0.045000  0.300000  0.240000  1.030000 1300.0000 298.00000  0.001000
$#     cp        pc     spall        it        d1        d2        d3        d4
    0.6740       0.0       0.0       1.0      1.70
$#     d5
     0.000
```

Fig. 16. Mat_Johnson_Cook input card

The flow stress values is calculated using the equation given in (22)

$$\sigma_y = \left(A + B \cdot \overline{\varepsilon}^{p^n}\right) \cdot \left(1 + C \cdot \ln \overline{\varepsilon}^*\right) \cdot (1 - T^{*m}) \tag{22}$$

where:

A, B, C, n, m – input constants;

$A = 0.05;\ B = 0.045;\ C = 0.24; n = 0.3;\ m = 1.03;$

$\overline{\varepsilon}^p$ - effective plastic strain

$\overline{\varepsilon}^* = \frac{\dot{\overline{\varepsilon}}}{EPSO}$ - effective total strain rate normalized by quasi-static threshold rate

T^*- homogenous temperature ($T^* = 0$ in our case)

The strain rate dependency of the material model is introduced through the effective total strain term ($\overline{\varepsilon}^*$) providing a better approximation for the steel projectile and theoretically a more accurate model.

3.2.3. Picture Frame Test

To determine the most appropriate relationship between shear stress and strain used in the ballistic model [51], additional picture frame tests were conducted [49]. The two preferred experimental methods for determining the shear characteristics of a fabric are the biaxial extension and the picture frame

test. In the biaxial extension, while the experimental setup is simpler, a combination of shear and tension is induced making the pure shear deformation harder to capture. The later, while the setup is more complicated, is favored for our purpose given that uniform measurable shear, easily recorded is produced in the fabric. The complete experimental setup is described in by Zhu in [52].

All tests were conducted in a 22 Kips servo-hydraulic test frame (MTS) operated under closed-loop control. A displacement control test procedure was used with the rate of displacement of actuator (stroke) at 0.2 in/min. Digital data acquisition was used to collect data every 0.5 second. A CCD monochrome camera was used to capture the images during loading process. Three different size specimens with corner cut-offs, i.e. 3”x3”, 4”x4” and 5”x5”, were tested with five replicates for each size specimen. Fig. 17 shows the test setup and one of the 5"x5" specimens in place at the beginning of the test.

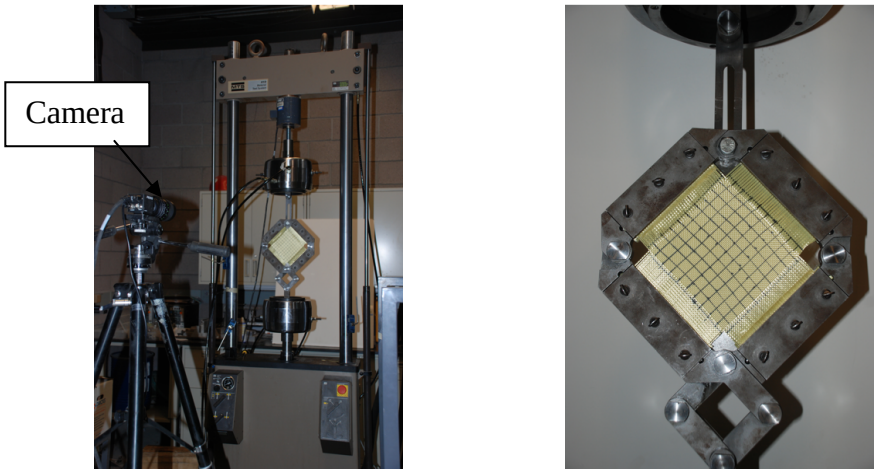

(a) (b)

Fig. 17. Picture frame test setup: (a) Instron machine and CCD camera, and (b) picture frame with specimen

Image analysis was used in the determination of the shear angle and in-planar displacement at pre-determined points on the surface of fabric specimen. Grid pattern was applied on the specimen surface before the test and used as the reference points for the image analysis. The number of points used to capture the displacement for the three specimen size are listed in Table 1.

Table 1
Number of point per test specimen.

Specimen size	Number of reference points
3”x3”	9
4”x4”	16
5”x5”	25

An example with the distribution and the location of the points, for the 4”x4”specimen, at the beginning of the test is shown in Fig. 18.

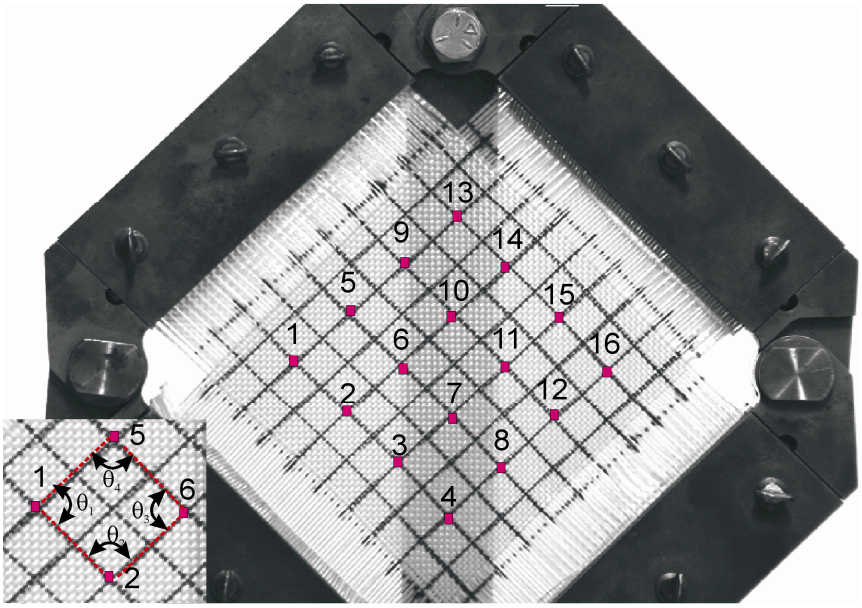

Fig. 18. Location of the reference points at the beginning of the test

Using image analysis, X and Y coordinates and displacements were computed at different time steps. The reference times used for collection and

comparison of data were 50, 100, 150, 200, 250 and 300 sec, respectively. Based on the collected data, a MATLAB code and a commercial image analysis software (VIC-2D - based on digital image correlation (DIC) method), the displacement field of specimen during the loading process and the shear modulus and shear strain were calculated.

The engineering shear stress versus shear strain obtained based on the experiments and later used in the FE simulation is shown in Fig. 19.

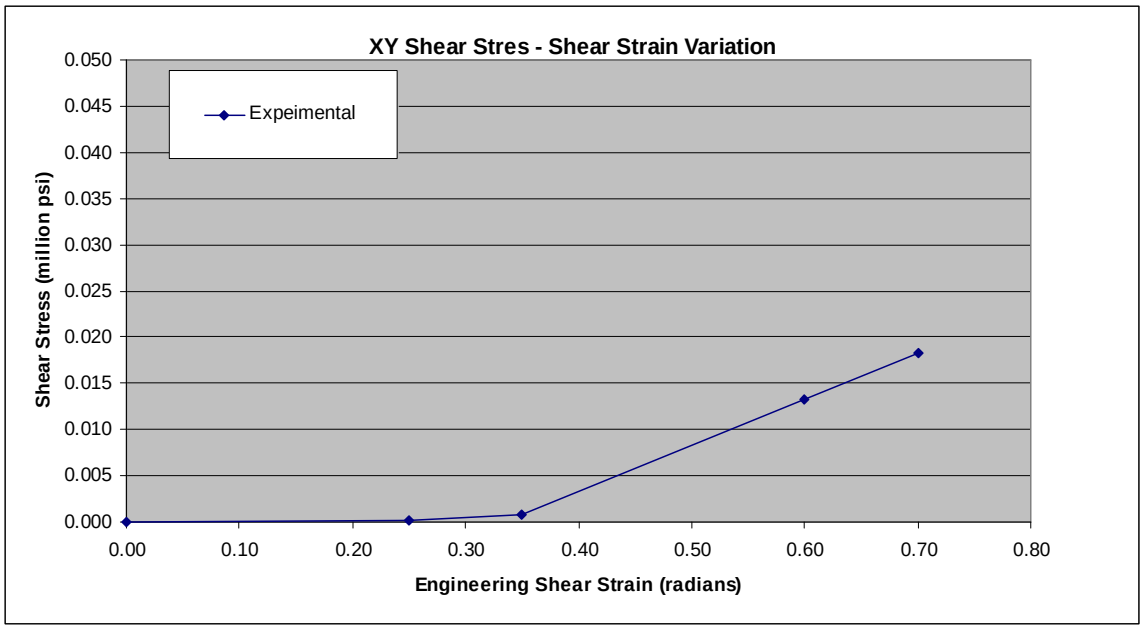

Fig. 19. Engineering shear stress versus engineering shear strain.

To better understand and verify the experimental picture frame test results, an FE model simulating the picture frame test was created. Because it provides a reasonable number of reference points and since the displacement of all three experimental setup was found to be consistent, the 4”x4” mesh with a total of sixteen reference points was used as a basis for comparison in our optimization problem. The FE model has the same dimensions and cross sectional properties as the experiment model. The FE model test setup is presented in Fig. 20.

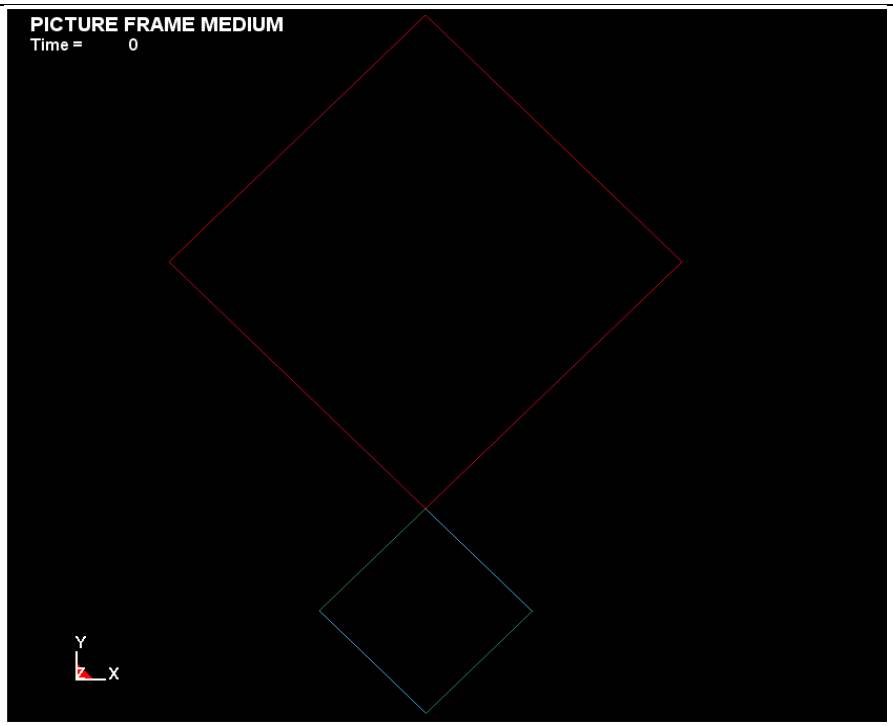

(a)

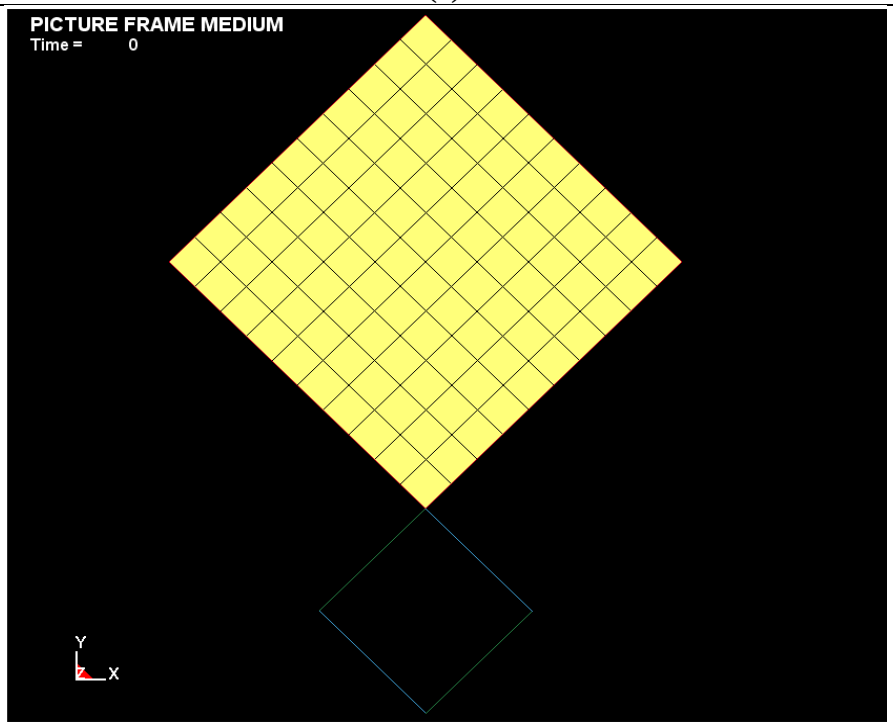

(b)

Fig. 20. Picture frame FE model: (a) Frame FE model only; (b) Frame and fabric FE model only

LS-DYNA v971 was used in the FE model and analysis. Beam elements (with linear, elastic steel properties) were used to model the edges of the picture frame and shell elements were used for the fabric (ASUumatv1.2).

In order to determine the shear strain-stress relationship for use in ASUumatv1.2, an optimization problem was formulated. A two level factorial design using three design variables was used. The variation of the shear stress – shear strain behavior was of two piecewise linear type. The three design variables chosen describe the shear stress versus shear strain behavior in the XY plane are: G_{xy1}, G_{xy2} and γ_1. Based on the problem formulation, the expected behavior is shown in Fig. 21.

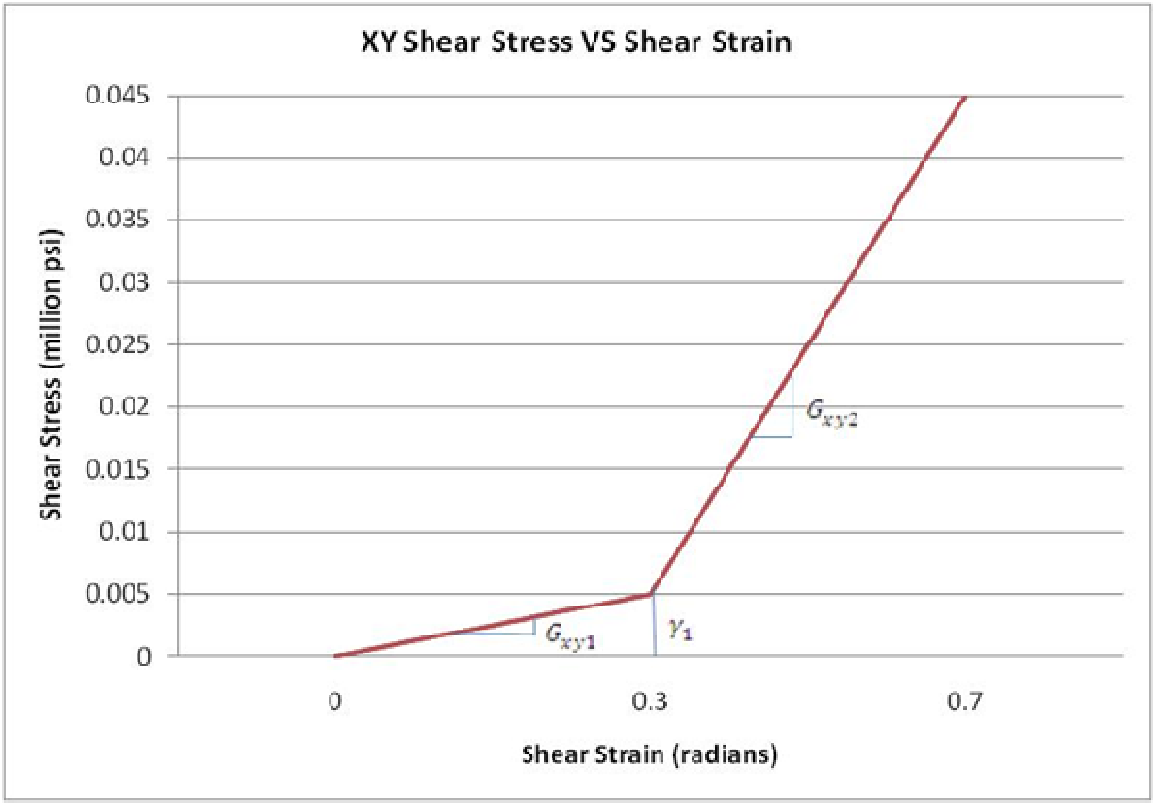

Fig. 21. Shear stress vs. shear strain predicted behavior

The three design variables in the two level factorial design require a total of $2^3 = 8$ responses, one for each of the three variables combination to be calculated. The experimental values from the image analysis for the X and Y displacement were compared to X and Y displacements values obtained from the FE analysis at six different reference times: 50, 100, 150, 200, 250 and 300 sec, respectively. The difference between the experiment and FE displacement in the X and Y direction was than minimized base on equation (23). The bounds for the three design variables were chosen as follows:

$$2(10^{-3})\frac{Mlb}{in^2} \leq G_{xy1} \leq 2(10^{-3})\frac{Mlb}{in^2}$$

$$150(10^{-3})\frac{Mlb}{in^2} \leq G_{xy2} \leq 250(10^{-3})\frac{Mlb}{in^2}$$

$$0.3 \leq \gamma_1 \leq 0.6$$

Several error estimate were attempted and are presented in Appendix A as $Error\ A$, $Error\ B$ and $Error\ C$. $Error\ C$, shown in Eqn. (23), is providing the best results for the error (residual) estimate in each of the eight runs and it and was used for all future calculations.

$$Error\ C = \sum_{1}^{16}\left\{\sum_{i=1}^{6}\left(\Delta X_{i,exp} - \Delta X_{i,FE}\right)^2 + \sum_{i=1}^{6}\left(\Delta Y_{i,exp} - \Delta Y_{i,FE}\right)^2\right\} \qquad (23)$$

$\Delta X_{i,exp}$ – change in the X-coordinates of the ith point in the measured during experiment compared to the unloaded state

$\Delta X_{i,FE}$ – change in the X-coordinates of the ith point in the measured during the FE simulation compared to the unloaded state

$\Delta Y_{i,exp}$ – change in the Y-coordinates of the ith point in the measured during experiment compared to the unloaded state

$\Delta Y_{i,FE}$ – change in the Y-coordinates of the ith point in the measured during the FE simulation compared to the unloaded state.

The eight runs combinations and the calculated error are listed in Table 2 while details on the calculation can be found in Appendix A.

Table 2
Optimization runs details

Run no.	γ_1	G_{xy1}	G_{xy2}	Error
1	0.3	8.E+03	1.50.E+05	28.167
2	0.6	8.E+03	2.50.E+05	24.185
3	0.3	2.E+03	1.50.E+05	50.158
4	0.3	8.E+03	2.50.E+05	69.679
5	0.6	2.E+03	1.50.E+05	24.216
6	0.6	2.E+03	2.50.E+05	24.216
7	0.3	2.E+03	2.50.E+05	72.943
8	0.6	8.E+03	1.50.E+05	24.281

The commercial software Design Expert [53] was used to evaluate and analyze the data. A third order polynomial considering all terms as significant was calculated and the expression obtained is shown in Eqn. (24).

$$\begin{aligned} R1 = {} & 41.20233 - 28.42667 \cdot \gamma_1 - 0.016729 \cdot G_{xy1} \\ & + 3.30533 \cdot 10^{-4} \cdot G_{xy2} + 0.027939 \cdot \gamma_1 \cdot G_{xy1} \\ & - 5.50356 \cdot 10^{-4} \cdot \gamma_1 \cdot G_{xy2} + 6.25833 \cdot 10^{-8} \\ & \cdot G_{xy1} \cdot G_{xy2} - 1.04572 \cdot 10^{-7} \cdot \gamma_1 \cdot G_{xy1} \cdot G_{xy2} \end{aligned} \quad (24)$$

Using non linear minimization on the expression above, the three design variable values at which the function minimum is achieved were calculated and are as follows:

$$G_{xy1} = 5 \cdot 10^3 \frac{Mlb}{in^2}$$

$$G_{xy2} = 200 \cdot 10^3 \frac{Mlb}{in^2}$$

$$\gamma_1 = 0.6rad$$

Additional details and the calculation used in the optimization can be found in Appendix A. The shear stress versus shear strain interaction curves based on the optimized design variables values are shown in Fig. 22.

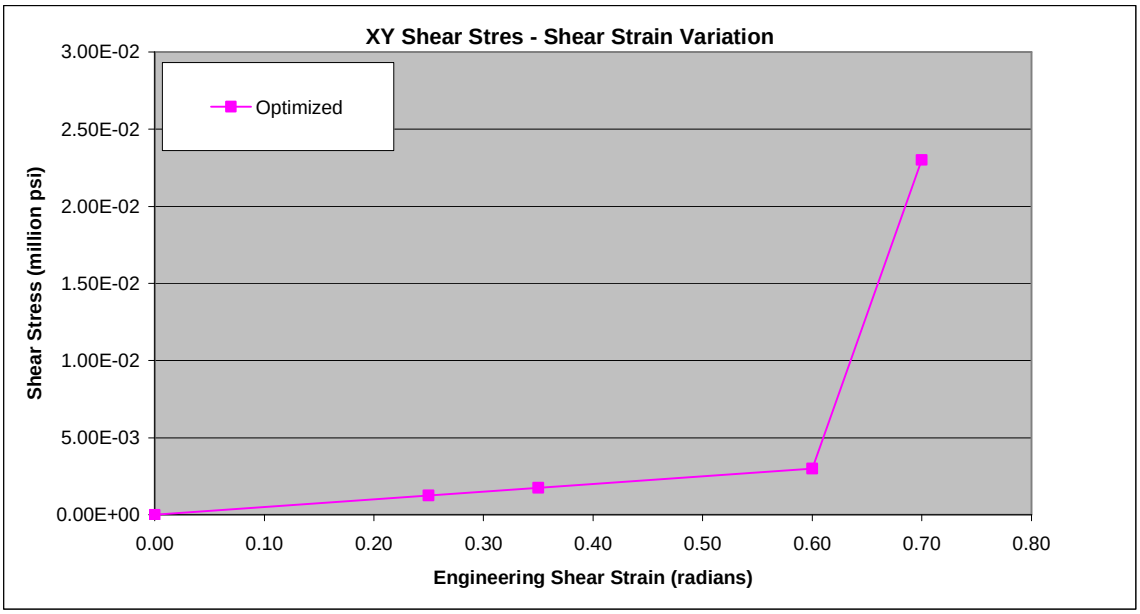

Fig. 22. Shear stress vs. shear strain

The minimum for the obtained function is 24.074 while the R-square for the curve obtained based on the eight residuals is 100% indicating a perfect fit.

A comparison of the experimental and the optimized shear strain versus shear stress is shown in Fig. 23.

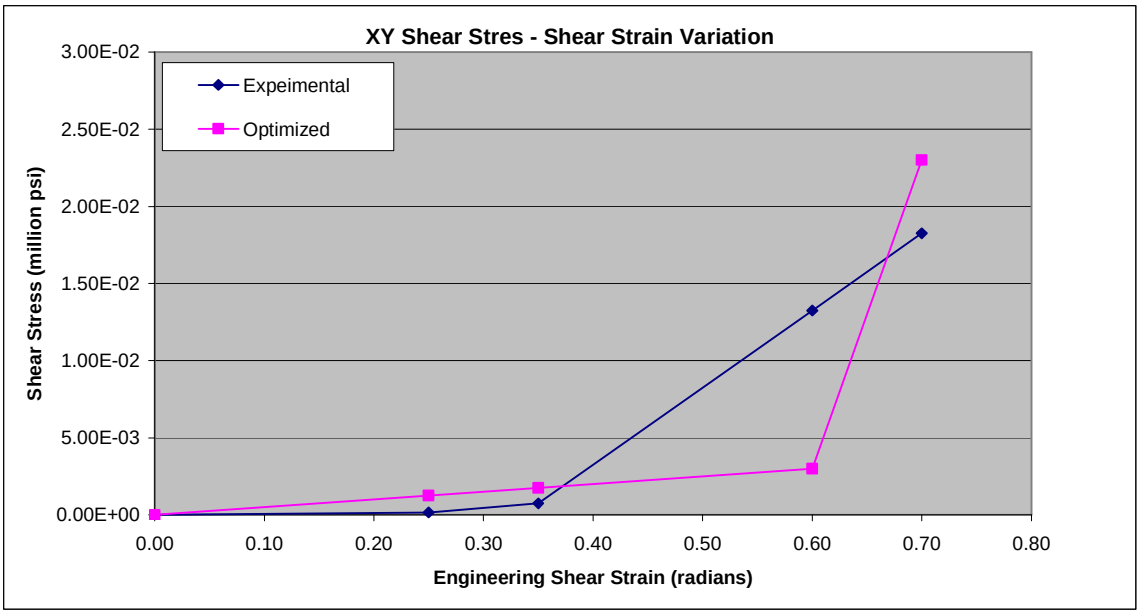

Fig. 23. Shear stress vs. shear strain, Experimental and Optimized

Comparing the displacement obtained from the experiment and the displacement obtained in the FE model, it can be observed that while the quantitative values may be slightly different, the displacement for all nodes takes place in the same direction indicating a qualitative concordance and thus validating the FE model. Table 3 presents the comparison at different time steps of the two models.

Table 3
Experiment versus FE model Prediction.

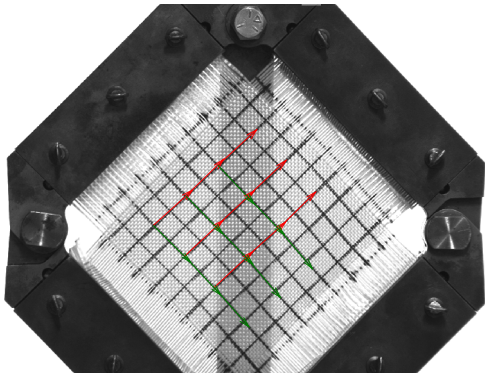 T=0 s	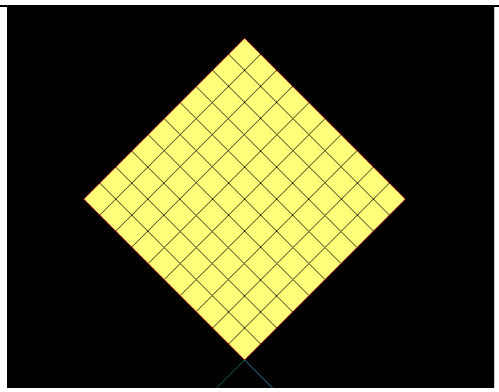 T=0 s
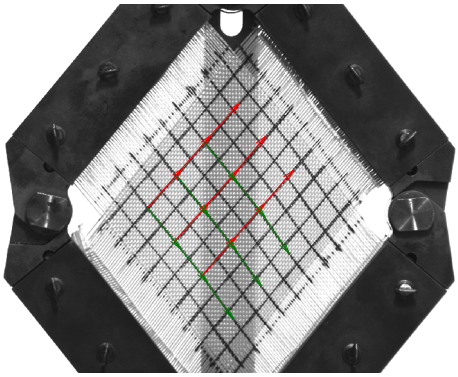 T=100 s	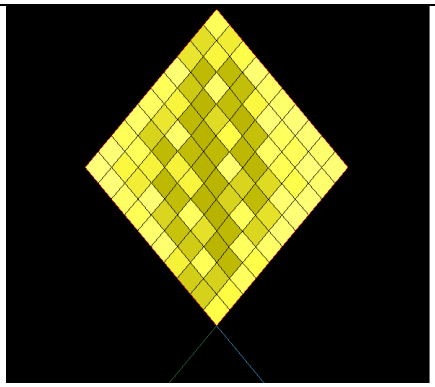 T=100 s
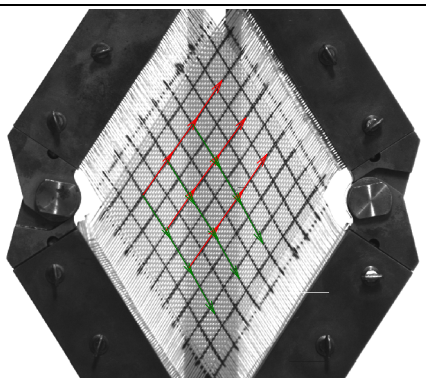 T=200 s	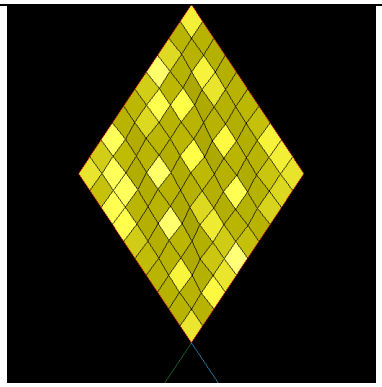 T=200 s

3.2.4. Angular Velocity

Analyzing the results of the NASA ballistic tests in Phase II it can be observed a variation in the position of the projectile in terms of the Euler angles (roll, pitch and yaw). In the suite of NASA experiments, the projectile's velocity

before impact, velocity after impact, and orientation was measured during each test using high speed cameras. The cameras tracked the position of various points on the projectile to determine its velocity and related the position to a fixed coordinate system to determine its orientation. Figures 24 and 25 are showing the local coordinate system of the projectile and the fixed or global coordinate system for a 0° and a non-0° test case, respectively.

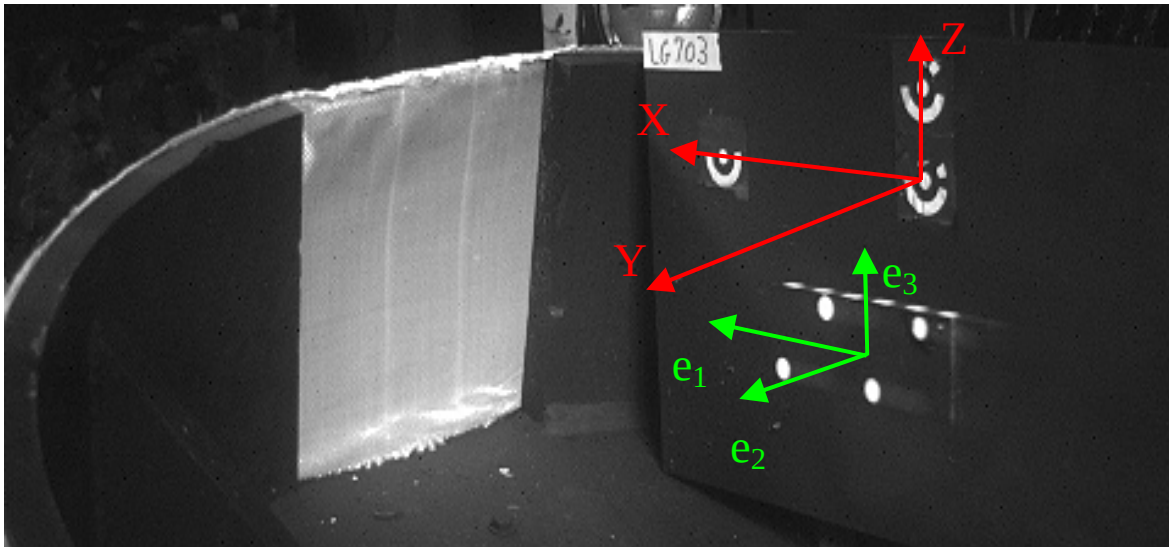

Fig. 24. NASA ballistic test showing global coordinate system (X-Y-Z) and local projectile coordinate system for a 0° projectile orientation

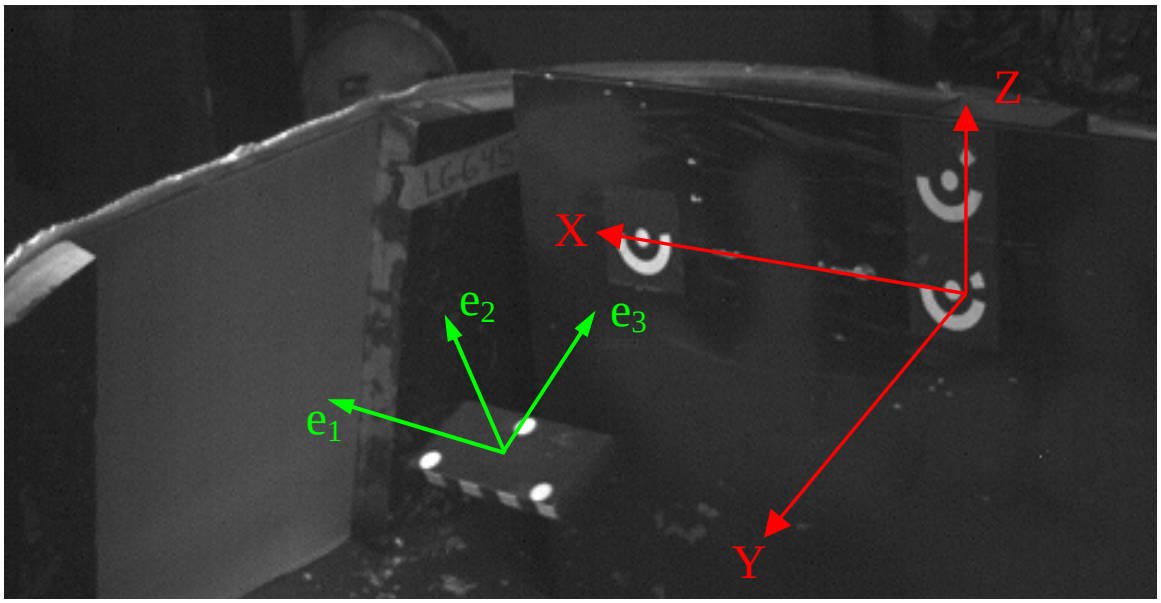

Fig. 25. NASA ballistic test showing global coordinate system (X-Y-Z) and local projectile coordinate system for non-0° projectile orientation

In the figures, the local coordinate system of the projectile is defined as **e** and the fixed coordinate system is shown. The orientation of the projectile was reported as Euler angles corresponding to roll, pitch, and yaw of the projectile. The roll, pitch and yaw angles are defined as the rotation about the e_1 axis, e_2 axis, and the e_3 axis, respectively, as shown in Fig. 26 where the local coordinate system is shown at the center of the projectile. A right hand rule is used to define positive and negative rotations. The order of rotation is important in this case because each angle is reported with respect to the projectile's local coordinate system. With each rotation, the local coordinate system changes and the next rotation are with respect to the new local coordinate system.

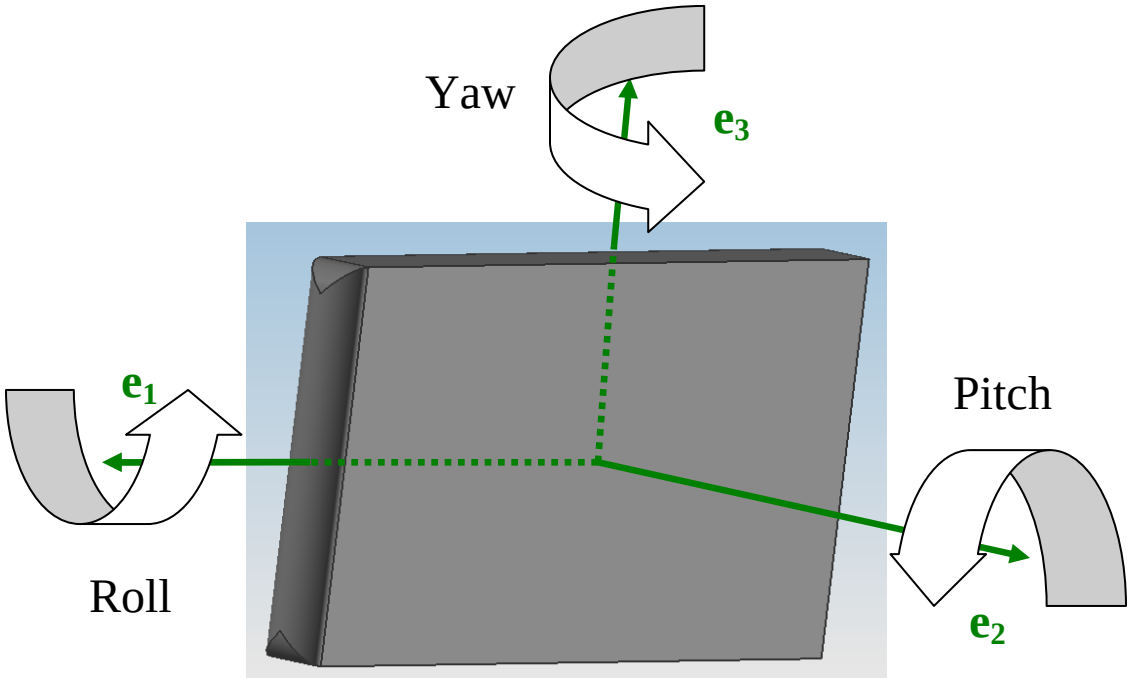

Fig. 26. Roll, pitch, and yaw angles of the projectile

Models with an observed variation at any time step of more than three degrees were selected and the angular velocities for each of the Euler angles were calculated.

Calculation was done based on the fitted curve slope as shown in Fig. 27. The roll, pitch and yaw position during the NASA test were measured and reported at different time interval. A fitted line through the reported position for each of the three orientations was created. In the line equation, the slope for the three directions is used to calculate the orientation and the magnitude of the angular velocity. A vector of angular velocity is so created, characterized by the three

direction cosines and its magnitude. The origin of the angular velocity vector is positioned at the center of the projectile for each one of the tests.

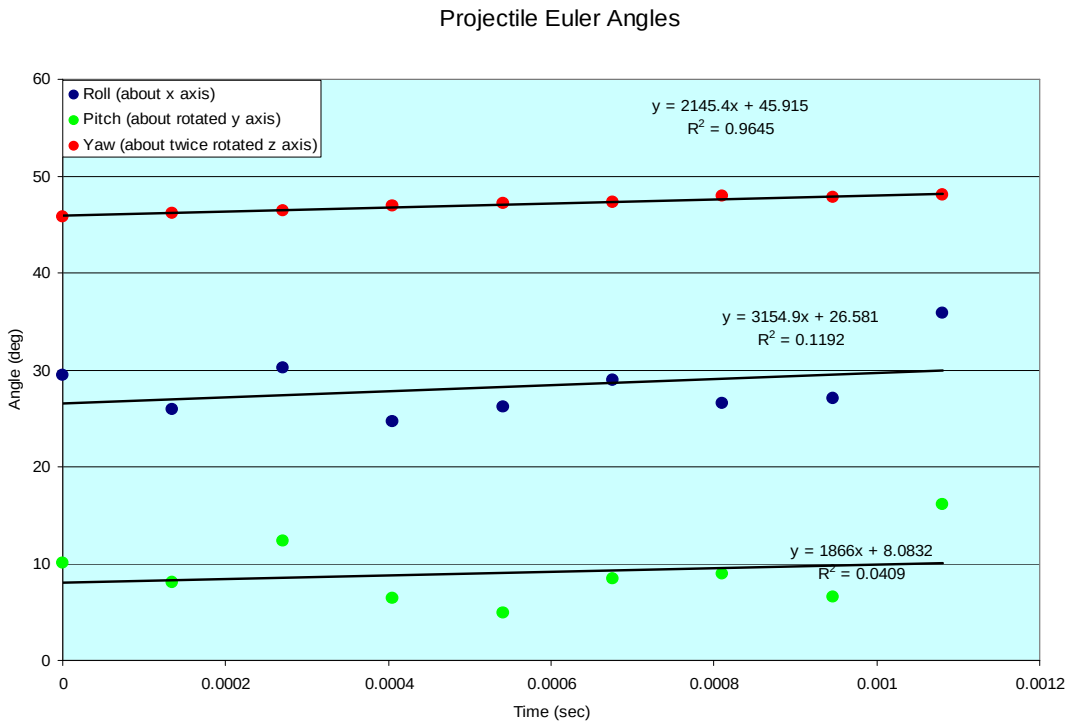

Fig. 27. Projectile position with time – LG594

Calculations performed for the four models subjected to angular velocities are presented below:

(1) Test case LG594

Values used in determining the angular velocity and the direction cosines for LG594 were extracted from the plot presented in Fig. 27.

- direction cosines

$$Nx = \frac{3154.9}{\sqrt{3154.9^2 + 1866.0^2 + 2145.4^2}} = 0.743$$

$$Ny = \frac{1866.0}{\sqrt{3154.9^2 + 1866^2 + 2145.4^2}} = 0.439$$

$$Nz = \frac{2145.4}{\sqrt{3154.9^2 + 1866.0^2 + 2145.4^2}} = 0.505$$

- Magnitude $\omega = \sqrt{3154.9^2 + 1866^2 + 2145.4^2} = 4247.1$ degrees/sec, transformed to

radians/second we have $\omega = 4247.1 \frac{\deg}{\sec} \cdot \frac{1\sec}{1000ms} \cdot \frac{3.1415rad}{180\deg} = 7.413e-2 \frac{rad}{ms}$

which is our input value for LS-DYNA analysis.

(2) Test case LG610

Values used in determining the angular velocity and the direction cosines for LG610 were extracted from the Fig. 28.

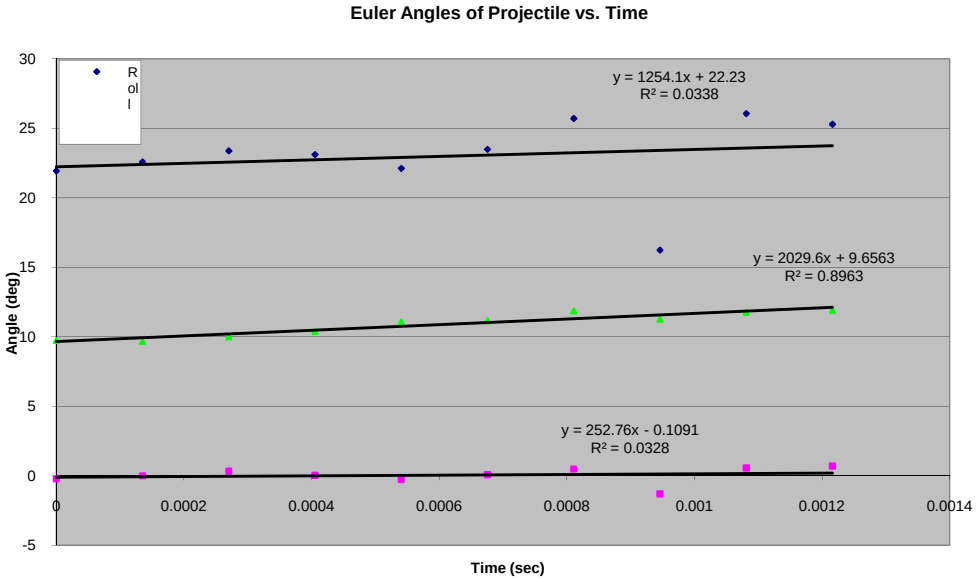

Fig. 28. Projectile position with time – LG610

- direction cosines

$$Nx = \frac{1254}{\sqrt{1254^2 + 252.7^2 + 2029.6^2}} = 0.523$$

$$Ny = \frac{252.7}{\sqrt{1254^2 + 252.7^2 + 2029.6^2}} = 0.105$$

$$Nz = \frac{2029.6}{\sqrt{1254^2 + 252.7^2 + 2029.6^2}} = 0.846$$

- Magnitude $\omega = \sqrt{1254^2 + 252.7^2 + 2029.6^2} = 2399.1$ degrees/sec, transformed to

radians/second we have $\omega = 2399.1 \frac{\text{deg}}{\text{sec}} \cdot \frac{1\text{sec}}{1000ms} \cdot \frac{3.1415rad}{180\,\text{deg}} = 4.187e-2 \frac{rad}{ms}$

which is our input value for LS-DYNA analysis.

(3) Test case LG655

Values used in determining the angular velocity and the direction cosines for LG655 were extracted from Fig. 29.

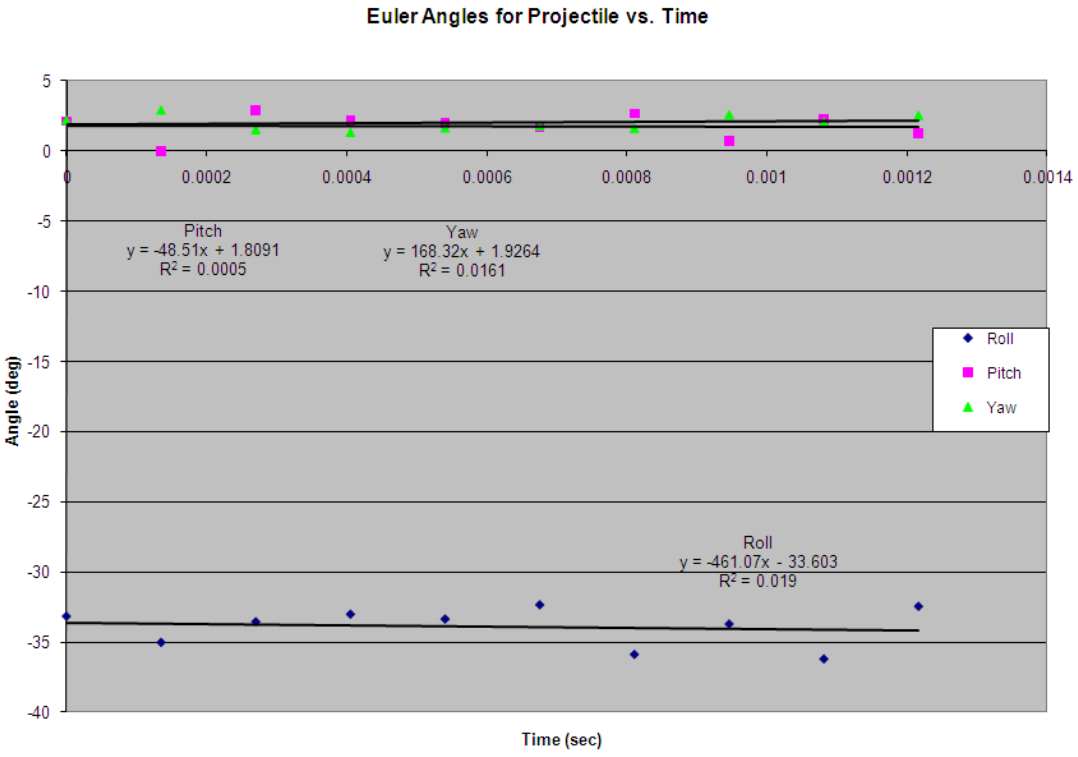

Fig. 29. Projectile position with time – LG655

- direction cosines
$$Nx = \frac{-461.07}{\sqrt{(-461.1)^2 + (-48.5)^2 + 168.3^2}} = -0.935$$
$$Ny = \frac{-48.5}{\sqrt{(-461.1)^2 + (-48.5)^2 + 168.3^2}} = -0.098$$
$$Nz = \frac{168.3}{\sqrt{(-461.1)^2 + (-48.5)^2 + 168.3^2}} = 0.341$$

- Magnitude $\omega = \sqrt{(-461.1)^2 + (-48.5)^2 + 168.3^2} = 493.2$ degrees/sec, transformed in radians/second we have $\omega = 493.2 \frac{\text{deg}}{\text{sec}} \cdot \frac{1\text{sec}}{1000ms} \cdot \frac{3.1415rad}{180\,\text{deg}} = 8.608e-3 \frac{rad}{ms}$ which is our input value for LS-Dyna analysis.

(4) Test case LG689

Values used in determining the angular velocity and the direction cosines for LG689 were extracted from Fig. 30.

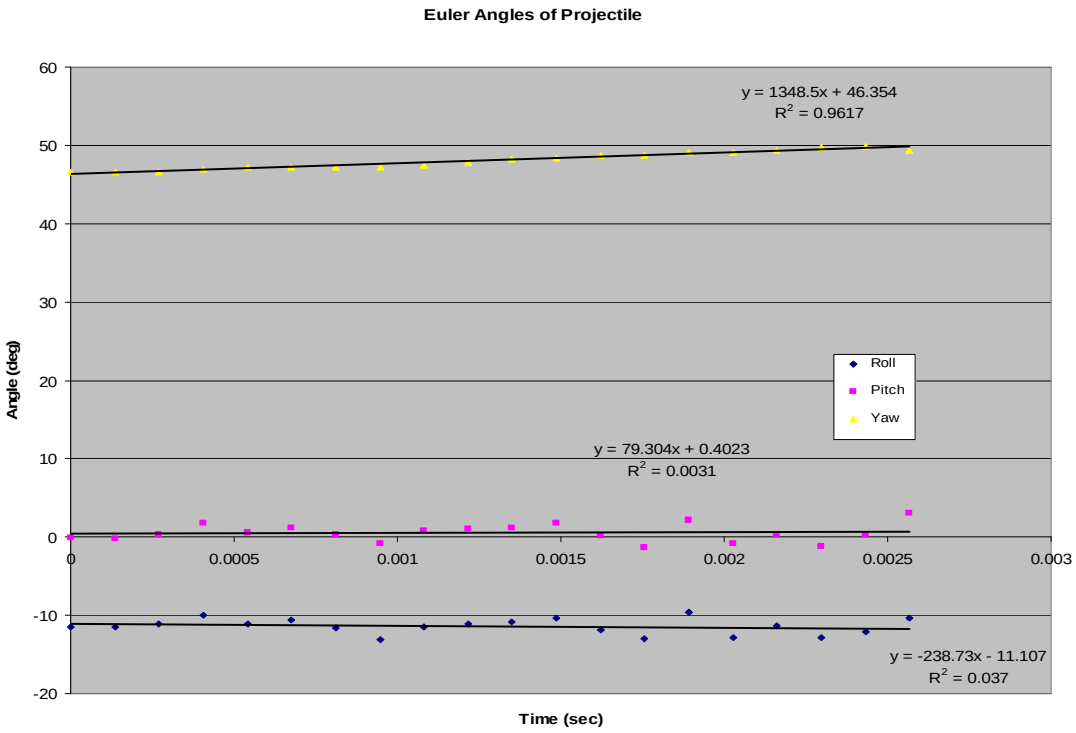

Fig. 30. Projectile position with time – LG689

- direction cosines
$$Nx = \frac{-238.7}{\sqrt{(-238.7)^2 + 79.3^2 + 1348.5^2}} = -0.174$$
$$Ny = \frac{79.3}{\sqrt{(-238.7)^2 + 79.3^2 + 1348.5^2}} = 0.058$$
$$Nz = \frac{1348.5}{\sqrt{(-238.7)^2 + 79.3^2 + 1348.5^2}} = 0.983$$

- Magnitude $\omega = \sqrt{(-238.7)^2 + 79.3^2 + 1348.5^2} = 1371.8$ degrees/sec, transformed in radians/second we have $\omega = 1371.7 \frac{\deg}{\sec} \cdot \frac{1\sec}{1000ms} \cdot \frac{3.1415rad}{180\deg} = 2.394e-2 \frac{rad}{ms}$ which is our input value for LS-DYNA analysis.

  The input data for all four cases are presented in the Table 4.

Table 4
Direction cosines and velocity magnitude for angular velocity.

Test	Direction Cosines			Magnitude (rad/ms)
	Nx	Ny	Nz	
LG594	0.743	0.439	0.505	7.413e-02
LG610	0.523	0.105	0.846	4.187e-02
LG655	-0.935	-0.098	0.341	8.608e-03
LG689	-0.178	0.058	0.983	2.349e-02

Simulations for the four cases subjected to angular velocities have been performed and the results are presented below in Table 5.

Table 5
Angular velocity cases and energy absorbed after adjustment

Test	Model Used	Initial transl. Velocity (ft/s)	Initial rot. velocity (deg/ms)	Initial Energy (J)	Final Velocity (ft/s)	Final Energy (J)	Absorbed Energy (%)
LG610	Original	888	0	11428	790	9045	**20.9%**
	Adjusted	888	4.25	11428	804	9368	**18.0%**
	Experiment	888	4.25	11428	810	9509	**16.8%**
LG655	Original	1132	0	19286	1016	15536	**19.4%**
	Adjusted	1132	2.4	19286	1018	15597	**19.1%**
	Experiment	1132	2.4	19286	831	10393	**46.1%**
LG594	Original	844	0	10158	366	1910	**81.2%**
	Adjusted	844	0.47	10158	295	1241	**87.8%**
	Experiment	844	0.47	10158	485	3354	**67.0%**
LG689	Original	897	0	12072	692	7185	**40.5%**
	Adjusted	896.67	1.35	12063	724	7865	**34.8%**
	Experiment	896.67	1.35	12063	655	6437	**46.6%**

Adjusted = with imposed angular velocity.

4. NUMERICAL RESULTS

4.1. Ballistic limit determination for single and multi layer models

A design engineer would use the FE models to predict the ballistic limit for a particular test scenario. The ballistic limit is defined as the maximum initial velocity of the projectile such that the projectile is completely contained in the fabric layers (exit velocity is zero).

Five FE models were created in order to model test case scenarios and determine the ballistic limit for four, eight, sixteen, twenty-four and thirty-two Kevlar fabric layers. To model the fabric layers, each four fabric layers were modeled into an equivalent FE layer. For the four fabric layer case, there was one FE layer, for the twelve fabric layer case there were three equivalents FE layers and so on. Table 6 shows the fabric layers and the equivalent FE layers for all the cases considered.

Table 6
Test layers and equivalent layers used in the FE model

Test Model	FE Model
12 fabric layers	3 FE layers
16 fabric layers	4 FE layers
24 fabric layers	6 FE layers
32 fabric layers	8 FE layers

There are two projectiles that have been used in the previously performed NASA ballistic tests. The ***Old*** projectile is a shorter, thicker less flexible projectile, while the ***New*** projectile is longer, shorter and more flexible projectile [3]. The Old projectile has a rectangular shaped, 10.2 cm (4 in) long, 5.1 cm (2 in) high and 0.8 cm (5/16 in) thick with a nominal mass of 320g while the New projectile has a length of 17.8 cm (7 in), a height of 3.8 cm (1.5 in), a thickness of

.54 cm (.2135 in) and the same nominal mass. The two projectiles are shown in Fig. 31(a) the Old projectile and Fig. 31(b) the New projectile. The two will be referred to as Old and New projectile for identification.

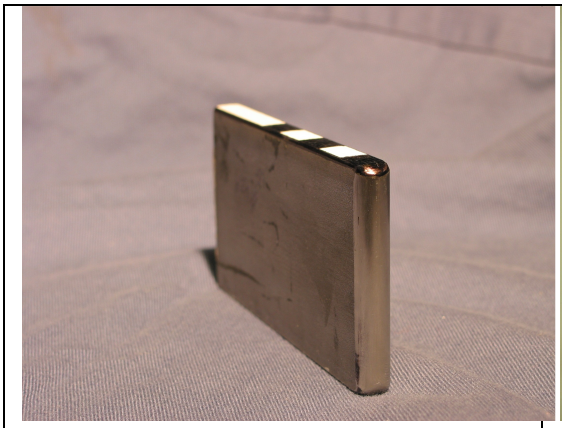

Fig. 31(a) – Old Projectile

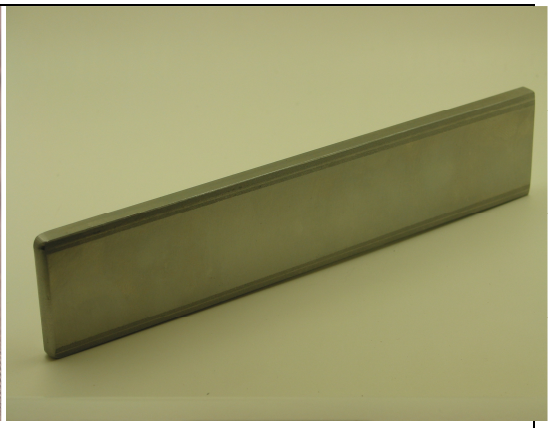

Fig. 31(b) – New Projectile

For all cases but one, the projectile orientation was chosen as a direct hit (zero rotation about the roll, pitch or yaw axes) as shown in Fig. 32.

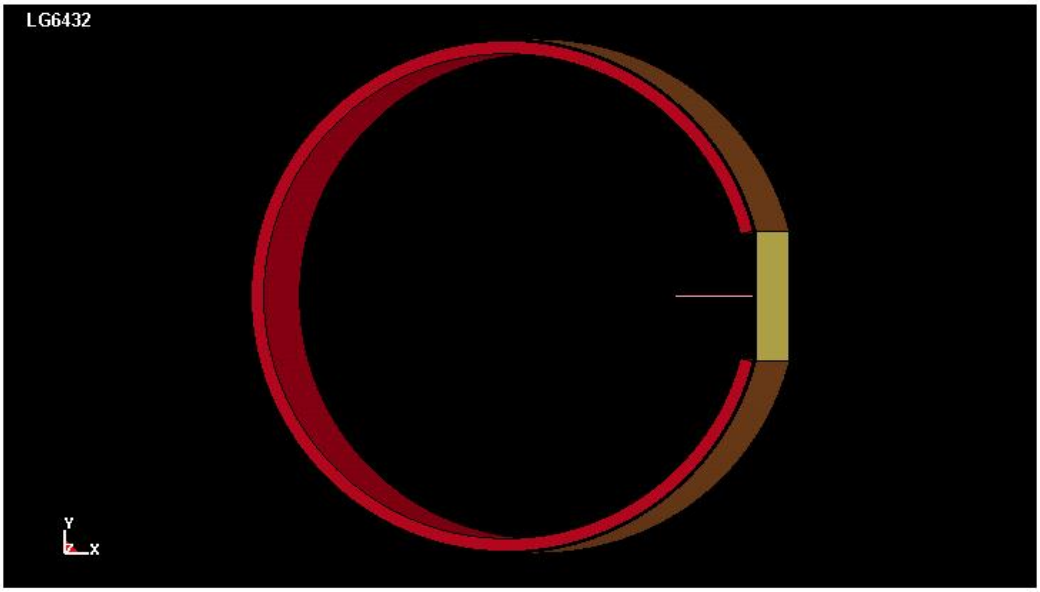

Fig. 32. Top view of the assembly with (zero rotation about the roll, pitch and yaw axis)

The ASU constitutive model v1.2 (ASUumatv1.2) for Kevlar was used to perform all the simulations.

(1) Old projectile, 24 layers model, elasto-plastic projectile material with direct hit (LG411)

In order to determine the ballistic limit for the twenty-four layer test model with the old projectile both a single layer and a multi layer model were created. Those models replicate the NASA ballistic test LG411 for which twenty-four fabric layers were used. For the multi layer model each four fabric layers were modeled into an equivalent FE layer as shown in Table 6 - for twenty-four fabric layer we have six FE layers. The projectile material model used was elasto-plastic and the estimated ballistic limit results based on the analysis are presented in Table 7.

Table 7
Estimated Ballistic Limit (LG411) - 24 fabric layers

Test case	24 Fabric Layers (fps)
Single Layer	925 - 950
Multi Layer	875 - 900

(2) Old projectile, 32 layers model, elasto-plastic projectile material, -22.16 deg Roll, 9.73 deg Pitch and 1.42 deg Yaw for projectile(LG657)

In order to determine the ballistic limit for the thirty-two layer test model with the new projectile a single layer and a multi layer model were created. Those models replicate the NASA ballistic test LG657 where thirty-two fabric layers were used. For the multi layer model each four fabric layers were modeled into an equivalent FE layer as previously described. As shown in Table 6 for thirty-two fabric layer we have eight FE layers. The projectile material model used was

elasto-plastic. The estimated ballistic limit results based on the analysis are presented in Table 8.

Table 8
Estimated Ballistic Limit (LG657) – 32 fabric layers

Test case	32 Layers (fps)
Single Layer	1042 – 1083
Multi Layer	875 – 917

(3) New projectile, four layers model, elasto-plastic projectile material, direct hit.

In order to determine the ballistic limit for the four layer test model with the new projectile both a single layer and a multi layer model were created. Those models do not replicate any of the NASA ballistic test. For this case there was no multi layer model, all four layers were modeled into a single equivalent FE layer as shown in Table 6 - for four fabric layer we have one equivalent FE layer. The projectile material model used was elasto-plastic and the estimated ballistic limit results based on the analysis are presented in Table 9.

Table 9
Estimated ballistic limit - 4 fabric layers

Test case	4 Fabric Layers (fps)
Single Layer	425 - 520
Multi Layer	-

(4) Old projectile, twelve layers model, elasto-plastic projectile material with, hit.

In order to determine the ballistic limit for the twelve layer test model with the new projectile both a single layer and a multi layer model were created. Those models do not replicate any of the NASA ballistic tests. For the multi layer model each four fabric layers were modeled into an equivalent FE layer as shown in

Table 6 - for twelve fabric layer we have three equivalent FE layers. The projectile material model used was elasto-plastic and the estimated ballistic limit results based on the analysis are presented in Table 10.

Table 10
Estimated ballistic limit - 12 fabric layers

Test case	12 Fabric Layers (fps)
Single Layer	725 – 775
Multi Layer	660 – 710

(5) New projectile, sixteen layers model, elasto-plastic projectile material, direct hit.

In order to determine the ballistic limit for the sixteen layer test model with the new projectile both a single layer and a multi layer model were created. Those models do not replicate any of the NASA ballistic tests. For the multi layer model each four fabric layers were modeled into an equivalent FE layer as shown in Table 6 - for sixteen fabric layer we have four equivalent FE layers. The projectile material model used was elasto-plastic and the estimated ballistic limit results based on the analysis are presented in Table 11.

Table 11
Estimated ballistic limit - 16 fabric layers

Test case	16 Fabric Layers (fps)
Single Layer	840 – 870
Multi Layer	775 – 800

(6) New projectile, twenty-four layers model, elasto-plastic projectile material, direct hit.

In order to determine the ballistic limit for the twenty-four layer test model with the new projectile both a single layer and a multi layer model were created. Those models do not replicate any of the NASA ballistic tests. For the multi layer model each four fabric layers were modeled into an equivalent FE layer as shown

in Table 6 - for twenty-four fabric layer we have six equivalent FE layers. The projectile material model used was elasto-plastic and the estimated ballistic limit results based on the analysis are presented in Table 12.

Table 12
Estimated ballistic limit - 24 fabric layers

Test case	24 Fabric Layers (fps)
Single Layer	950 – 975
Multi Layer	825 – 860

A summary of the ballistic limit determination is presented in Table 13 and Table 14. Final results for the ballistic limit of the three cases analyzed as well as the NASA ballistic test are summarized in Table 14.

Table 13
Estimated ballistic limit – New projectile with direct hit

Test case	4 Layers (fps)	12 Layers (fps)	16 Layers (fps)	24 Layers (fps)
Single Layer	475 - 525	725 - 775	840 – 870	950 – 975
Multi Layer	-	660 - 710	775 – 800	825 – 860

Table 14
Estimated Ballistic Limits – All cases

Test case	Projectile	Projectile Angels			4 Layers	12 Layers	16 Layers	24 Layers	32 Layers
		Pitch	Roll	Yaw					
		(deg)	(deg)	(deg)	(fps)	(fps)	(fps)	(fps)	(fps)
Single Layer	New	0	0	0	475 - 525	725 – 775	840 – 870	950 – 975	
Multi Layer	New	0	0	0	-	660 - 710	775 – 800	825 – 860	
Single Layer (LG411)	Old	0	0	0				925 - 950	
Multi Layer (LG411)	Old	0	0	0				875 - 900	
Single Layer	Old	0	0	0					1042 - 1083
Multi Layer	Old	0	0	0					875 - 917
Single Layer (LG657*)	Old	9.73	-22.16	1.42					Contained
Multi Layer (LG657*)	Old	9.73	-22.16	1.42					Contained
LG657* (NASA Test)	Old	9.73	-22.16	1.42					Contained

*LG 657 Initial Velocity is 830 fps.

4.2. Ballistic test reanalysis for single and multi layer models

4.2.1. QA Checks

The numerical stability during the simulation is ensured by conducting following checks. Summary of these tests is shown in Table 15.

1) Ratio of global kinetic energy/global total energy and global internal energy/ global total energy should be less than unity. A ratio of greater than unity indicates the numerical errors.

2) Ratio of global hourglass energy/global total energy and global sliding energy/ global total energy should be less than 0.1.

3) Variation in energy ratio should be less than 0.1.

4) Hourglass energy/total energy for the fabric directly in contact with the projectile should be less than 0.1. To track hourglass energy of fabric directly in contact with projectile, each layer of fabric is modeled using two parts. One part representing fabric on the ring cutout and other part representing fabric over the solid ring.

Table 15
Energy ratios and values used for QA check of FE simulations

Column Number	Variable Name		Variable Definition	Acceptable limit
1	Test Case		Test Case number	-
2	Fabric Layers		Number of fabric layers in the test case	-
3	Min energy ratio		Minimum ratio of (current total energy)/(initial total energy + external work)	> 0.90
4	Max energy ratio		Maximum ratio of (current total energy)/(initial total energy + external work)	< 1.1
5	Min sliding energy ratio		Minimum ratio of (sliding energy)/(total energy)	> -0.1
6	Max sliding energy ratio		Maximum ratio of (sliding energy)/(total energy)	< 0.1
7	Max kinetic energy ratio		Maximum ratio of (kinetic energy)/(total energy)	< 1.0
8	Max internal energy ratio		Maximum ratio of (internal energy)/(total energy)	< 1.0
9	Hourglass energy ratio	Global	Maximum ratio of (global hourglass energy)/(global total energy)	< 0.1
10		Fabric	Maximum ratio of (hourglass energy)/(total energy) for fabric directly in contact with projectile for single layer model.	< 0.1

As presented in Section 3.2 of this document, for a closer modeling of the NASA ballistic tests and to improve the current ASU models a few changes were necessary. They are again presented below and are as follows:

(a) Strain at failure increased form the current level of 0.1 to 0.16 based on the new stress strain data presented in section 3.2.2.

(b) Increase in the stress value for the beginning of the post-peak non-linear region from 5000 psi to 10000 psi based on the data presented in section 3.2.2.

(c) New elasto-plastic material model for projectile.

(d) Viscous Damping Coefficients in the contact cards for all parts was changed from 0 to 50, as recommended by the LS-DYNA manual. This change resulted in no noticeable improvements to the results.

4.2.2. Single layer model

Shell elements were used to represent the fabric and solid elements were used to represent the steel ring and steel projectiles. The fabric was modeled with a uniform mesh containing 0.25” shell elements. The steel ring was modeled with 0.25” x 0.25” x 1.0” hexagonal elements (1.0” through the ring thickness) since the ring is consider not to have an impact on the FE analysis results. One layer of shell elements was used to represent the fabric irrespective of the actual number of fabric layers. Thus for an 8-layer test case, the shell element thickness was taken as the thickness of one fabric layer multiplied by 8, or 0.011” x 8 = 0.088”. Using this approach we fail to incorporate one important factor, that is the friction between the fabric layers. In the model the center of the shell elements was placed at a distance of one half the shells element thickness away from the ring facilitating contact between the shell elements and the ring at the start of the analysis.

The fabric model was meshed using two different parts. The fabric directly in contact with projectile is given separate part id than rest of the fabric. This type of configuration facilitates tracing of energy balance for this area separately. Fig. 33 shows the typical ring and fabric model used for these simulations.

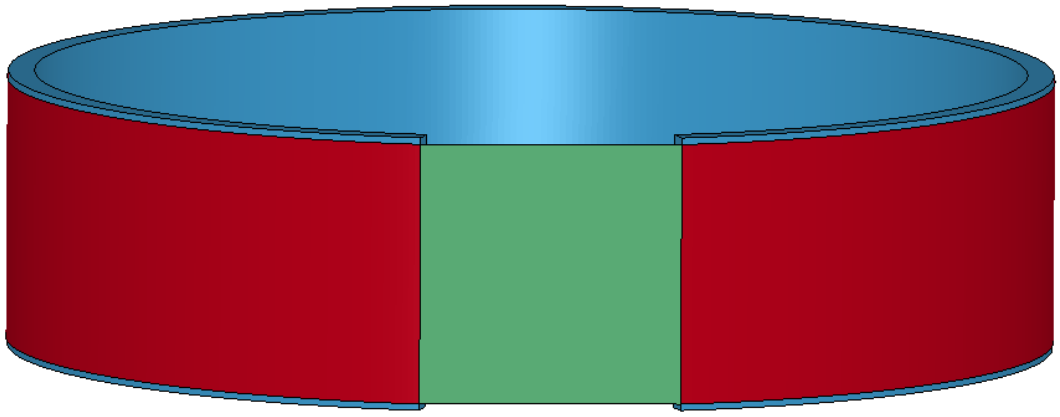

Fig. 33. Single FE layer ballistic test model

Table 16 shows a comparison between the absorbed energy during experiment and its corresponding LS-DYNA simulation. The % difference values shown in the table were computed based on following formula.

% Diff. = (Exp. Absorbed Energy %) – (Sim. Absorbed Energy %) (25)

Hence a positive % difference corresponds to the FE simulation under predicting the absorbed energy and a negative % difference corresponds to the FE simulation over predicting the absorbed energy.

Table 16

Single layer, experiment and FE model energy absorbtion

				NASA TEST					
File Run	Mesh	Material Model	Fabric Layers	Before Impact		After Impact		Absorbed Energy	
				Velocity	Energy	Velocity	Energy		
				(ft/sec)	(J)	(ft/sec)	(J)	(J)	%
LG403	ASU	ASU 1.2	4	898.95	11952	846.46	10597	1355	11.3%
LG404	ASU	ASU 1.2	8	895.7	11843	820.2	9931	1911	16.1%
LG409	ASU	ASU 1.2	8	889.1	11604	807.1	9562	2042	17.6%
LG410	ASU	ASU 1.2	4	912.1	12226	866.1	11026	1200	9.8%
LG411	ASU	ASU 1.2	24	885.8	11474	413.4	2499	8976	78.2%
LG424	ASU	ASU 1.2	8	833.3	10352	744.8	8268	2084	20.1%
LG427	ASU	ASU 1.2	24	915.4	12373	607.0	5440	6933	56.0%
LG429	ASU	ASU 1.2	16	915.4	12307	718.5	7583	4724	38.4%
LG432	ASU	ASU 1.2	16	895.7	11925	649.6	6273	5652	47.4%
LG609	ASU	ASU 1.2	8	913.7	12110	825.4	9883	2228	18.4%
LG610	ASU	ASU 1.2	8	888.1	11440	809.7	9510	1931	16.9%
LG611	ASU	ASU 1.2	8	905.7	12348	798.1	9588	2760	22.4%
LG612	ASU	ASU 1.2	8	898.3	12146	822.7	10190	1957	16.1%
LG618	ASU	ASU 1.2	8	866.4	10889	558.9	4531	6358	58.4%
LG656	ASU	ASU 1.2	32	967.3	14086	469.2	3315	10771	76.5%
LG657	ASU	ASU 1.2	32	829.7	10363	0.0	0	10363	100.0%
LG692	ASU	ASU 1.2	8	885.3	11799	602.6	5466	6333	53.7%
LG594	ASU	ASU 1.2	8	843.9	10147	484.5	3345	6802	67.0%
LG689	ASU	ASU 1.2	8	896.3	12061	655.1	6443	5618	46.6%
LG620	ASU	ASU 1.2	8	893.8	11735	580.8	4954	6780	57.8%

Table 16 (cont)

		MODEL						% Difference
File Run	FE Layers	Before Impact		After Impact		Absorbed Energy		ASUSL v1.2
		Velocity	Energy	Velocity	Energy			
		(ft/sec)	(J)	(ft/sec)	(J)	(J)	%	
LG403	1	899.17	11958	862.00	10990	**968**	**8.1%**	**3.2%**
LG404	1	895.83	11847	805.00	9566	**2281**	**19.3%**	**-3.1%**
LG409	1	889.17	11605	815.00	9750	**1855**	**16.0%**	**1.6%**
LG410	1	911.67	12216	877.00	11304	**911**	**7.5%**	**2.4%**
LG411	1	885.83	11475	0.00	0	**11475**	**100.0%**	**-21.8%**
LG424	1	833.33	10352	732.00	7987	**2364**	**22.8%**	**-2.7%**
LG427	1	915.00	12363	0.00	0	**12363**	**100.0%**	**-44.0%**
LG429	1	915.02	12298	613.00	5519	**6778**	**55.1%**	**-16.7%**
LG432	1	895.83	11929	601.00	5369	**6560**	**55.0%**	**-7.6%**
LG609	1	914.25	12124	867.00	10904	**1221**	**10.1%**	**8.3%**
LG610	1	888.33	11447	805.00	9400	**2047**	**17.9%**	**-1.0%**
LG611	1	905.83	12352	813.00	9950	**2402**	**19.4%**	**2.9%**
LG612	1	898.31	12148	814.00	9975	**2173**	**17.9%**	**-1.8%**
LG618	1	866.72	10896	437.00	2770	**8126**	**74.6%**	**-16.2%**
LG656	1	967.50	14091	730.00	8022	**6069**	**43.1%**	**33.4%**
LG657	1	829.64	10362	0.00	0	**10362**	**100.0%**	**0.0%**
LG692	1	885.00	11791	668.00	6717	**5073**	**43.0%**	**10.6%**
LG594	1	844.22	10156	227.00	734	**9422**	**92.8%**	**-25.7%**
LG689	1	896.67	12072	691.00	7169	**4903**	**40.6%**	**6.0%**
LG620	1	894.25	11746	667.00	6535	**5211**	**44.4%**	**13.4%**

Table 17 shows statistics of the results when comparing absorbed energy –the average difference between the simulations and the experimental tests, the maximum difference or largest under prediction between the simulations and the experimental tests, the minimum difference or largest over prediction between the simulations and the experimental tests, and the standard deviation of the difference between the simulations and the experimental tests for single model with Version 1.2.

Table 17
Comparison between FE Simulation and Experimental Tests (Single layer results for ASUumatv1.2)

	ASUumatv1.2		
	Phase I	Phase II	Overall
Number of Tests	9	11	20
AVG:	-9.9%	2.7%	-2.9%
MAX:	3.2%	33.4%	33.4%
MIN:	-44.0%	-25.7%	-44.0%
STDEV:	15.4%	15.4%	16.3%

Table 18
Comparison between FE Simulation and Experimental Tests (Single layer results for ASUumatv1.1 and ASUumatv1.2)

	ASUumatv1.0			**ASUumatv1.1**			**ASUumatv1.2**		
	Phase I	**PhaseII**	**Overall**	**Phase I**	**Phase II**	**Overall**	**Phase I**	**Phase II**	**Overall**
AVG:	-13.1%	7.0%	-3.8%	-14.0%	5.3%	-5.1%	-9.9%	2.7%	-2.9%
MAX:	9.2%	29.5%	29.5%	9.6%	26.8%	26.8%	3.2%	33.4%	33.4%
MIN:	-49.8%	-19.1%	-49.8%	-53.2%	-11.6%	-53.2%	-44.0%	-25.7%	-44.0%
STDEV:	19.1%	15.4%	19.9%	21.5%	11.7%	19.8%	15.4%	15.4%	16.3%

For simulations of the Phase I, ASUumatv1.2 provides an improved average and standard deviation compared to both ASUumatv1.0 and ASUumatv1.1 as shown in Table 18 above. The overall average for Phase I is negative for all three versions indicating a conservative prediction. For Phase II simulations, all three versions under predict the experimental data. From the data obtained using ASUumatv1.2 the average is improved while the standard deviation is within the same range of values as obtained by the earlier versions. For the overall comparison of the three phases, ASUumatv1.2 provides a better performance than the two earlier versions. The only underperformance in the overall statistical results can be observed at the overall maximum where the under prediction of the ASUumatv1.2 has a slightly higher value compared to the earlier versions. However

the difference is only 6.4% compared to the ASUumatv1.1 which has “the best” overall under prediction and 3.9% compared to ASUumatv1.0. The minimum representing the highest over prediction has improved compared to the two earlier versions, “the best” overall over prediction given by ASUumatv1.2 has improved by 5.8% compared to ASUumatv1.0 and by 9.2% compared to ASUumatv1.1.

Table 19 below shows the QA checks for the stability of the single layer FE models. As mentioned in section 4.2.1 the energy ratios are checked. From the table it can be observed that all models perform well and all values are within the required ranges. Compared to ASUumatv1.1 the two bad performing cases LG405 and LG657 were eliminated so there are no bad performing cases.

Table 19
QA check for single layer FE models

Test Case	Fabric Layers	Min energy ratio	Max energy ratio	Min sliding energy ratio	Max sliding energy ratio
(1)	(2)	(3)	(4)	(5)	(6)
LG403.in	1	1.0000	1.0000	0.0000	0.0011
LG404.in	1	1.0000	1.0000	0.0000	0.0059
LG409.in	1	1.0000	1.0000	0.0000	0.0034
LG410.in	1	1.0000	1.0000	0.0000	0.0014
LG411.in	1	1.0000	1.0000	0.0000	0.0599
LG424.in	1	1.0000	1.0000	0.0000	0.0043
LG427.in	1	1.0000	1.0000	0.0000	0.0659
LG429.in	1	1.0000	1.0000	0.0000	0.0111
LG432.in	1	0.9990	1.0000	0.0000	0.0106
LG594.in	1	1.0000	1.0600	0.0000	0.0803
LG609.in	1	1.0000	1.0000	0.0000	0.0006
LG610.in	1	0.9990	1.0000	0.0000	0.0028
LG611.in	1	1.0000	1.0000	0.0000	0.0028
LG612.in	1	1.0000	1.0000	0.0000	0.0039
LG618.in	1	1.0000	1.0000	0.0000	0.0447
LG620.in	1	1.0000	1.0000	-0.0005	0.0148
LG656.in	1	0.9980	1.0000	0.0000	0.0200
LG657.in	1	1.0000	1.0000	0.0000	0.0558
LG689.in	1	1.0000	1.0000	0.0000	0.0129
LG692.in	1	0.9990	1.0000	0.0000	0.0077

Table 19(cont.)

Test Case	Max kinetic energy ratio	Max internal energy ratio	Hourglass energy ratio Global	Hourglass energy ratio Fabric
(1)	(7)	(8)	(9)	(10)
LG403.in	1.0000	0.0165	0.0013	0.0184
LG404.in	1.0000	0.0476	0.0046	0.0209
LG409.in	1.0000	0.0398	0.0034	0.0199
LG410.in	1.0000	0.0114	0.0006	0.0126
LG411.in	1.0000	0.3420	0.1060	0.2580
LG424.in	1.0000	0.0595	0.0045	0.0176
LG427.in	1.0000	0.3160	0.1080	0.2250
LG429.in	1.0000	0.1340	0.0152	0.0314
LG432.in	1.0000	0.1430	0.0180	0.0273
LG594.in	1.0000	0.2440	0.0689	0.1570
LG609.in	1.0000	0.0129	0.0010	0.0154
LG610.in	1.0000	0.0419	0.0038	0.0181
LG611.in	1.0000	0.0446	0.0044	0.0197
LG612.in	1.0000	0.0404	0.0028	0.0202
LG618.in	1.0000	0.1930	0.0590	0.0629
LG620.in	1.0000	0.1100	0.0326	0.0362
LG656.in	1.0000	0.1420	0.0411	0.1190
LG657.in	1.0000	0.3470	0.1120	0.3130
LG689.in	1.0000	0.0772	0.0238	0.0420
LG692.in	1.0000	0.0793	0.0215	0.0488

4.2.3. Multi layer model

Shell elements were used to represent the fabric and solid elements were used to represent the steel ring and steel projectiles. The fabric was modeled with a uniform mesh containing 0.25” shell elements. The steel ring was modeled with 0.25” x 0.25” x 1.0” hexagonal elements (1.0” through the ring thickness) since the ring is not of interest with respect to the FE analysis results. One layer of shell elements was used to represent the four fabric layers. Thus for an 8-fabric layer test case, there are two finite element layers with shell element thickness of one fabric layer multiplied by 4, or 0.011” x 4 = 0.044”. With this methodology, the friction between the fabric layers can also be captured.

In the model, the center of the shell elements was placed at a distance of one half the shell element thickness away from the ring and one shell element away from adjacent shell layer to facilitating contact between them at the start of the analysis. Fig. 34 shows the FE mesh of the ring and the fabric for 16 fabric layer (4 FE layer) model.

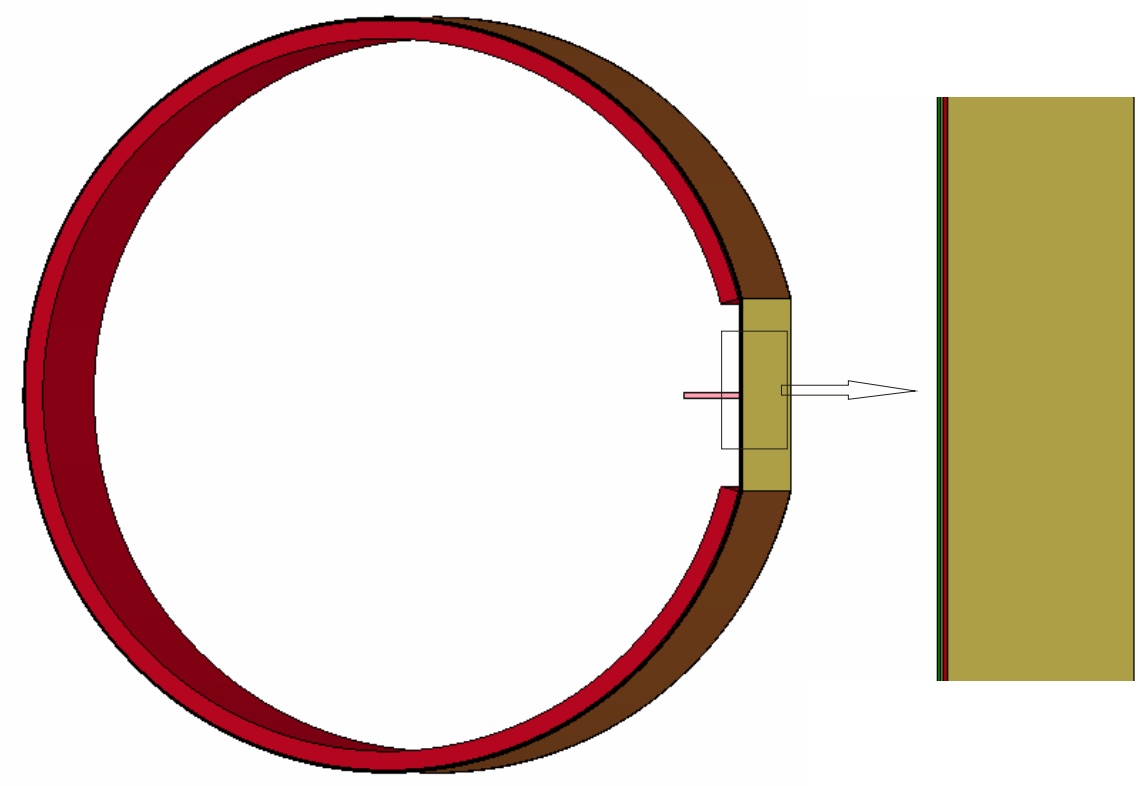

Fig. 34. Multi FE layer ballistic test model

Table 20 shows a comparison between the absorbed energy of the fabric for each experimental test case and its corresponding LS-DYNA simulation result. The % difference values shown in the table were computed based on following formula.

% Diff. = (Exp. Absorbed Energy %) – (FE Model Absorbed Energy %) (26)

Hence a positive % difference corresponds to the FE simulation under predicting the absorbed energy and a negative % difference corresponds to the FE simulation over predicting the absorbed energy.

Table 20
Multi-layer Results

				NASA TEST					
File Run	Mesh	Material Model	Fabric Layers	Before Impact		After Impact		Absorbed Energy	
				Velocity	Energy	Velocity	Energy		
				(ft/sec)	(J)	(ft/sec)	(J)	(J)	%
LG404	ASU	ASU 1.2	8	895.7	11843	820.2	9931	1911	16.1%
LG409	ASU	ASU 1.2	8	889.1	11604	807.1	9562	1506	17.6%
LG411	ASU	ASU 1.2	24	885.8	11474	413.4	2499	8976	78.2%
LG424	ASU	ASU 1.2	8	833.3	10352	744.8	8268	1537	20.1%
LG427	ASU	ASU 1.2	24	915.4	12373	607.0	5440	5113	56.0%
LG429	ASU	ASU 1.2	16	915.4	12307	718.5	7583	3484	38.4%
LG432	ASU	ASU 1.2	16	895.7	11925	649.6	6273	5652	47.4%
LG609	ASU	ASU 1.2	8	913.7	12110	825.4	9883	2228	18.4%
LG610	ASU	ASU 1.2	8	888.1	11440	809.7	9510	1931	16.9%
LG611	ASU	ASU 1.2	8	905.7	12348	798.1	9588	2760	22.4%
LG612	ASU	ASU 1.2	8	898.3	12146	822.7	10190	1957	16.1%
LG618	ASU	ASU 1.2	8	866.4	10889	558.9	4531	6358	58.4%
LG656	ASU	ASU 1.2	32	967.3	14086	469.2	3315	10771	76.5%
LG657	ASU	ASU 1.2	32	829.7	10363	0.0	0	10363	100.0%
LG692	ASU	ASU 1.2	8	885.3	11799	602.6	5466	6333	53.7%
LG594	ASU	ASU 1.2	8	843.9	10147	484.5	3345	6802	67.0%
LG689	ASU	ASU 1.2	8	896.3	12061	655.1	6443	5618	46.6%
LG620	ASU	ASU 1.2	8	893.8	11735	580.8	4954	6780	57.8%

Table 20 (cont.)

		MODEL						Absolute %
File Run	FE Layers	Before Impact		After Impact		Absorbed Energy		ASU ML v 1.2 (a)+(b)+(c)
		Velocity	Energy	Velocity	Energy			
		(ft/sec)	(J)	(ft/sec)	(J)	(J)	%	
LG404	2	895.83	11847	808.71	9655	**2192**	**18.5%**	**-2.4%**
LG409	2	889.17	11605	808.10	9586	**2020**	**17.4%**	**0.2%**
LG411	6	885.83	11475	427.46	2672	**8803**	**76.7%**	**1.5%**
LG424	2	833.33	10352	713.64	7592	**2760**	**26.7%**	**-6.5%**
LG427	2	915.00	12363	686.44	6958	**5405**	**43.7%**	**12.3%**
LG429	4	915.00	12297	746.13	8177	**4120**	**33.5%**	**4.9%**
LG432	4	895.83	11929	715.73	7615	**4314**	**36.2%**	**11.2%**
LG609	2	914.25	12124	870.50	10992	**1133**	**9.3%**	**9.1%**
LG610	2	888.42	11449	790.26	9059	**2390**	**20.9%**	**-4.0%**
LG611	2	905.83	12352	849.58	10866	**1486**	**12.0%**	**10.3%**
LG612	2	898.31	12148	808.33	9836	**2312**	**19.0%**	**-2.9%**
LG618	2	866.75	10897	0.00	0	**10897**	**100.0%**	**-41.6%**
LG656	8	967.50	14091	466.57	3277	**10814**	**76.7%**	**-0.3%**
LG657	8	829.67	10362	0.00	0	**10362**	**100.0%**	**0.0%**
LG692	2	885.00	11791	762.35	8749	**3042**	**25.8%**	**27.9%**
LG594	2	844.25	10157	307.70	1349	**8808**	**86.7%**	**-19.7%**
LG689	2	896.67	12072	635.27	6060	**6013**	**49.8%**	**-3.2%**
LG620	2	894.25	11746	598.18	5256	**6490**	**55.3%**	**2.5%**

Table 21 shows statistics of the results when comparing absorbed energy – the average difference between the simulations and the experimental tests, the maximum difference or largest under prediction between the simulations and the experimental tests, the minimum difference or largest over prediction between the simulations and the experimental tests, and the standard deviation of the difference between the simulations and the experimental tests for multilayer model with Version 1.2.

Table 21
Comparison between FE Simulation and Experimental Tests (Multi layer results for ASUumatv1.2)

	ASUumatv1.2		
	Phase I	Phase II	Overall
Number of Tests	7	11	18
AVG:	3.0%	-2.0%	0.0%
MAX:	12.3%	27.9%	27.9%
MIN:	-6.5%	-41.6%	-41.6%
STDEV:	6.9%	17.6%	14.3%

Table 22
Comparison between FE Simulation and Experimental Tests (Multi layer results for ASUumatv1.1 and ASUumatv1.2)

	ASUumatv1.1			**ASUumatv1.2**		
	Phase I	**Phase II**	**Overall**	**Phase I**	**Phase II**	**Overall**
AVG:	5.2%	4.7%	4.7%	3.0%	-2.0%	0.0%
MAX:	16.1%	29.3%	29.3%	12.3%	27.9%	27.9%
MIN:	-3.1%	-41.6%	-41.6%	-6.5%	-41.6%	-41.6%
STDEV:	7.4%	18.2%	14.9%	6.9%	17.6%	14.3%

Table 22 shows the comparison between ASUumatv1.1 and ASUumatv1.2. The average and the standard deviation both show improved values with the new version. The overall maximum and minimum from ASUumatv1.1 and ASUumatv1.2 do not change as they are generated by the same test cases – LG 618 for the minimum and LG 692 for the maximum. A comparison of the two material models for both phases shows that for Phase I ASUumatv1.2 provides an improved overall average over ASUumatv1.1 of 2.2% as well as a small improvement of 0.5% in standard deviation. For the second phase, the maximum is improved by 3.8% while the minimum is more conservative than in the earlier version by 3.4%.

Analyzing the entire test suite, there are 12 models that have 8 fabric layers and 6 models that have more than 8 layers (2 models with 16 layers, 2 model with 24 layers and 2 models with 32 layers). Table 23 presents the statistics based on the number of layers. While the initial velocity of all cases is between 830 and 967 fps, it can be observed that overall the test cases with the higher number of layers have a better predictive performance than the 8 layer cases. The extreme cases (where the overall maximum and minimum occurs) are part of the 8 layer models.

Table 23
Multi layer results comparing 8 fabric layers to more than 8 fabric layers

	ASUumatv1.2	
	8 Layers	More than 8 Layers
Number of Tests	12	6
AVG:	-2.5%	4.9%
MAX:	27.9%	12.3%
MIN:	-41.6%	-0.3%
STDEV:	18.6%	5.6%

Table 24 below shows the QA checks for the stability of the single layer FE models. From the table it can be observed that all models perform well and all values are within the acceptable range. In ASUumatv1.2 compared to ASUumatv1.1, the two bad performing (outliers) cases LG405 and LG657 were eliminated.

Table 24
QA Check (single layer FE models)

Test case	Fabric layers	FE fabric layers	Min energy ratio	Max energy ratio	Min sliding energy ratio	Max sliding energy ratio	Max kinetic energy ratio	Max internal energy ratio
1	2	3	4	5	6	7	8	9
LG404	8	2	1.0000	1.0000	0.0000	0.0052	1.0000	0.0454
LG409	8	2	1.0000	1.0000	0.0000	0.0047	1.0000	0.0449
LG411	24	6	0.9990	1.0000	-0.0263	0.0174	1.0000	0.2570
LG424	8	2	1.0000	1.0000	0.0000	0.0079	1.0000	0.0674
LG427	24	6	0.9990	1.0000	0.0000	0.0151	1.0000	0.1330
LG429	16	4	1.0000	1.0000	0.0000	0.0123	1.0000	0.0849
LG432	16	4	0.9990	1.0000	0.0000	0.0118	1.0000	0.0961
LG594	8	2	0.9990	1.0300	-0.0009	0.0606	1.0000	0.2310
LG609	8	2	1.0000	1.0000	-0.0004	0.0006	1.0000	0.0188
LG610	8	2	1.0000	1.0000	0.0000	0.0023	1.0000	0.0374
LG611	8	2	1.0000	1.0000	0.0000	0.0032	1.0000	0.0308
LG612	8	2	1.0000	1.0000	0.0000	0.0058	1.0000	0.0467
LG618	8	2	1.0000	1.0100	-0.0118	0.0606	1.0000	0.5170
LG620	8	2	1.0000	1.0000	-0.0003	0.0316	1.0000	0.1330
LG655	32	8	0.9990	1.0100	-0.0606	0.0302	1.0000	0.2410
LG656	32	8	0.9990	1.0000	-0.2910	0.0250	1.0000	0.5250
LG689	8	2	0.9980	1.0000	0.0000	0.0222	1.0000	0.0971
LG692	8	2	1.0000	1.0000	-0.0001	0.0065	1.0000	0.0600

Table 24 (cont.)

Test case	Hourglass energy ratio								
	Global	1st FE layer	2nd FE layer	3rd FE layer	4th FE layer	5th FE layer	6th FE layer	7th FE layer	8th FE layer
1	10	11	12	13	14	15	16	17	18
LG404	0.0036	0.0213	0.0156	0.0000	0.0000	0.0000	0.0000	0.0000	0.0000
LG409	0.0035	0.0169	0.0188	0.0000	0.0000	0.0000	0.0000	0.0000	0.0000
LG411	0.0385	0.0453	0.0662	0.0748	0.0703	0.0503	0.0555	0.0000	0.0000
LG424	0.0059	0.0311	0.0205	0.0000	0.0000	0.0000	0.0000	0.0000	0.0000
LG427	0.0145	0.0420	0.0393	0.0349	0.0274	0.0286	0.0266	0.0000	0.0000
LG429	0.0069	0.0207	0.0190	0.0215	0.0149	0.0000	0.0000	0.0000	0.0000
LG432	0.0088	0.0300	0.0183	0.0178	0.0171	0.0000	0.0000	0.0000	0.0000
LG594	0.0399	0.1530	0.1010	0.0000	0.0000	0.0000	0.0000	0.0000	0.0000
LG609	0.0015	0.0281	0.0229	0.0000	0.0000	0.0000	0.0000	0.0000	0.0000
LG610	0.0024	0.0150	0.0124	0.0000	0.0000	0.0000	0.0000	0.0000	0.0000
LG611	0.0018	0.0175	0.0266	0.0000	0.0000	0.0000	0.0000	0.0000	0.0000
LG612	0.0039	0.0234	0.0172	0.0000	0.0000	0.0000	0.0000	0.0000	0.0000
LG618	0.0729	0.3020	0.1970	0.0000	0.0000	0.0000	0.0000	0.0000	0.0000
LG620	0.0279	0.0388	0.0320	0.0000	0.0000	0.0000	0.0000	0.0000	0.0000
LG655	0.0316	0.2240	0.1590	0.0659	0.0565	0.0749	0.0764	0.0880	0.0844
LG656	0.0624	0.0637	0.0507	0.1210	0.0917	0.1170	0.1220	0.1420	0.1490
LG689	0.0221	0.0401	0.0487	0.0000	0.0000	0.0000	0.0000	0.0000	0.0000
LG692	0.0093	0.0389	0.0174	0.0000	0.0000	0.0000	0.0000	0.0000	0.0000

4.3. Displacement comparison between ASU model and ballistic tests

In addition to using absorbed energy as a metric, in this section the fabric displacement is used as an additional metric. The fabric displacement data are available only for ten test cases from the NASA suite. To compare the maximum displacements, the three most displaced fabric elements in any model were selected and the maximum displacement in the direction of the projectile movement was plotted. For the cases used in FE analysis, the displacements are shown in Figures 35 to 44.

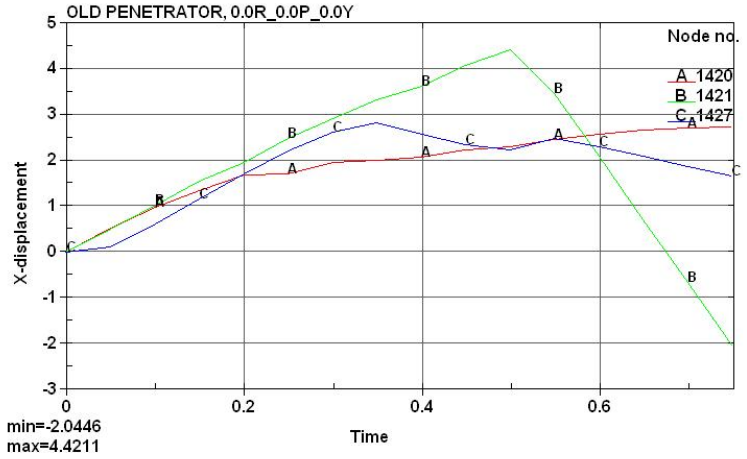

Fig. 35. Displacement plot for LG403

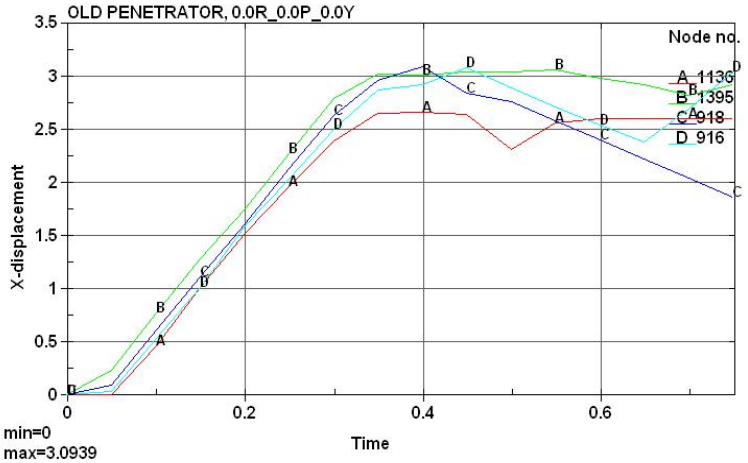

Fig. 36. Displacement plot for LG404

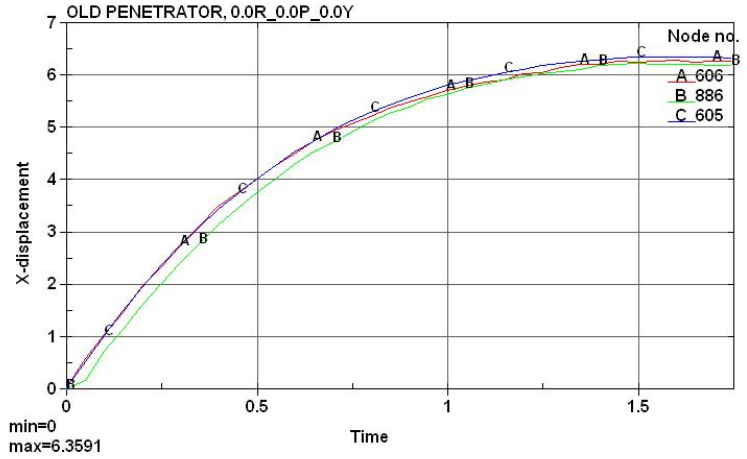

Fig. 37. Displacement plot for LG405

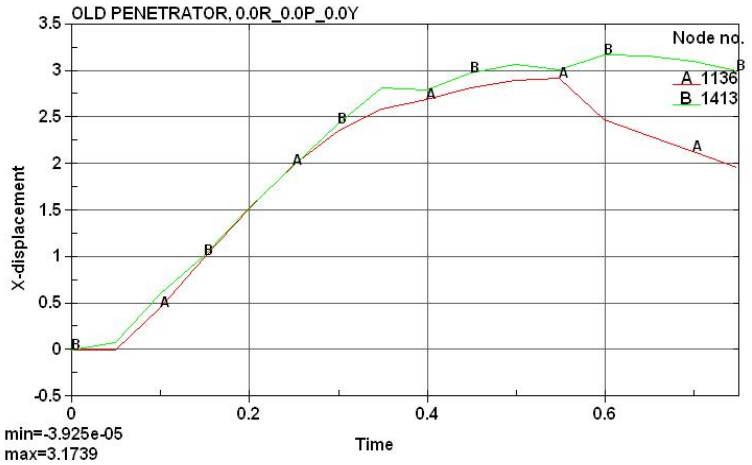

Fig. 38. Displacement plot for LG409

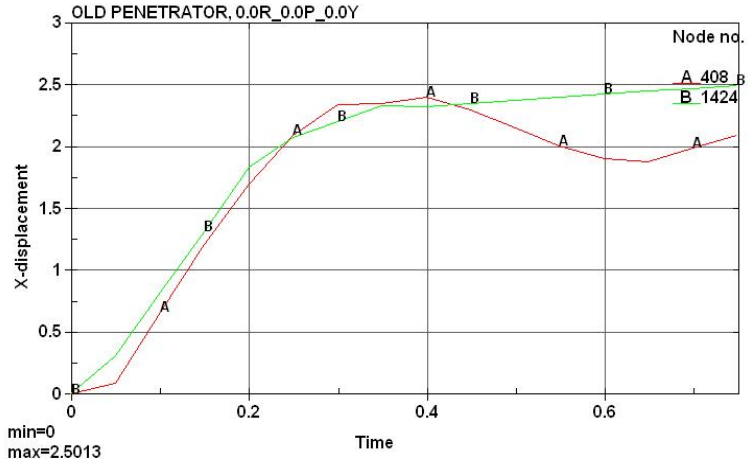

Fig. 39. Displacement plot for LG410

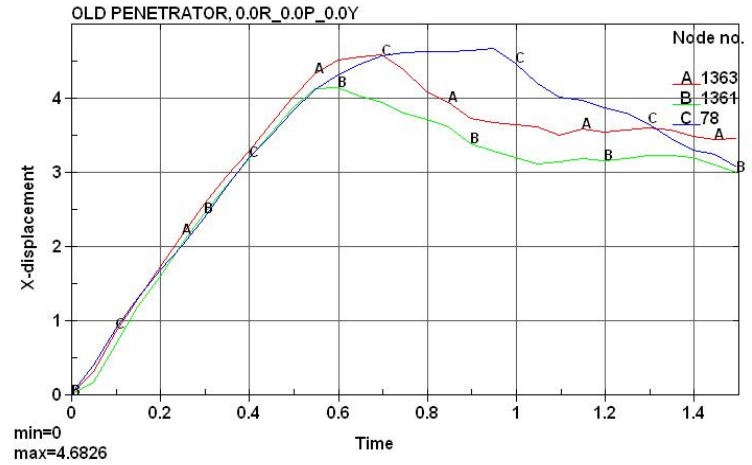

Fig. 40. Displacement plot for LG411

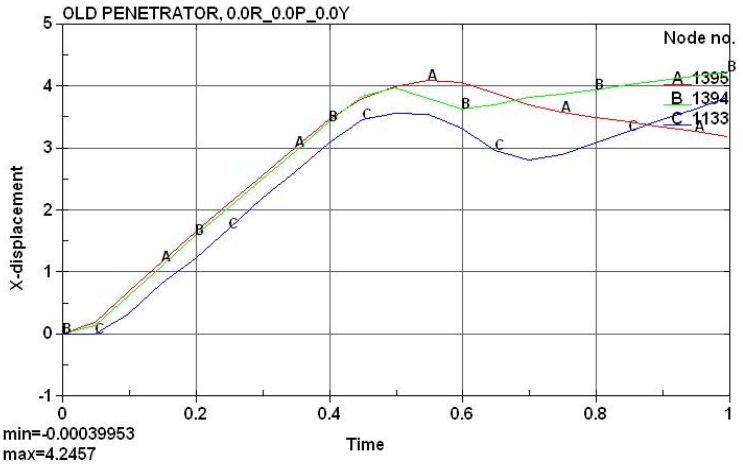

Fig. 41. Displacement plot for LG424

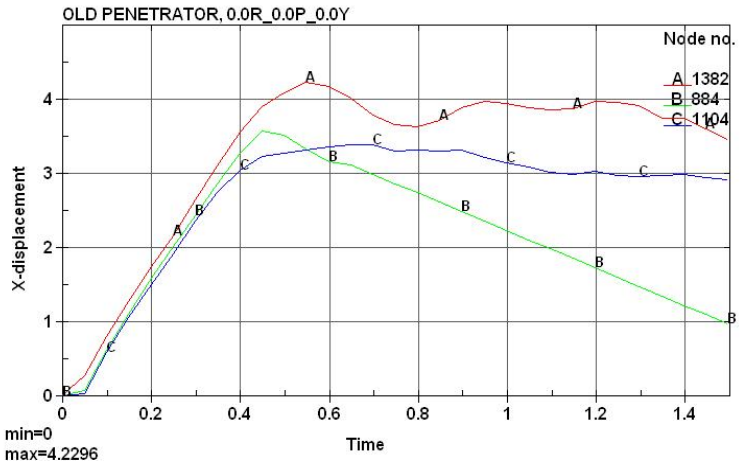

Fig. 42. Displacement plot for LG427

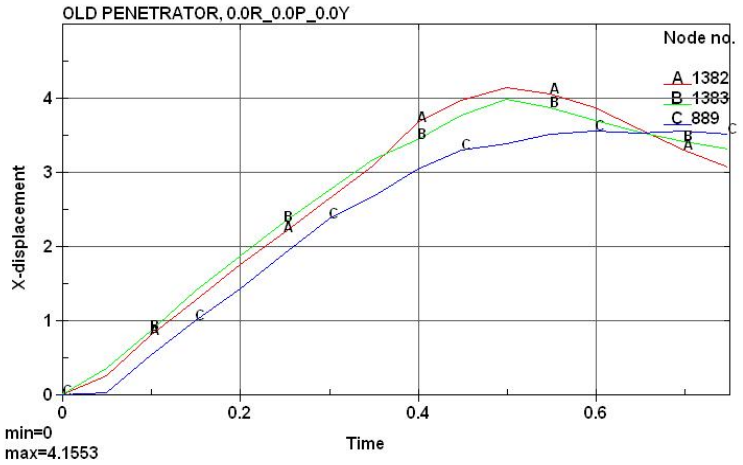

Fig. 43. Displacement plot for LG429

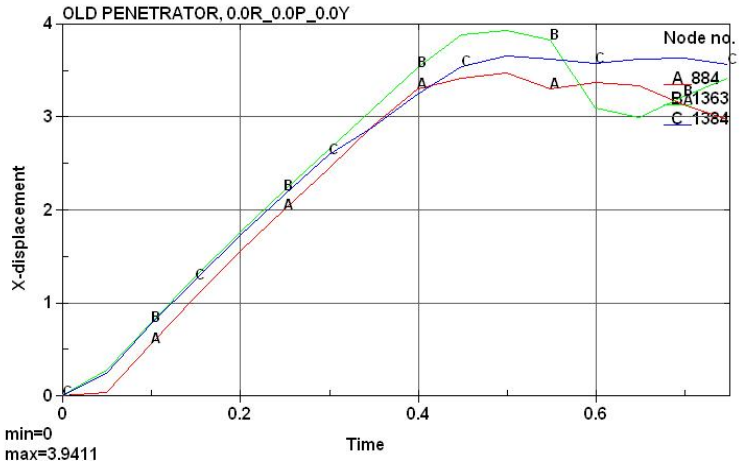

Fig. 44. Displacement plot for LG432

Table 25 shows the comparison of the experimental reported displacement and the FE model.

Table 25
Displacement comparison - experiments and FE model

Test	NASA test		ASU model
	Report displacement	Graph displacement*	
LG403	8.30	12.50	7.11
LG404	8.90	12.50	7.85
LG405	11.40	13.00	16.15
LG409	8.30	12.50	8.05
LG410	7.60	12.50	6.35
LG411	12.70	15.00	11.89
LG424	8.30	12.50	10.80
LG427	8.90	12.00	10.74
LG429	8.90	16.00	10.55
LG432	10.20	13.00	10.01

*Displacement measured on the graph in NASA report

It can be observed that the displacement obtained from the FE model are close to the displacements provided in the NASA report indicating good correlation.

4.4. Mesh convergence study

The importance of studying the effect of mesh size on the final output of a finite element model is widely recognized and is one of first steps in verification and validation of the any FE modeling scheme. One would expect with increasing mesh density the results would be more accurate but with a corresponding increase in computational cost. The optimal solution is a mesh that obtains the solution with the desired accuracy with the lowest computational time.

Following the initial material model mesh convergence study presented in [4], for checking the new material model version (umat v1.2) mesh convergence study, two cases were selected (LG404 and LG414 single layer). Test case LG404 (single layer) is shown in Fig. 45.

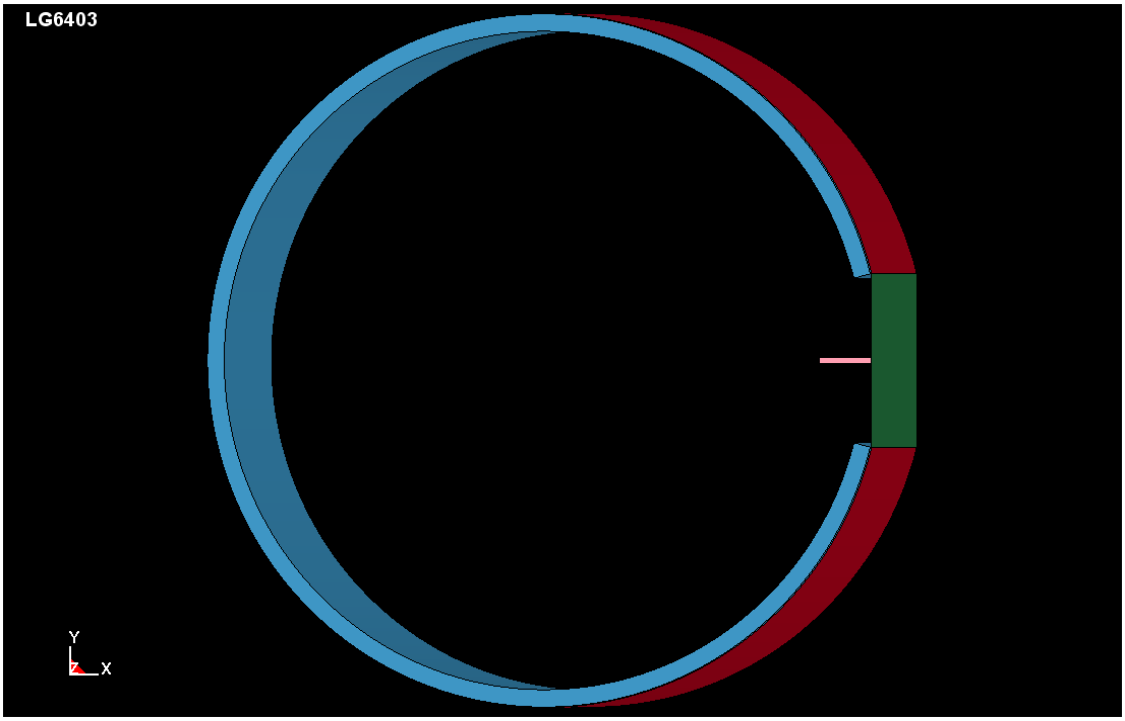

Fig. 45. LG 404 - Single layer FE model

Two element types are used in the model – shell elements for modeling the Kevlar fabric as shown in Fig. 46 and solid elements for modeling the steel ring and the projectile as shown in Fig. 47.

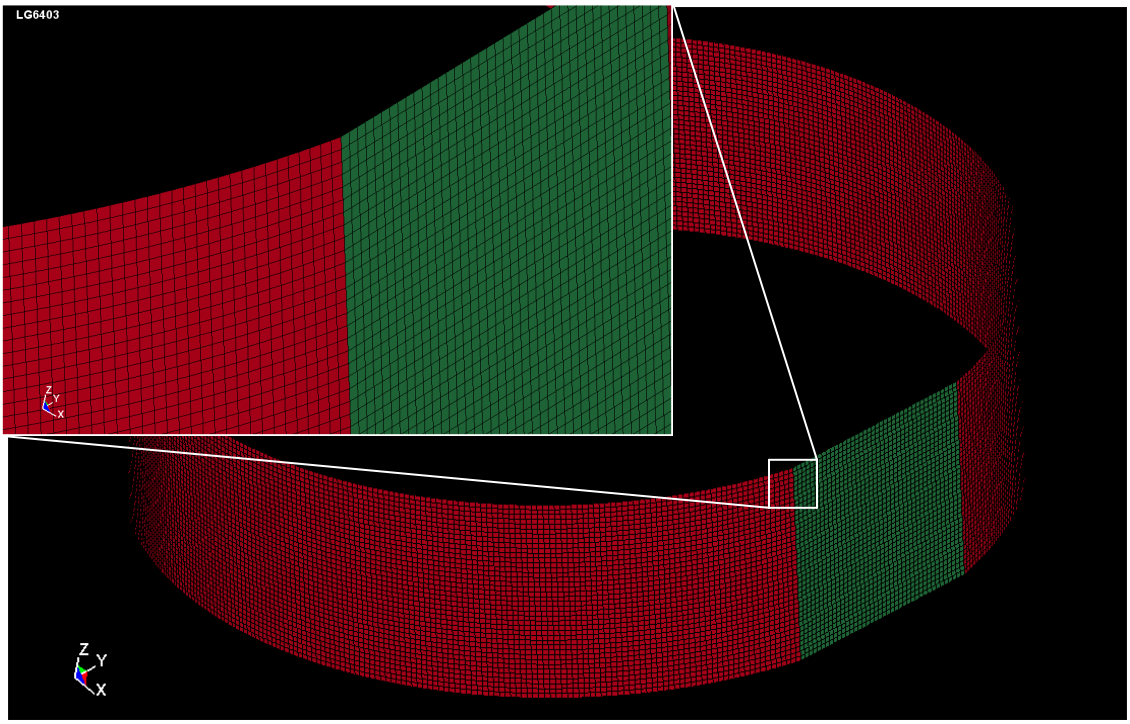

Fig. 46. Fabric mesh

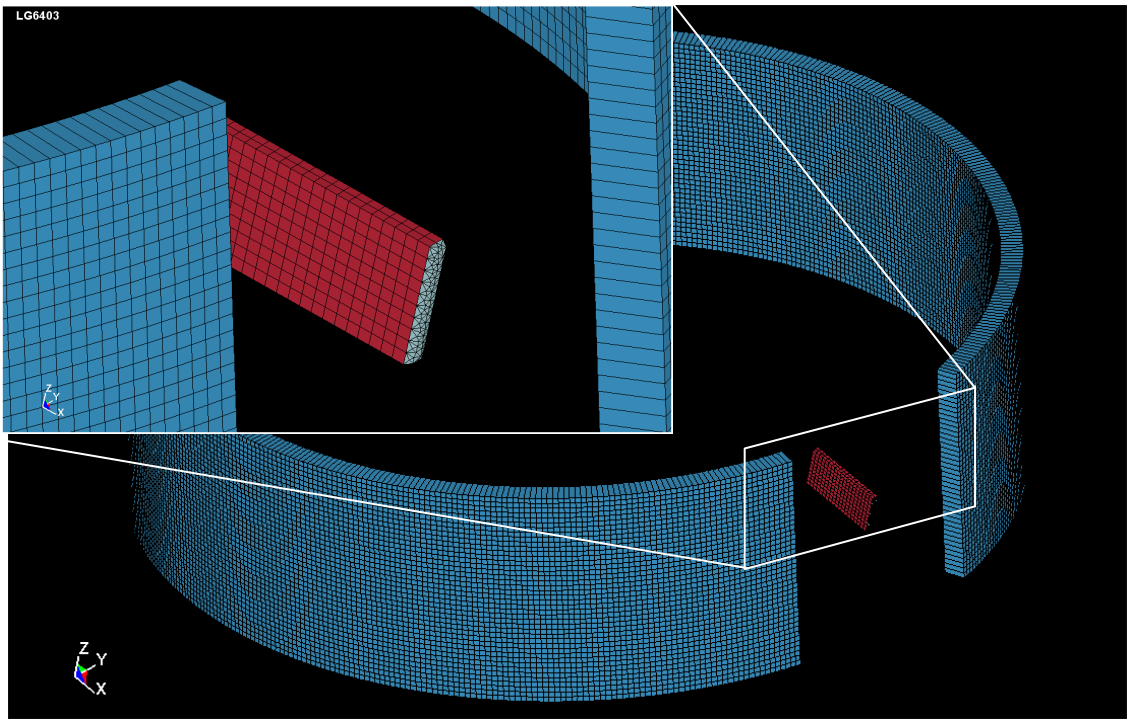

Fig. 47. Ring and projectile mesh

Since the mesh density of the steel ring does not influence the final result, only the fabric mesh density is varied in this study.

LG404 is an 8 layers test case while LG411 is a 24 layers test case. The fabric models used in the analysis were modeled with a single FE layer with the corresponding required thickness. The Kevlar fabric typically has 17 yarns per inch in both the warp and fill direction. To avoid modeling each individual yarn, a minimum number of two yarns in each direction are required per each mesh element. The resulting minimum dimension for the elements is 0.125”x0.125”. Doubling the dimension each time results in two other mesh densities: 0.25”x0.25” and 0.5”x0.5”.

For case LG404, Table 26 shows the numerical details of the analysis and Fig. 48 shows the convergence trend.

Table 26
Analysis of test case LG404

	Yarns/FE element*	Initial Velocity (fps)	Final Velocity (fps)	NASA Test Final Velocity (fps)
Test case	**LG404**			
0.5 x 0.5	9	895.83	709.87	820.2
0.25 x 0.25	4	895.83	808.35	
0.125 x 0.125	2	895.83	834.5	

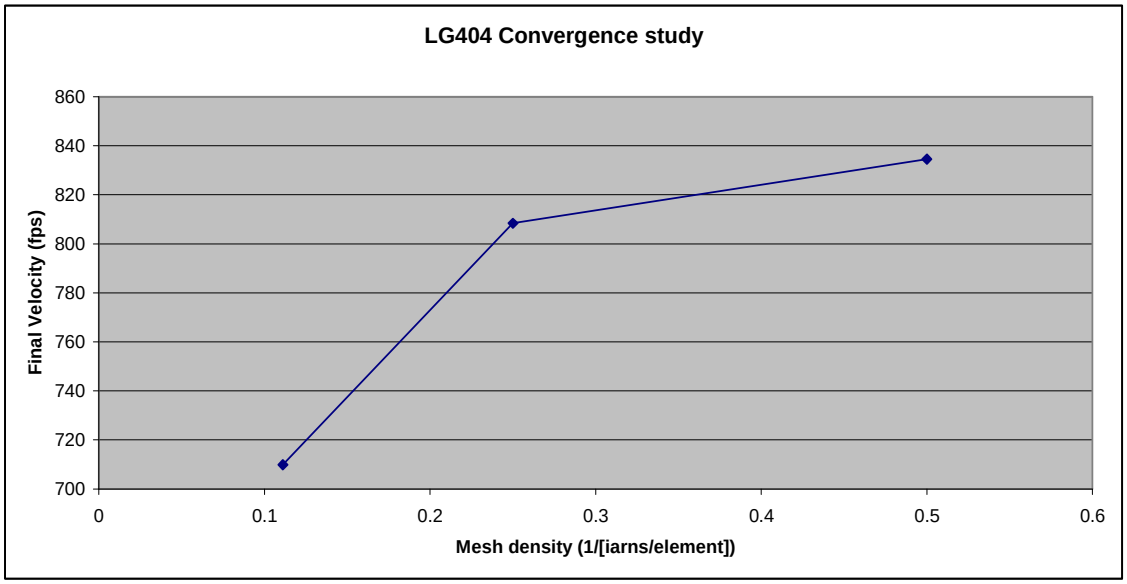

Fig. 48. Convergence trend for model LG404

For model LG411, Table 27 shows the numerical details of the analysis and Fig. 49 shows the convergence trend.

Table 27
Analysis of test case LG411

	Yarns/FE element*	Initial Velocity (fps)	Final Velocity (fps)	Analysis time (ms)	Total CPU time (h/m/s)	NASA Test Final Velocity (fps)
Test case	**LG411**					
0.5 x 0.5	9	885.83	0	3.0	0h37m45s	413.4
0.25 x 0.25	4	885.83	546.36	1.5	0h35m0s	
0.125 x 0.125	2	885.83	506.89	1.5	3h28m39s	
0.0625 x 0.0625	1	895.83	716.49	1.5	19h35m58s	

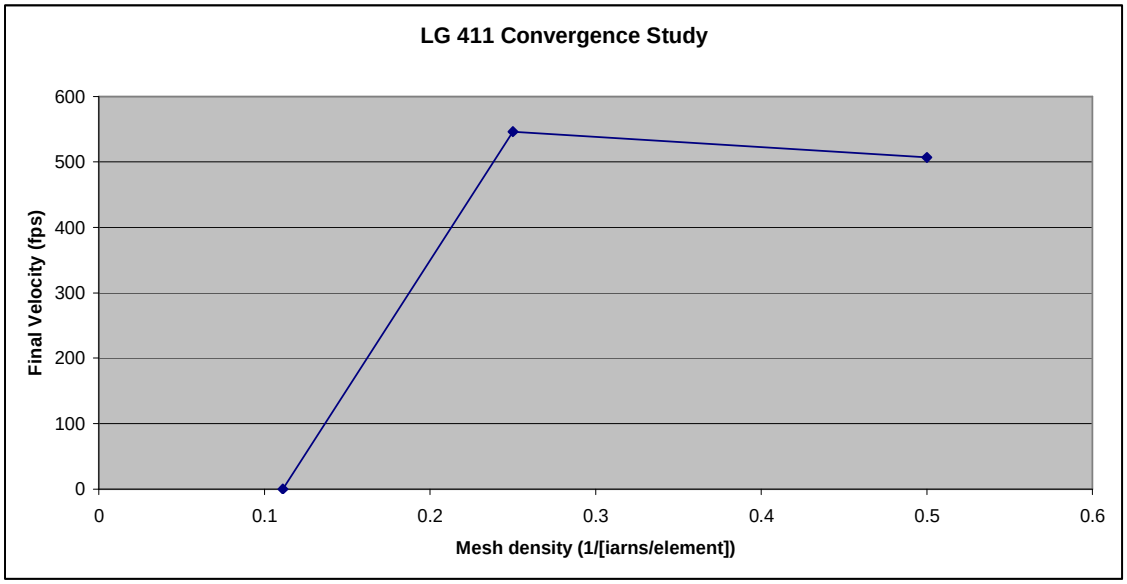

Fig. 49. Convergence trend for model LG411

The results show that 0.25” x 0.25” mesh density obtains the most cost-effective solution (accuracy versus computational time). It should be noted that one cannot increase the mesh density indefinitely especially when element erosion is a part of the analysis. Fig. 4.4.6 (a) to (h) show the deformation of the fabric after impact and a very fine mesh would create an unrealistic response after impact (Fig. 50(g) and (h)).

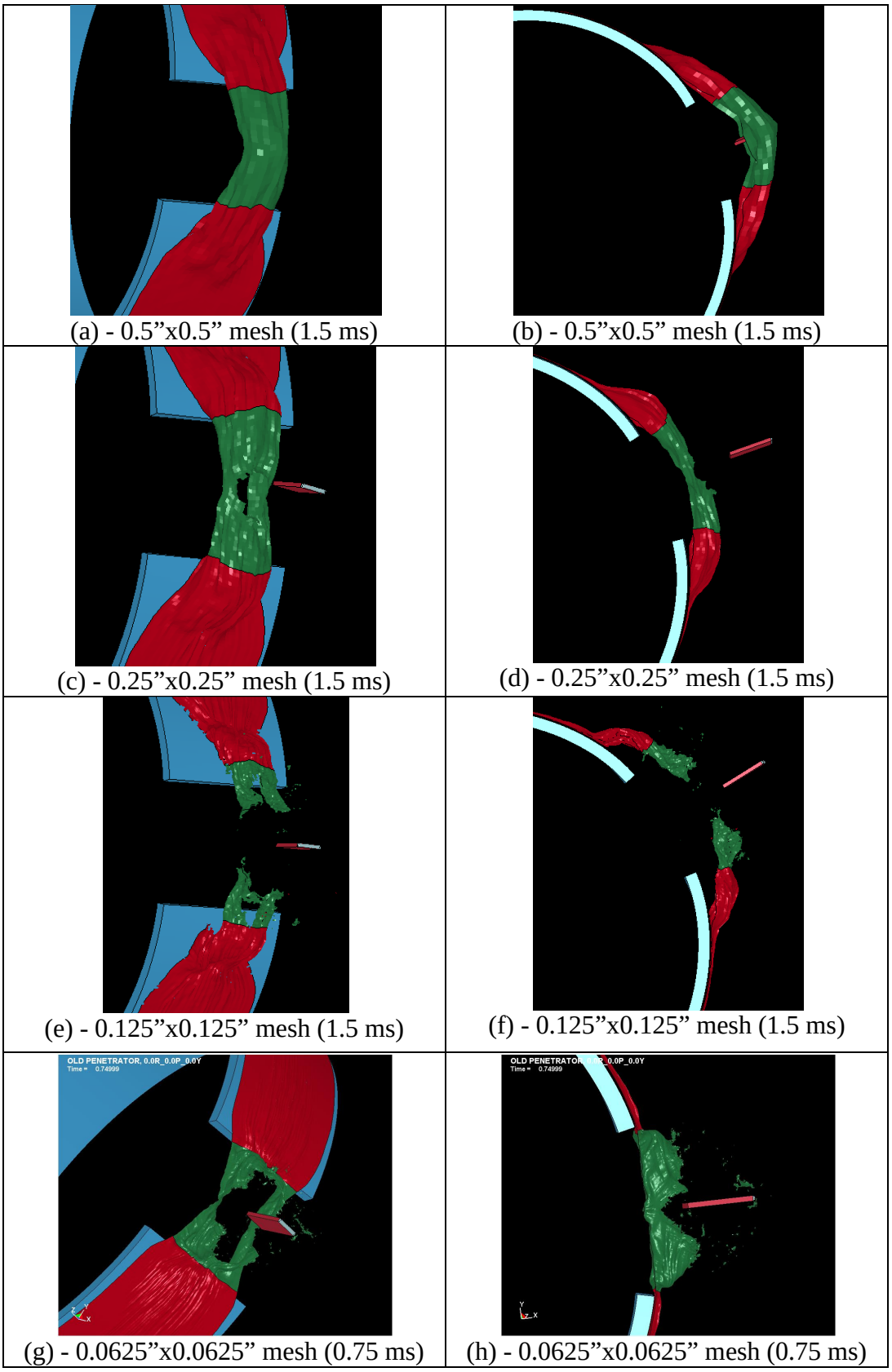

(a) - 0.5”x0.5” mesh (1.5 ms)
(b) - 0.5”x0.5” mesh (1.5 ms)
(c) - 0.25”x0.25” mesh (1.5 ms)
(d) - 0.25”x0.25” mesh (1.5 ms)
(e) - 0.125”x0.125” mesh (1.5 ms)
(f) - 0.125”x0.125” mesh (1.5 ms)
(g) - 0.0625”x0.0625” mesh (0.75 ms)
(h) - 0.0625”x0.0625” mesh (0.75 ms)

Fig. 50. Mesh deformation for test case LG411

5. CONCLUDING REMARKS AND FUTURE WORK

In this thesis, the material model for Kevlar 49 previously developed at Arizona State University was improved based on new experimental data and a detailed analysis of NASA ballistic test data. New changes include consideration of the rotational velocity, fabric displacement, modified strain failure values and a new material model for projectile. The picture frame test conducted using Kevlar was modeled and the shear moduli were determine and compared with the experimental results. Prediction of the ballistic limit using the ASU material model was performed and the accuracy of those predictions will be checked against future tests planed at NASA-GRC.

5.1. Remarks on the ASU continuum model and improvements.

(a) The new tension test conducted at Arizona State University provides additional data based on which the material model was modified. The changes made – bidirectional failure and increase in the stress at which the post peak non-linear curve begins - and implemented in the material model parameters are providing a closer simulation of the Kevlar behavior as shown during experiments as described in section 3.2.1.

(b) The projectile material model used in the ballistic test simulations was changed from elastic to elasto-plastic. By using elasto-plastic material model, the plastic deformations that occur during a

ballistic test and that can be observed in the videos of several test cases are better captured in the FE simulations.

(c) Using the picture frame test, new values of the parameters to be used for the shear modulus of the Kevlar were determined. The FE model simulation of the picture frame test data together with the experimental data were used to formulate a two level factorial design. The commercial software Design Expert, was used to determine optimum parameters to characterize the shearing behavior of Kevlar. The optimized values obtained were then used in the FE models of the NASA ballistic tests for reanalysis. The results obtained using the new shear modulus parameters did not improved the overall results for the models. In determining the displacements for the sixteen points used to compare the FE model and the experimental model, the time was used to track the position of the representative points. This may be detrimental, and the use of a combination time and force for matching of the displacement could have provided an improved outcome of the optimization formulation.

(d) In previous models, it was assumed that the projectile had only translational velocities. The NASA test data were reanalyzed and some test cases revealed rotational (or angular) velocities in addition to translational velocities. The reanalysis of those specific

test cases with imposed the angular velocity showed small changes in the absorbed energy.

(e) A mesh convergence study is a required part of any FE modeling studies. In this research, two FE models were selected and a mesh convergence study was performed. The study indicates that the 0.25” x 25” shell elements currently used are adequate in terms of accuracy and computational expense. An increase in the mesh density would lead to an unnecessary increase in the computational time without a significant increase in accuracy.

(f) The usage of the ASU material model in predicting the ballistic limit for a specific test setup is an indication of how well the material model approximates the Kevlar behavior. The currently developed model has been used in predicting the ballistic limits of several NASA test setups. These results will be used in generating the test setup for future planned tests at NASA-GRC.

(g) In addition to using absorbed energy as a metric, a displacement analysis of the fabric and comparison of the FE model with the ballistic tests is essential as a secondary metric. The limited displacement data from the experiments allowed only a few test cases to be compared. The comparison indicates a good correlation of the test cases provided by the current material model with the experiment data.

5.2. Future work

There are several areas of improvement for the current model.

(a) The strain rate test data for Kevlar is scarce and it does not reach the rates achieved in the ballistic tests. A simple sensitivity analysis has shown that strain rate model plays a very important role in predicting the amount of absorbed energy [3]. More test data would help in confirming the current approach of the ASU material model.

(b) In the current model, the stress-strain relationships in the two principal material directions are uncoupled. The coupling of the two directions by implementing a Poisson's ratio type effect would make bring the material model closer to reality.

(c) The steel projectile is possibly subjected to high strain rate effects. Using a strain rate dependent material model for the projectile could improve the outcome and create a more realistic FE model.

(d) The displacement data in future tests should be captured for all test cases. This will provide an important secondary metric that can then be used to improve the FE model.

6. REFERENCES

[1] Sharda, J. Experimental methods and numerical simulation of fabrics for engine containment systems. M.S. Thesis, Department of Civil Engineering, Arizona State University, August 2002.

[2] D. Naik, S. Sankaran, B. Mobasher, S. D. Rajan and J. M. Pereira. Development of Reliable Modeling Methodologies for Fan Blade-Out Containment Analysis. Part I: Experimental Studies. J of Impact Engineering, 36:1, 1-11, 2009.

[3] Stahlecker, K. Z. The development of a fabric material model for use in modeling engine containment systems. MS thesis, Arizona State University, March 2007.

[4] Stahlecker Z., Mobasher B., Rajan S.D. and Pereira J. M. Development of Reliable Modeling Methodologies for Fan Blade-Out Containment Analysis. Part II: Finite Element Analysis. J of Impact Engineering, 36:3, 447-459, 2009.

[5] Tabiei, A., and Yi, W. Comparative study of predictive methods for woven fabric composite elastic properties. J Comp Stru 2002, 58: 149-64.

[6] Scida, D., Aboura, Z., Benzeggagh, M.L., and Bocherens, E. A micromechanics model for 3D elasticity and failure of woven-fibre composite materials. J Compos Sci Tech 1999, 59:505-17.

[7] Peng, X.Q., and Cao, J. Numerical determination of mechanical elastic constants of textile composites. 15th Annual Technical Conference of the American Society for Composites, College Station, TX, 2000.

[8] Tabiei, A., and Ivanov, I. Computational micro-mechanical model of flexible woven fabric for finite element impact simulation. 7th International LS-DYNA Users Conference, 2002, 8-15-8-40.

[9] Roylance, D., Chammas, P., Ting, J., Chi, H., and Scott, B. Numerical modeling of fabric impact. Proceedings of the National Meeting of the American Society of Mechanical Engineers (ASME), San Fransisco, CA, 1995.

[10] Xia, Y., and Wang, Y. The effects of strain rate on the mechanical behavior of Kevlar fibre bundles: an experimental and theoretical study. Comp Part A 1998, 29A: 1411-15.

[11] Xia, Y., Wang, Y. Experimental and theoretical study on the strain rate and temperature dependence of mechanical behavior of Kevlar fibre. Comp Part A 1999, 30: 1251-57.

[12] Bansal K. S. Development of micro-mechanical model for dry fabrics. MS thesis, Arizona State University, December 2007.

[13] S. Bansal, B. Mobasher, S.D. Rajan and I. Vintilescu. Numerical Modeling of Engine Fan Blade-Out Events. *ASCE* J of Aerospace Engineering, 22, 249-259, 2009.

[14] Ishikawa, T., and Chou, T.W. Stiffness and strength behavior of woven fabric composites. J Compos Mater 1982, 17:3211-220.

[15] Ishikawa, T., and Chou, T.W. Elastic behavior of woven hybrid composites. J Compos Mater 1982, 16:2-19.

[16] Ishikawa, T., and Chou, T.W. One-dimensional micromechanical analysis of woven fabric composites. AIAA Jr 1983, 21(12):1714-21.

[17] Ishikawa, T., Matsusima, M., Hayashi, Y., and Chou, T. Experimental confirmation of the theory of elastic moduli of fabric composites. J Compos Mater 1985, 19:443-58.

[18] Scida, D., Aboura, Z., Benzeggagh, M.M. and Boherens, E. A micromechanics modelfor 3D elasticity and failure of woven-fibre composite materials. Composite Science and Technology 1999, 59: 505–517.

[19] Jiang, Y., Tabiei, A., and Simitses, G.J. A novel micromechanics-based approach to the derivation of constitutive equations for local/global analysis of plain-weave fabric composite. J Compos Sci Tech 2000, 60: 1825-33

[20] Tabiei, A., and Jiang, Y. Woven fabric composite material model with material nonlinearity for nonlinear finite element simulation. J Solids Structures 1999, 36: 2757-71.

[21] Tanov, R., and Tabiei, A. Computationally efficient micro-mechanical woven fabric constitutive. J Models Appl Mech 2001, 68(4): 553-60.

[22] Naik, N.K., and Ganesh, V.K. Failure behavior of plain weave fabric laminates under on-axis uniaxial tensile loading: I-Laminate geometry. J Compos Mater 1996, 30(16): 1748-78.

[23] Naik, N.K., and Ganesh, V.K. Failure behavior of plain weave fabric laminates under on-axis uniaxial tensile loading: II-Analytical predictions. J Compos Mater 1996, 30(16): 1779-1822.

[24] Naik, N.K., and Ganesh, V.K. Failure behavior of plain weave fabric laminates under on-axis uniaxial tensile loading: III-Effect of fabric geometry. J Compos Mater 1996, 30(16): 1823-1856.

[25] Vandeurzen, Ph., Ivens, J., and Verpoest, I. A three-dimensional micromechanical analysis of woven-fabric composites: I. Geometric analysis. J Compos Sci Tech 1996, 56: 1303-15.

[26] Vandeurzen, Ph., Ivens, J., and Verpoest, I. A three-dimensional micromechanical analysis of woven-fabric composites: II. Elastic analysis. J Compos Sci Tech 1996, 56: 1317-27.

[27] Peng XQ, Cao J. Numerical determination of mechanical elastic constants of textile composites. In: Fifteenth annual technical conference of the American Society for Composites, College Station, TX, USA; 2000.

[28] Barbero, E.J., Lonetti, P., and Sikkil, K.K. Finite element continuum damage modeling of plain weave reinforced composites. Comp Part B 2006, 37: 137-47.

[29] Barbero, E.J., et al., Finite element modeling of plain weave fabrics from photomicrograph measurements, J Comp Stru 2006, 73(1): 41-52.

[30] Srirengan, K., Whitcomb, J., and Chapman, C. Modal technique for three-dimensional global/local stress analysis of plain weave composites. J Comp Stru 1997, 39: 145-56.

[31] Kollegal, G.M., and Sridharan, S. Strength prediction of plain woven fabrics. J Compos Mater 2000, 34(3): 240-57.

[32] Kollegal, M., Chatterjee, S.N., and Flanagan, G. Progressive failure analysis of plain weaves using damage mechanics based constitutive laws. J Damage Mech 2001, 10:301-23.

[33] Xue, P., Xiongqi, P., and Cao, J. A non-orthogonal constitutive model for characterizing woven composites. Comp Part A 2003, 34: 183-93.

[34] Gu, B. Analytical modeling for the ballistic perforation of planar plain-woven fabric target by projectile. Comp Part B 2003, 34: 361-71.

[35] Roylance D. Numerical modeling of fabric impact. In: Proceedings of national meeting of the American Society of Mechanical Engineers (ASME), San Francisco, CA; 1995.

[36] Shim, V.P.W., Tan, V.B.C., and Tay, T.E. Modeling deformation and damage characteristics of woven fabric under small projectile impact. Int J Impact Engng 1995, 16(4): 585-605.

[37] Lim, C.T., Shim, V.P.W., and Ng, Y.H. Finite-element modeling of the ballistic impact of fabric armor. Int J Impact Engng 2003, 28: 13-31.

[38] Iannucci, L., and Willows, M.L. An energy based damage mechanics approach to modeling impact onto woven composite materials-Part I: Numerical models. Comp Part A 2006, 37(11): 2041-56.

[39] Johnson, A.F., and Simon, J. Modeling fabric reinforced composites under impact loads. EUROMECH 400: Impact and Damage Tolerance Modeling of Composite Materials and Structures Imperial College of Science Technology and Medicine, London, 1999.

[40] Krishnan, K. Using virtual testing for topology optimization, M.S. Thesis, Department of Civil & Environmental Engineering, Arizona State University, May 2007.

[41] Cheng, M., Chen, W., and Weerasooriya, T. Mechanical properties of Kevlar KM2 single fiber. J Engng Mat Tech 2005, 127(2): 197-203.

[42] Rodriquez, J., Shocron, I.S., Martinez, M.A., and Sanchez-Galvez, V. High strain rate properties of aramid and polyethylene woven fabric composites. Comp Part B 1996, 27B: 147-54.

[43] Shim, V.P.W., Lim, C.T., and Foo, K.J. Dynamic mechanical properties of fabric armour. Int J Impact Engng 2001, 25: 1-15.

[44] Söderberg, A., and Sellgren, U. Modeling of strain hardening and strain rate hardening of dual phase steels in finite element analysis of energy-absorbing components. NAFEMS World Congress 2005, No. 69.

[45] ABAQUS. Theory Manual. ABAQUS, Inc., Pawtucket RI, 2006.

[46] Belytschko, T., and Hughes, T.J.R., Computational Methods for Transient Analysis, Elsevier Science Publishing Company, New York, New York, 1983.

[47] Belytschko, T., Liu, W. K. and Moran, B., Nonlinear Finite Elements for Continua and Structures, J. Wiley and Sons, New York, New York, 2000.

[48] Sharda, J. Experimental methods and numerical simulation of fabrics for engine containment systems. M.S. Thesis, Department of Civil Engineering, Arizona State University, August 2002.

[49] Arizona State University. FAA Development of Reliable Modeling Methodologies for Fan Blade-Out Containment Analysis: Experimental Study on Aging effects on Kevlar and Zylon Fabrics. Unpublished, 2009.

[50] Blandford R. K., Morton D. K., Snow S. D. and Rahl T. E. Tensile Stress-Strain Results for 304L and 316L Stainless Steel Plate at Temperature. ASME Pressure Vessels and Piping Division Conference July 2007.

[51] Arizona State University. FAA development of reliable modeling methodologies for fan blade out analysis: Shear modulus test using picture frame tests. Unpublished, 2005.

[52] Zhu D. Experimental study and finite element modeling of woven fabrics. PhD Dissertation, Arizona State University, December 2009.

[53] Stat-Ease. Design-Expert 7.1 User's Guide. Stat-Ease, Inc, Minneapolis, MN 2006.

[54] Agilent Technologies. The Fundamentals of Signal Analysis. Application Note 243, 2000.

[55] Antoniou, A. Digital Filters: Analysis, Design, and Applications. Second Edition, McGraw-Hill, 1993.

[56] Arizona State University. FAA development of reliable modeling methodologies for fan blade out analysis: Friction Tests. Unpublished, November 2004.

[57] Arizona State University. FAA development of reliable modeling methodologies for fan blade out analysis: Picture Frame Test of Kevlar 49 Fabric. Unpublished, 2009.

[58] Cowper, G.R., and Symonds, P.S. Strain hardening and strain rate effect in the impact loading of cantilever beams. Brown University, Division of Applied Mathematics report, 1957; 28

[59] Iannucci, L., and Willows, M.L. An energy based damage mechanics approach to modeling impact onto woven composite materials-Part II: Experimental and numerical results. Comp Part A 2007, 38(2): 540-54.

[60] LS-DYNA, "Theoretical Manual. Livermore Software Technology Corp. Livermore CA, 1998.

[61] LS-DYNA. Keyword User's Manual: Version 971. Livermore Software Technology Corp., Livermore CA, 2003.

[62] Shim, V.P.W., Lim, C.T., and Foo, K.J. Dynamic mechanical properties of fabric armour. Int J Impact Engng 2001, 25: 1-15.

[63] J. Sharda, C. Deenadayalu, B. Mobasher and S. D. Rajan. Modeling of Multi-Layer Composite Fabrics for Gas Turbine Engine Containment Systems. ASCE J of Aerospace Engineering, 19:1, 38-45, 2006.

APPENDIX A

DETAILS OF THE OPTIMIZATION PROBLEM

Details on the calculations of the overall error are shown below for each of the eight runs. The experimental and the FE displacements are listed for the x and the Y direction. The overall error is calculated based on the denoted as $C\ Error$ formula and listed below. Formulas denoted as $A\ Error$ and $B\ Error$ were tested but did not provide quality results.

$$A\ Error = \sum_{1}^{16}\left(1 - \frac{\sum \Delta X_{i,exp}}{\sum \Delta X_{i,FE}}\right)^2$$

$$B\ Error = \sum_{1}^{16}\left\{\sum_{i=1}^{6}\left(1 - \frac{\Delta X_{i,exp}}{\Delta X_{i,FE}}\right)^2\right\}$$

$$C\ Error = \sum_{1}^{16}\left\{\sum_{i=1}^{6}\left(\Delta X_{i,exp} - \Delta X_{i,FE}\right)^2 + \sum_{i=1}^{6}\left(\Delta Y_{i,exp} - \Delta Y_{i,FE}\right)^2\right\}$$

Run 1 – C Error = 24.216

	Test case: 1_06_2e3_250e3															
	X dir - DIC															
Time	1 (54)		2 (56)		3 (64)		4 (66)		5 (74)		6 (77)		7 (79)		8 (84)	
	Exp Disp	FE Displ	Exp Disp	FE Displ	Exp Disp	FE Displ	Exp Disp	FE Displ	Exp Disp	FE Displ	Exp Disp	FE Displ	Exp Disp	FE Displ	Exp Disp	FE Displ
50	0.121	-0.045	0.079	-0.001	0.037	-0.002	-0.005	0.041	0.080	0.085	-0.039	0.044	0.000	0.127	-0.043	0.085
100	0.240	-0.101	0.159	0.003	0.076	-0.003	0.000	0.100	0.162	0.192	0.083	0.111	0.000	0.279	-0.078	0.182
150	0.373	-0.155	0.249	-0.006	0.121	0.037	-0.002	0.163	0.253	0.308	0.130	0.182	0.002	0.453	-0.119	0.295
200	0.525	-0.215	0.351	-0.006	0.172	0.085	0.001	0.259	0.358	0.460	0.185	0.270	0.008	0.708	-0.163	0.429
250	0.699	-0.288	0.465	-0.007	0.227	0.191	0.002	0.431	0.476	0.673	0.247	0.427	0.010	1.092	-0.214	0.622
300	0.902	-0.443	0.609	0.000	0.305	0.261	0.014	0.510	0.605	0.837	0.244	0.585	0.020	1.250	-0.266	0.826
	2.861	-1.247	1.912	-0.017	0.938	0.569	0.010	1.503	1.934	2.555	0.849	1.619	0.039	3.909	-0.883	2.441
A		10.853		13255.2		0.422		0.987		0.059		0.226		0.980		1.855
B		69.502		2E+06		1172.2		6.2114		0.2719		4.3422		5.9241		11.745
C		3.638		0.793		0.019		0.525		0.106		0.166		3.396		2.431
	Y dir - DIC															
Time	1 (54)		2 (56)		3 (64)		4 (66)		5 (74)		6 (77)		7 (79)		8 (84)	
	Exp Disp	FE Displ	Exp Disp	FE Displ	Exp Disp	FE Displ	Exp Disp	FE Displ	Exp Disp	FE Displ	Exp Disp	FE Displ	Exp Disp	FE Displ	Exp Disp	FE Displ
50	0.242	0.279	0.276	0.321	0.312	0.239	0.352	0.280	0.203	0.162	0.239	0.201	0.276	0.201	0.315	0.242
100	0.446	0.559	0.504	0.644	0.574	0.480	0.727	0.570	0.375	0.330	0.440	0.411	0.474	0.411	0.576	0.494
150	0.652	0.833	0.744	0.963	0.841	0.740	0.946	0.868	0.551	0.493	0.645	0.621	0.739	0.620	0.839	0.752
200	0.859	1.104	0.980	1.289	1.111	0.999	1.253	1.166	0.726	0.668	0.849	0.837	0.973	0.837	1.108	1.017
250	1.067	1.348	1.215	1.594	1.370	1.263	1.540	1.479	0.903	0.842	1.056	1.062	1.205	1.049	1.365	1.299
300	1.227	1.602	1.399	1.916	1.580	1.496	1.773	1.728	1.037	0.998	1.210	1.270	1.387	1.205	1.572	1.527
	4.493	5.725	5.117	6.726	5.789	5.217	6.592	6.090	3.795	3.494	4.439	4.402	5.054	4.323	5.776	5.330
A		0.046		0.057		0.012		0.007		0.007		0.000		0.029		0.007
B		0.2535		0.3056		0.173		0.1584		0.1098		0.0444		0.2694		0.1441
C		0.313		0.557		0.047		0.025		0.014		0.006		0.096		0.028

Run 1 (cont.)

-

	Test case: 1_06_2e3_250e3															
	X dir - DIC															
Time	9 (91)		10 (93)		11 (98)		12 (104)		13 (107)		14 (109)		15 (114)		16 (118)	
	Exp Disp	FE Displ	Exp Disp	FE Displ	Exp Disp	FE Displ	Exp Disp	FE Displ	Exp Disp	FE Displ	Exp Disp	FE Displ	Exp Disp	FE Displ	Exp Disp	FE Displ
50	0.038	-0.127	-0.004	-0.088	-0.047	-0.086	-0.086	-0.044	-0.004	0.000	-0.046	-0.043	-0.092	0.042	-0.131	-0.003
100	0.079	-0.279	-0.001	-0.189	-0.083	-0.195	-0.161	-0.093	-0.004	0.004	-0.083	-0.099	-0.169	0.095	-0.245	-0.004
150	0.124	-0.458	-0.001	-0.294	-0.126	-0.312	-0.248	-0.142	-0.004	0.014	-0.128	-0.150	-0.257	0.155	-0.375	-0.013
200	0.174	-0.682	0.001	-0.433	-0.173	-0.485	-0.342	-0.210	-0.002	0.021	-0.173	-0.237	-0.351	0.217	-0.519	-0.028
250	0.230	-1.012	0.001	-0.581	-0.230	-0.700	-0.455	-0.295	-0.004	0.052	-0.230	-0.403	-0.467	0.271	-0.691	-0.081
300	0.291	-1.220	0.002	-0.754	-0.292	-0.899	-0.581	-0.304	-0.008	0.060	-0.294	-0.460	-0.599	0.337	-0.884	-0.049
	0.936	-3.778	-0.002	-2.339	-0.951	-2.678	-1.874	-1.088	-0.027	0.152	-0.955	-1.393	-1.934	1.116	-2.846	-0.179
A		1.557		0.998		0.416		0.522		1.381		0.099		7.465		222.859
B		9.5662		5.9055		2.2151		3.5599		403.51		0.4396		47.022		6368.8
C		4.923		1.191		0.723		0.133		0.009		0.062		1.929		1.458

	Y dir - DIC															
Time	9 (91)		10 (93)		11 (98)		12 (104)		13 (107)		14 (109)		15 (114)		16 (118)	
	Exp Disp	FE Displ	Exp Disp	FE Displ	Exp Disp	FE Displ	Exp Disp	FE Displ	Exp Disp	FE Displ	Exp Disp	FE Displ	Exp Disp	FE Displ	Exp Disp	FE Displ
50	0.167	0.199	0.203	0.238	0.241	0.159	0.279	0.198	0.133	0.080	0.168	0.118	0.209	0.120	0.245	0.158
100	0.307	0.392	0.373	0.472	0.441	0.311	0.509	0.394	0.247	0.157	0.311	0.227	0.381	0.248	0.447	0.319
150	0.454	0.578	0.545	0.699	0.641	0.447	0.739	0.593	0.365	0.232	0.458	0.334	0.556	0.374	0.651	0.479
200	0.595	0.762	0.717	0.924	0.841	0.572	0.971	0.787	0.477	0.317	0.599	0.436	0.727	0.512	0.853	0.640
250	0.741	0.935	0.893	1.141	1.045	0.698	1.202	0.981	0.594	0.404	0.747	0.514	0.903	0.646	1.060	0.797
300	0.851	1.127	1.024	1.355	1.200	0.863	1.384	1.179	0.684	0.479	0.857	0.619	1.038	0.766	1.216	0.947
	3.114	3.994	3.755	4.829	4.410	3.051	5.084	4.132	2.499	1.669	3.140	2.248	3.814	2.666	4.472	3.341
A		0.049		0.049		0.199		0.053		0.247		0.157		0.185		0.115
B		0.2707		0.2712		1.2513		0.4502		1.7512		0.953		1.5325		0.8933
C		0.159		0.239		0.351		0.153		0.124		0.155		0.227		0.224

Run 2 – C Error = 24.281

	Test case: 2_06_8e3_150e3															
	X dir - DIC															
Time	1 (54)		2 (56)		3 (64)		4 (66)		5 (74)		6 (77)		7 (79)		8 (84)	
	Exp Disp	FE Displ	Exp Disp	FE Displ	Exp Disp	FE Displ	Exp Disp	FE Displ	Exp Disp	FE Displ	Exp Disp	FE Displ	Exp Disp	FE Displ	Exp Disp	FE Displ
50	0.121	-0.049	0.079	0.000	0.037	0.001	-0.005	0.047	0.080	0.091	-0.039	0.050	0.000	0.131	-0.043	0.091
100	0.240	-0.116	0.159	0.007	0.076	0.002	0.000	0.109	0.162	0.199	0.083	0.116	0.000	0.279	-0.078	0.199
150	0.373	-0.160	0.249	0.015	0.121	0.019	-0.002	0.159	0.253	0.307	0.130	0.169	0.002	0.435	-0.119	0.303
200	0.525	-0.168	0.351	-0.003	0.172	-0.006	0.001	0.169	0.358	0.399	0.185	0.162	0.008	0.615	-0.163	0.404
250	0.699	-0.273	0.465	-0.048	0.227	-0.136	0.002	0.114	0.476	0.525	0.247	0.179	0.010	0.770	-0.214	0.530
300	0.902	-0.374	0.609	-0.067	0.305	-0.045	0.014	0.206	0.605	0.682	0.244	0.237	0.020	1.074	-0.266	0.678
	2.861	-1.140	1.912	-0.096	0.938	-0.164	0.010	0.804	1.934	2.203	0.849	0.912	0.039	3.303	-0.883	2.204
A		12.322		433.626		44.977		0.976		0.015		0.005		0.977		1.962
B		73.877		674216		3645.9		6.0743		0.1123		3.5239		5.908		11.942
C		3.366		0.907		0.297		0.106		0.013		0.015		2.263		1.961

	Y dir - DIC															
Time	1 (54)		2 (56)		3 (64)		4 (66)		5 (74)		6 (77)		7 (79)		8 (84)	
	Exp Disp	FE Displ	Exp Disp	FE Displ	Exp Disp	FE Displ	Exp Disp	FE Displ	Exp Disp	FE Displ	Exp Disp	FE Displ	Exp Disp	FE Displ	Exp Disp	FE Displ
50	0.242	0.280	0.276	0.322	0.312	0.239	0.352	0.280	0.203	0.161	0.239	0.200	0.276	0.201	0.315	0.242
100	0.446	0.559	0.504	0.648	0.574	0.477	0.727	0.568	0.375	0.324	0.440	0.401	0.474	0.405	0.576	0.488
150	0.652	0.821	0.744	0.962	0.841	0.716	0.946	0.849	0.551	0.490	0.645	0.603	0.739	0.610	0.839	0.738
200	0.859	1.068	0.980	1.247	1.111	0.935	1.253	1.113	0.726	0.645	0.849	0.787	0.973	0.799	1.108	0.979
250	1.067	1.267	1.215	1.498	1.370	1.133	1.540	1.356	0.903	0.792	1.056	0.971	1.205	0.961	1.365	1.198
300	1.227	1.524	1.399	1.813	1.580	1.379	1.773	1.620	1.037	0.979	1.210	1.168	1.387	1.177	1.572	1.433
	4.493	5.519	5.117	6.491	5.789	4.879	6.592	5.786	3.795	3.390	4.439	4.129	5.054	4.153	5.776	5.079
A		0.035		0.045		0.035		0.019		0.014		0.006		0.047		0.019
B		0.2032		0.2558		0.2661		0.2007		0.149		0.0674		0.3565		0.1893
C		0.202		0.373		0.149		0.091		0.028		0.016		0.156		0.079

Run 2 (cont.)

	Test case: 2_06_8e3_150e3															
	X dir - DIC															
Time	**9 (91)**		**10 (93)**		**11 (98)**		**12 (104)**		**13 (107)**		**14 (109)**		**15 (114)**		**16 (118)**	
	Exp Disp	Exp Displ	Exp Disp	Exp Displ	Exp Disp	Exp Displ	Exp Disp	Exp Displ	Exp Disp	Exp Displ	Exp Disp	Exp Displ	Exp Disp	Exp Displ	Exp Disp	Exp Displ
50	0.038	-0.131	-0.004	-0.091	-0.047	-0.091	-0.086	-0.048	-0.004	0.000	-0.046	-0.046	-0.092	0.050	-0.131	-0.003
100	0.079	-0.281	-0.001	-0.200	-0.083	-0.200	-0.161	-0.105	-0.004	-0.012	-0.083	-0.102	-0.169	0.119	-0.245	-0.021
150	0.124	-0.444	-0.001	-0.289	-0.126	-0.294	-0.248	-0.153	-0.004	-0.007	-0.128	-0.153	-0.257	0.171	-0.375	-0.048
200	0.174	-0.826	0.001	-0.491	-0.173	-0.419	-0.342	-0.279	-0.002	-0.041	-0.173	-0.320	-0.351	0.217	-0.519	-0.173
250	0.230	-1.393	0.001	-0.812	-0.230	-0.702	-0.455	-0.487	-0.004	-0.089	-0.230	-0.607	-0.467	0.284	-0.691	-0.405
300	0.291	-1.449	0.002	-0.846	-0.292	-0.813	-0.581	-0.501	-0.008	0.046	-0.294	-0.592	-0.599	0.399	-0.884	-0.354
	0.936	-4.523	-0.002	-2.728	-0.951	-2.519	-1.874	-1.572	-0.027	-0.102	-0.955	-1.821	-1.934	1.240	-2.846	-1.003
A		1.457		0.998		0.387		0.037		0.546		0.226		6.550		3.373
B		9.2124		5.9072		2.1098		1.3926		117.42		0.9112		40.287		2306.2
C		7.010		1.712		0.585		0.022		0.012		0.253		2.086		0.607

	Y dir - DIC															
Time	**9 (91)**		**10 (93)**		**11 (98)**		**12 (104)**		**13 (107)**		**14 (109)**		**15 (114)**		**16 (118)**	
	Exp Disp	FE Displ	Exp Disp	FE Displ	Exp Disp	FE Displ	Exp Disp	FE Displ	Exp Disp	FE Displ	Exp Disp	FE Displ	Exp Disp	FE Displ	Exp Disp	FE Displ
50	0.167	0.197	0.203	0.237	0.241	0.156	0.279	0.197	0.133	0.076	0.168	0.117	0.209	0.118	0.245	0.159
100	0.307	0.391	0.373	0.474	0.441	0.308	0.509	0.396	0.247	0.150	0.311	0.228	0.381	0.240	0.447	0.315
150	0.454	0.570	0.545	0.697	0.641	0.444	0.739	0.587	0.365	0.226	0.458	0.336	0.556	0.365	0.651	0.467
200	0.595	0.744	0.717	0.909	0.841	0.563	0.971	0.740	0.477	0.283	0.599	0.424	0.727	0.478	0.853	0.603
250	0.741	0.892	0.893	1.078	1.045	0.656	1.202	0.884	0.594	0.340	0.747	0.515	0.903	0.579	1.060	0.733
300	0.851	1.082	1.024	1.309	1.200	0.796	1.384	1.095	0.684	0.458	0.857	0.612	1.038	0.733	1.216	0.864
	3.114	3.875	3.755	4.703	4.410	2.923	5.084	3.899	2.499	1.533	3.140	2.232	3.814	2.512	4.472	3.140
A		0.039		0.041		0.259		0.092		0.397		0.165		0.269		0.180
B		0.2246		0.2351		1.5353		0.6154		2.6253		0.9874		1.9723		1.1643
C		0.113		0.176		0.439		0.268		0.175		0.162		0.305		0.335

Run 3 – C Error = 50.518

	Test case: 3_03_2e3_150e3															
	X dir - DIC															
Time	**1 (54)**		**2 (56)**		**3 (64)**		**4 (66)**		**5 (74)**		**6 (77)**		**7 (79)**		**8 (84)**	
	Exp Disp	FE Displ	Exp Disp	FE Displ	Exp Disp	FE Displ	Exp Disp	FE Displ	Exp Disp	FE Displ	Exp Disp	FE Displ	Exp Disp	FE Displ	Exp Disp	FE Displ
50	0.121	-0.045	0.079	-0.001	0.037	-0.002	-0.005	0.041	0.080	0.085	-0.039	0.044	0.000	0.127	-0.043	0.085
100	0.240	-0.101	0.159	0.003	0.076	-0.003	0.000	0.100	0.162	0.192	0.083	0.111	0.000	0.279	-0.078	0.182
150	0.373	-0.155	0.249	-0.006	0.121	0.037	-0.002	0.163	0.253	0.308	0.130	0.182	0.002	0.453	-0.119	0.295
200	0.525	-0.207	0.351	-0.019	0.172	0.069	0.001	0.223	0.358	0.436	0.185	0.235	0.008	0.678	-0.163	0.387
250	0.699	-0.429	0.465	-0.086	0.227	0.085	0.002	0.254	0.476	0.501	0.247	0.208	0.010	0.765	-0.214	0.372
300	0.902	-0.653	0.609	-0.302	0.305	-0.705	0.014	1.067	0.605	-0.010	0.244	-0.252	0.020	2.014	-0.266	1.527
	2.861	-1.590	1.912	-0.410	0.938	-0.518	0.010	1.848	1.934	1.513	0.849	0.528	0.039	4.316	-0.883	2.849
A		7.838		32.038		7.901		0.990		0.078		0.369		0.982		1.716
B		61.816		12630		1178.2		6.2323		4008.6		7.6779		5.9271		12.167
C		4.533		1.341		1.058		1.251		0.388		0.260		5.218		4.047

	Y dir - DIC															
Time	**1 (54)**		**2 (56)**		**3 (64)**		**4 (66)**		**5 (74)**		**6 (77)**		**7 (79)**		**8 (84)**	
	Exp Disp	FE Displ	Exp Disp	FE Displ	Exp Disp	FE Displ	Exp Disp	FE Displ	Exp Disp	FE Displ	Exp Disp	FE Displ	Exp Disp	FE Displ	Exp Disp	FE Displ
50	0.242	0.279	0.276	0.321	0.312	0.239	0.352	0.280	0.203	0.162	0.239	0.201	0.276	0.201	0.315	0.242
100	0.446	0.559	0.504	0.644	0.574	0.480	0.727	0.570	0.375	0.330	0.440	0.411	0.474	0.411	0.576	0.494
150	0.652	0.833	0.744	0.963	0.841	0.740	0.946	0.868	0.551	0.493	0.645	0.621	0.739	0.620	0.839	0.752
200	0.859	1.094	0.980	1.267	1.111	0.961	1.253	1.123	0.726	0.648	0.849	0.812	0.973	0.814	1.108	0.986
250	1.067	1.169	1.215	1.355	1.370	1.021	1.540	1.191	0.903	0.686	1.056	0.856	1.205	0.869	1.365	1.034
300	1.227	2.150	1.399	2.355	1.580	2.325	1.773	2.125	1.037	1.979	1.210	2.510	1.387	0.894	1.572	1.737
	4.493	6.084	5.117	6.904	5.789	5.766	6.592	6.156	3.795	4.300	4.439	5.410	5.054	3.808	5.776	5.244
A		0.068		0.067		0.000		0.005		0.014		0.032		0.107		0.010
B		0.3443		0.3456		0.3946		0.2772		0.4355		0.3667		0.6907		0.2597
C		0.952		1.066		0.715		0.274		0.945		1.732		0.402		0.165

Run 3 (cont.)

	Test case: 3_03_2e3_150e3															
	X dir - DIC															
Time	9 (91)		10 (93)		11 (98)		12 (104)		13 (107)		14 (109)		15 (114)		16 (118)	
	Exp Disp	Exp Displ	Exp Disp	Exp Displ	Exp Disp	Exp Displ	Exp Disp	Exp Displ	Exp Disp	Exp Displ	Exp Disp	Exp Displ	Exp Disp	Exp Displ	Exp Disp	Exp Displ
50	0.038	-0.127	-0.004	-0.088	-0.047	-0.086	-0.086	-0.044	-0.004	0.000	-0.046	-0.043	-0.092	0.042	-0.131	-0.003
100	0.079	-0.279	-0.001	-0.189	-0.083	-0.195	-0.161	-0.093	-0.004	0.004	-0.083	-0.099	-0.169	0.095	-0.245	-0.004
150	0.124	-0.458	-0.001	-0.294	-0.126	-0.312	-0.248	-0.142	-0.004	0.015	-0.128	-0.150	-0.257	0.155	-0.375	-0.013
200	0.174	-0.645	0.001	-0.407	-0.173	-0.400	-0.342	-0.206	-0.002	0.016	-0.173	-0.197	-0.351	0.176	-0.519	-0.038
250	0.230	-0.799	0.001	-0.607	-0.230	-0.619	-0.455	-0.298	-0.004	-0.090	-0.230	-0.215	-0.467	0.106	-0.691	-0.027
300	0.291	-1.371	0.002	-1.046	-0.292	-1.345	-0.581	-0.822	-0.008	-0.147	-0.294	-1.236	-0.599	-0.623	-0.884	-0.606
	0.936	-3.680	-0.002	-2.631	-0.951	-2.956	-1.874	-1.605	-0.027	-0.203	-0.955	-1.940	-1.934	-0.050	-2.846	-0.691
A		1.573		0.998		0.460		0.028		0.755		0.258		1441.6		9.723
B		9.6905		5.9045		2.2237		2.8413		402.91		0.6537		63.421		6486.4
C		4.857		1.727		1.346		0.114		0.027		0.888		0.793		0.898

	Y dir - DIC															
Time	9 (91)		10 (93)		11 (98)		12 (104)		13 (107)		14 (109)		15 (114)		16 (118)	
	Exp Disp	FE Displ	Exp Disp	FE Displ	Exp Disp	FE Displ	Exp Disp	FE Displ	Exp Disp	FE Displ	Exp Disp	FE Displ	Exp Disp	FE Displ	Exp Disp	FE Displ
50	0.167	0.199	0.203	0.238	0.241	0.159	0.279	0.198	0.133	0.080	0.168	0.118	0.209	0.120	0.245	0.158
100	0.307	0.392	0.373	0.472	0.441	0.311	0.509	0.394	0.247	0.157	0.311	0.227	0.381	0.248	0.447	0.319
150	0.454	0.578	0.545	0.699	0.641	0.447	0.739	0.592	0.365	0.232	0.458	0.334	0.556	0.374	0.651	0.479
200	0.595	0.769	0.717	0.926	0.841	0.592	0.971	0.774	0.477	0.312	0.599	0.453	0.727	0.487	0.853	0.632
250	0.741	0.816	0.893	0.986	1.045	0.638	1.202	0.826	0.594	0.320	0.747	0.473	0.903	0.496	1.060	0.664
300	0.851	1.705	1.024	1.993	1.200	0.390	1.384	2.189	0.684	-0.259	0.857	2.961	1.038	3.014	1.216	2.485
	3.114	4.459	3.755	5.315	4.410	2.537	5.084	4.973	2.499	0.842	3.140	4.565	3.814	4.739	4.472	4.737
A		0.091		0.086		0.545		0.001		3.874		0.097		0.038		0.003
B		0.4298		0.4105		5.5331		0.723		15.392		1.4078		2.4186		1.3313
C		0.783		1.017		0.929		0.857		1.011		4.542		4.172		1.852

Run 4 – C Error = 72.943

	Test case: 4_03_2e3_250e3															
	X dir - DIC															
Time	1 (54)		2 (56)		3 (64)		4 (66)		5 (74)		6 (77)		7 (79)		8 (84)	
	Exp Disp	FE Displ	Exp Disp	FE Displ	Exp Disp	FE Displ	Exp Disp	FE Displ	Exp Disp	FE Displ	Exp Disp	FE Displ	Exp Disp	FE Displ	Exp Disp	FE Displ
50	0.121	-0.045	0.079	-0.001	0.037	-0.002	-0.005	0.041	0.080	0.085	-0.039	0.044	0.000	0.127	-0.043	0.085
100	0.240	-0.101	0.159	0.003	0.076	-0.003	0.000	0.100	0.162	0.192	0.083	0.111	0.000	0.279	-0.078	0.182
150	0.373	-0.155	0.249	-0.006	0.121	0.037	-0.002	0.163	0.253	0.308	0.130	0.182	0.002	0.453	-0.119	0.295
200	0.525	-0.201	0.351	-0.017	0.172	0.074	0.001	0.230	0.358	0.437	0.185	0.227	0.008	0.683	-0.163	0.370
250	0.699	-0.360	0.465	0.173	0.227	0.109	0.002	0.322	0.476	0.588	0.247	0.207	0.010	0.945	-0.214	0.468
300	0.902	-1.219	0.609	0.408	0.305	0.348	0.014	0.806	0.605	1.112	0.244	0.666	0.020	0.901	-0.266	1.160
	2.861	-2.081	1.912	0.559	0.938	0.562	0.010	1.663	1.934	2.723	0.849	1.437	0.039	3.387	-0.883	2.561
A		5.639		5.845		0.447		0.988		0.084		0.168		0.977		1.809
B		61.409		12723		1174.1		6.2273		0.3371		4.2		5.9086		11.998
C		6.456		0.333		0.034		0.812		0.279		0.192		2.326		2.970

	Y dir - DIC															
Time	1 (54)		2 (56)		3 (64)		4 (66)		5 (74)		6 (77)		7 (79)		8 (84)	
	Exp Disp	FE Displ	Exp Disp	FE Displ	Exp Disp	FE Displ	Exp Disp	FE Displ	Exp Disp	FE Displ	Exp Disp	FE Displ	Exp Disp	FE Displ	Exp Disp	FE Displ
50	0.242	0.279	0.276	0.321	0.312	0.239	0.352	0.280	0.203	0.162	0.239	0.201	0.276	0.201	0.315	0.242
100	0.446	0.559	0.504	0.644	0.574	0.480	0.727	0.570	0.375	0.330	0.440	0.411	0.474	0.411	0.576	0.494
150	0.652	0.833	0.744	0.963	0.841	0.740	0.946	0.868	0.551	0.493	0.645	0.621	0.739	0.620	0.839	0.752
200	0.859	1.083	0.980	1.253	1.111	0.946	1.253	1.109	0.726	0.638	0.849	0.801	0.973	0.801	1.108	0.970
250	1.067	1.138	1.215	1.329	1.370	0.987	1.540	1.170	0.903	0.657	1.056	0.837	1.205	0.828	1.365	1.000
300	1.227	2.287	1.399	2.479	1.580	2.244	1.773	2.301	1.037	3.219	1.210	2.261	1.387	2.990	1.572	2.141
	4.493	6.179	5.117	6.988	5.789	5.638	6.592	6.299	3.795	5.499	4.439	5.132	5.054	5.851	5.776	5.599
A		0.074		0.072		0.001		0.002		0.096		0.018		0.019		0.001
B		0.3677		0.3633		0.4184		0.3194		0.7146		0.3297		0.7381		0.3566
C		1.212		1.305		0.631		0.447		4.834		1.156		2.760		0.489

Run 4 (Cont.)

	Test case: 4_03_2e3_250e3															
	X dir - DIC															
Time	9 (91)		10 (93)		11 (98)		12 (104)		13 (107)		14 (109)		15 (114)		16 (118)	
	Exp Disp	Exp Displ	Exp Disp	Exp Displ	Exp Disp	Exp Displ	Exp Disp	Exp Displ	Exp Disp	Exp Displ	Exp Disp	Exp Displ	Exp Disp	Exp Displ	Exp Disp	Exp Displ
50	0.038	-0.127	-0.004	-0.088	-0.047	-0.086	-0.086	-0.044	-0.004	0.000	-0.046	-0.043	-0.092	0.042	-0.131	-0.003
100	0.079	-0.279	-0.001	-0.189	-0.083	-0.195	-0.161	-0.093	-0.004	0.004	-0.083	-0.099	-0.169	0.095	-0.245	-0.004
150	0.124	-0.458	-0.001	-0.294	-0.126	-0.312	-0.248	-0.142	-0.004	0.015	-0.128	-0.150	-0.257	0.155	-0.375	-0.013
200	0.174	-0.631	0.001	-0.400	-0.173	-0.386	-0.342	-0.202	-0.002	0.010	-0.173	-0.188	-0.351	0.158	-0.519	-0.033
250	0.230	-0.715	0.001	-0.546	-0.230	-0.557	-0.455	-0.248	-0.004	-0.061	-0.230	-0.179	-0.467	0.117	-0.691	-0.005
300	0.291	-2.846	0.002	-2.239	-0.292	-2.890	-0.581	-1.473	-0.008	-1.080	-0.294	-2.221	-0.599	0.344	-0.884	-0.126
	0.936	-5.056	-0.002	-3.755	-0.951	-4.425	-1.874	-2.202	-0.027	-1.113	-0.955	-2.882	-1.934	0.911	-2.846	-0.184
A		1.404		0.999		0.616		0.022		0.953		0.447		9.747		209.017
B		9.5401		5.9032		2.3513		3.5892		403.11		0.8944		67.731		23062
C		11.746		5.573		6.934		0.871		1.153		3.716		1.677		1.430

	Y dir - DIC															
Time	9 (91)		10 (93)		11 (98)		12 (104)		13 (107)		14 (109)		15 (114)		16 (118)	
	Exp Disp	FE Displ	Exp Disp	FE Displ	Exp Disp	FE Displ	Exp Disp	FE Displ	Exp Disp	FE Displ	Exp Disp	FE Displ	Exp Disp	FE Displ	Exp Disp	FE Displ
50	0.167	0.199	0.203	0.238	0.241	0.159	0.279	0.198	0.133	0.080	0.168	0.118	0.209	0.120	0.245	0.158
100	0.307	0.392	0.373	0.472	0.441	0.311	0.509	0.394	0.247	0.157	0.311	0.227	0.381	0.248	0.447	0.319
150	0.454	0.578	0.545	0.699	0.641	0.447	0.739	0.592	0.365	0.232	0.458	0.334	0.556	0.374	0.651	0.479
200	0.595	0.758	0.717	0.917	0.841	0.584	0.971	0.764	0.477	0.306	0.599	0.448	0.727	0.476	0.853	0.625
250	0.741	0.798	0.893	0.964	1.045	0.642	1.202	0.808	0.594	0.319	0.747	0.474	0.903	0.484	1.060	0.652
300	0.851	1.937	1.024	2.176	1.200	2.363	1.384	2.272	0.684	2.745	0.857	2.410	1.038	1.363	1.216	2.113
	3.114	4.662	3.755	5.466	4.410	4.506	5.084	5.028	2.499	3.838	3.140	4.011	3.814	3.065	4.472	4.345
A		0.110		0.098		0.000		0.000		0.122		0.047		0.060		0.001
B		0.4852		0.4471		1.461		0.779		2.7115		1.3221		2.1558		1.2998
C		1.226		1.396		1.624		1.015		4.372		2.529		0.385		1.060

Run 5 – C Error = 69.679

	Test case: 5_03_8e3_250e3															
	X dir - DIC															
Time	1 (54)		2 (56)		3 (64)		4 (66)		5 (74)		6 (77)		7 (79)		8 (84)	
	Exp Disp	FE Displ	Exp Disp	FE Displ	Exp Disp	FE Displ	Exp Disp	FE Displ	Exp Disp	FE Displ	Exp Disp	FE Displ	Exp Disp	FE Displ	Exp Disp	FE Displ
50	0.121	-0.049	0.079	0.000	0.037	0.001	-0.005	0.047	0.080	0.091	-0.039	0.050	0.000	0.131	-0.043	0.091
100	0.240	-0.116	0.159	0.007	0.076	0.002	0.000	0.109	0.162	0.199	0.083	0.116	0.000	0.279	-0.078	0.199
150	0.373	-0.160	0.249	0.015	0.121	0.019	-0.002	0.159	0.253	0.307	0.130	0.169	0.002	0.435	-0.119	0.303
200	0.525	-0.130	0.351	0.022	0.172	-0.016	0.001	0.142	0.358	0.403	0.185	0.165	0.008	0.569	-0.163	0.409
250	0.699	-0.112	0.465	0.067	0.227	0.001	0.002	0.175	0.476	0.625	0.247	0.202	0.010	0.769	-0.214	0.593
300	0.902	0.204	0.609	0.040	0.305	0.353	0.014	0.673	0.605	0.962	0.244	0.667	0.020	1.242	-0.266	1.085
	2.861	-0.363	1.912	0.151	0.938	0.360	0.010	1.304	1.934	2.587	0.849	1.368	0.039	3.424	-0.883	2.679
A		78.782		136.913		2.572		0.985		0.064		0.144		0.978		1.768
B		121.89		656441		198967		6.173		0.2872		3.8241		5.9107		11.422
C		1.887		0.651		0.101		0.512		0.155		0.191		2.589		2.998

	Y dir - DIC															
Time	1 (54)		2 (56)		3 (64)		4 (66)		5 (74)		6 (77)		7 (79)		8 (84)	
	Exp Disp	FE Displ	Exp Disp	FE Displ	Exp Disp	FE Displ	Exp Disp	FE Displ	Exp Disp	FE Displ	Exp Disp	FE Displ	Exp Disp	FE Displ	Exp Disp	FE Displ
50	0.242	0.280	0.276	0.322	0.312	0.239	0.352	0.280	0.203	0.161	0.239	0.200	0.276	0.201	0.315	0.242
100	0.446	0.559	0.504	0.648	0.574	0.477	0.727	0.568	0.375	0.324	0.440	0.401	0.474	0.405	0.576	0.488
150	0.652	0.821	0.744	0.962	0.841	0.716	0.946	0.849	0.551	0.490	0.645	0.603	0.739	0.610	0.839	0.738
200	0.859	1.019	0.980	1.179	1.111	0.886	1.253	1.045	0.726	0.597	0.849	0.741	0.973	0.742	1.108	0.910
250	1.067	1.085	1.215	1.264	1.370	0.949	1.540	1.120	0.903	0.639	1.056	0.792	1.205	0.790	1.365	0.964
300	1.227	2.646	1.399	2.486	1.580	2.777	1.773	2.036	1.037	2.520	1.210	2.586	1.387	1.471	1.572	1.739
	4.493	6.410	5.117	6.861	5.789	6.043	6.592	5.898	3.795	4.730	4.439	5.323	5.054	4.218	5.776	5.082
A		0.089		0.065		0.002		0.014		0.039		0.028		0.039		0.019
B		0.4146		0.343		0.6135		0.3539		0.6734		0.4664		0.5901		0.3729
C		2.069		1.273		1.682		0.302		2.290		1.975		0.255		0.244

Run 5 (Cont.)

	Test case: 5_03_8e3_250e3															
	X dir - DIC															
Time	9 (91)		10 (93)		11 (98)		12 (104)		13 (107)		14 (109)		15 (114)		16 (118)	
	Exp Disp	Exp Displ	Exp Disp	Exp Disp	Exp Disp	Exp Displ	Exp Disp	Exp Displ	Exp Disp	Exp Displ	Exp Disp	Exp Displ	Exp Disp	Exp Displ	Exp Disp	Exp Displ
50	0.038	-0.131	-0.004	-0.091	-0.047	-0.091	-0.086	-0.048	-0.004	0.000	-0.046	-0.046	-0.092	0.050	-0.131	-0.003
100	0.079	-0.281	-0.001	-0.200	-0.083	-0.200	-0.161	-0.105	-0.004	-0.012	-0.083	-0.102	-0.169	0.119	-0.245	-0.021
150	0.124	-0.444	-0.001	-0.289	-0.126	-0.294	-0.248	-0.153	-0.004	-0.007	-0.128	-0.153	-0.257	0.171	-0.375	-0.048
200	0.174	-0.774	0.001	-0.464	-0.173	-0.383	-0.342	-0.222	-0.002	-0.020	-0.173	-0.288	-0.351	0.240	-0.519	-0.132
250	0.230	-0.795	0.001	-0.541	-0.230	-0.415	-0.455	-0.230	-0.004	-0.090	-0.230	-0.315	-0.467	0.360	-0.691	-0.151
300	0.291	-0.637	0.002	-0.521	-0.292	0.164	-0.581	0.366	-0.008	0.978	-0.294	0.495	-0.599	0.572	-0.884	0.353
	0.936	-3.062	-0.002	-2.106	-0.951	-1.218	-1.874	-0.391	-0.027	0.849	-0.955	-0.410	-1.934	1.512	-2.846	-0.002
A		1.705		0.998		0.048		14.348		1.064		1.769		5.195		#######
B		10.231		5.9109		9.1475		9.2466		116.98		2.8361		35.742		2333
C		3.163		0.874		0.317		0.973		0.979		0.645		2.607		2.095

	Y dir - DIC															
Time	9 (91)		10 (93)		11 (98)		12 (104)		13 (107)		14 (109)		15 (114)		16 (118)	
	Exp Disp	FE Displ	Exp Disp	FE Displ	Exp Disp	FE Displ	Exp Disp	FE Displ	Exp Disp	FE Displ	Exp Disp	FE Displ	Exp Disp	FE Displ	Exp Disp	FE Displ
50	0.167	0.197	0.203	0.237	0.241	0.156	0.279	0.197	0.133	0.076	0.168	0.117	0.209	0.118	0.245	0.159
100	0.307	0.391	0.373	0.474	0.441	0.308	0.509	0.396	0.247	0.150	0.311	0.228	0.381	0.240	0.447	0.315
150	0.454	0.570	0.545	0.697	0.641	0.444	0.739	0.587	0.365	0.226	0.458	0.336	0.556	0.365	0.651	0.467
200	0.595	0.710	0.717	0.865	0.841	0.555	0.971	0.717	0.477	0.278	0.599	0.420	0.727	0.441	0.853	0.576
250	0.741	0.764	0.893	0.920	1.045	0.592	1.202	0.758	0.594	0.279	0.747	0.457	0.903	0.466	1.060	0.621
300	0.851	2.374	1.024	2.255	1.200	3.045	1.384	3.086	0.684	3.810	0.857	3.699	1.038	3.206	1.216	3.346
	3.114	5.005	3.755	5.448	4.410	5.101	5.084	5.741	2.499	4.819	3.140	5.257	3.814	4.836	4.472	5.484
A		0.143		0.097		0.018		0.013		0.232		0.162		0.045		0.034
B		0.5489		0.442		1.8985		1.0915		3.8218		1.6291		2.9738		1.7628
C		2.350		1.562		3.736		3.188		9.935		8.211		5.022		4.846

Run 6 – C Error = 24.185

	Test case: 6_06_8e3_250e3															
	X dir - DIC															
Time	1 (54)		2 (56)		3 (64)		4 (66)		5 (74)		6 (77)		7 (79)		8 (84)	
	Exp Disp	FE Displ	Exp Disp	FE Displ	Exp Disp	FE Displ	Exp Disp	FE Displ	Exp Disp	FE Displ	Exp Disp	FE Displ	Exp Disp	FE Displ	Exp Disp	FE Displ
50	0.121	-0.049	0.079	0.000	0.037	0.001	-0.005	0.047	0.080	0.091	-0.039	0.050	0.000	0.131	-0.043	0.091
100	0.240	-0.116	0.159	0.007	0.076	0.002	0.000	0.109	0.162	0.199	0.083	0.116	0.000	0.279	-0.078	0.199
150	0.373	-0.160	0.249	0.015	0.121	0.019	-0.002	0.159	0.253	0.307	0.130	0.169	0.002	0.435	-0.119	0.303
200	0.525	-0.168	0.351	-0.003	0.172	-0.006	0.001	0.169	0.358	0.399	0.185	0.162	0.008	0.615	-0.163	0.404
250	0.699	-0.273	0.465	-0.048	0.227	-0.136	0.002	0.114	0.476	0.525	0.247	0.179	0.010	0.770	-0.214	0.530
300	0.902	-0.371	0.609	-0.064	0.305	-0.045	0.014	0.207	0.605	0.681	0.244	0.230	0.020	1.065	-0.266	0.679
	2.861	-1.136	1.912	-0.093	0.938	-0.164	0.010	0.805	1.934	2.202	0.849	0.905	0.039	3.294	-0.883	2.206
A		12.374		465.9		44.957		0.976		0.015		0.004		0.977		1.961
B		74.027		674227		3645.8		6.0745		0.1121		3.5269		5.9076		11.939
C		3.358		0.902		0.297		0.107		0.013		0.015		2.243		1.964

	Y dir - DIC															
Time	1 (54)		2 (56)		3 (64)		4 (66)		5 (74)		6 (77)		7 (79)		8 (84)	
	Exp Disp	FE Displ	Exp Disp	FE Displ	Exp Disp	FE Displ	Exp Disp	FE Displ	Exp Disp	FE Displ	Exp Disp	FE Displ	Exp Disp	FE Displ	Exp Disp	FE Displ
50	0.242	0.280	0.276	0.322	0.312	0.239	0.352	0.280	0.203	0.161	0.239	0.200	0.276	0.201	0.315	0.242
100	0.446	0.559	0.504	0.648	0.574	0.477	0.727	0.568	0.375	0.324	0.440	0.401	0.474	0.405	0.576	0.488
150	0.652	0.821	0.744	0.962	0.841	0.716	0.946	0.849	0.551	0.490	0.645	0.603	0.739	0.610	0.839	0.738
200	0.859	1.068	0.980	1.247	1.111	0.935	1.253	1.113	0.726	0.645	0.849	0.787	0.973	0.799	1.108	0.979
250	1.067	1.267	1.215	1.498	1.370	1.133	1.540	1.356	0.903	0.792	1.056	0.971	1.205	0.961	1.365	1.198
300	1.227	1.525	1.399	1.811	1.580	1.378	1.773	1.617	1.037	0.976	1.210	1.164	1.387	1.175	1.572	1.430
	4.493	5.520	5.117	6.489	5.789	4.878	6.592	5.783	3.795	3.388	4.439	4.125	5.054	4.151	5.776	5.076
A		0.035		0.045		0.035		0.020		0.014		0.006		0.047		0.019
B		0.2033		0.2555		0.2662		0.201		0.1493		0.0676		0.3573		0.1897
C		0.202		0.372		0.149		0.092		0.028		0.016		0.157		0.080

Run 6 (Cont.)

	Test case: 6_06_8e3_250e3															
	X dir - DIC															
Time	9 (91)		10 (93)		11 (98)		12 (104)		13 (107)		14 (109)		15 (114)		16 (118)	
	Exp Disp	Exp Displ	Exp Disp	Exp Displ	Exp Disp	Exp Displ	Exp Disp	Exp Displ	Exp Disp	Exp Displ	Exp Disp	Exp Displ	Exp Disp	Exp Displ	Exp Disp	Exp Displ
50	0.038	-0.131	-0.004	-0.091	-0.047	-0.091	-0.086	-0.048	-0.004	0.000	-0.046	-0.046	-0.092	0.050	-0.131	-0.003
100	0.079	-0.281	-0.001	-0.200	-0.083	-0.200	-0.161	-0.105	-0.004	-0.012	-0.083	-0.102	-0.169	0.119	-0.245	-0.021
150	0.124	-0.444	-0.001	-0.289	-0.126	-0.294	-0.248	-0.153	-0.004	-0.007	-0.128	-0.153	-0.257	0.171	-0.375	-0.048
200	0.174	-0.826	0.001	-0.491	-0.173	-0.419	-0.342	-0.279	-0.002	-0.041	-0.173	-0.320	-0.351	0.217	-0.519	-0.173
250	0.230	-1.393	0.001	-0.812	-0.230	-0.702	-0.455	-0.487	-0.004	-0.089	-0.230	-0.607	-0.467	0.284	-0.691	-0.405
300	0.291	-1.431	0.002	-0.840	-0.292	-0.805	-0.581	-0.495	-0.008	0.046	-0.294	-0.582	-0.599	0.402	-0.884	-0.347
	0.936	-4.505	-0.002	-2.722	-0.951	-2.511	-1.874	-1.566	-0.027	-0.103	-0.955	-1.811	-1.934	1.243	-2.846	-0.996
A		1.459		0.998		0.386		0.039		0.548		0.223		6.532		3.451
B		9.2185		5.9072		2.1051		1.3975		117.43		0.9025		40.235		2306.3
C		6.948		1.701		0.576		0.023		0.012		0.247		2.092		0.614

	Y dir - DIC															
Time	9 (91)		10 (93)		11 (98)		12 (104)		13 (107)		14 (109)		15 (114)		16 (118)	
	Exp Disp	FE Displ	Exp Disp	FE Displ	Exp Disp	FE Displ	Exp Disp	FE Displ	Exp Disp	FE Displ	Exp Disp	FE Displ	Exp Disp	FE Displ	Exp Disp	FE Displ
50	0.167	0.197	0.203	0.237	0.241	0.156	0.279	0.197	0.133	0.076	0.168	0.117	0.209	0.118	0.245	0.159
100	0.307	0.391	0.373	0.474	0.441	0.308	0.509	0.396	0.247	0.150	0.311	0.228	0.381	0.240	0.447	0.315
150	0.454	0.570	0.545	0.697	0.641	0.444	0.739	0.587	0.365	0.226	0.458	0.336	0.556	0.365	0.651	0.467
200	0.595	0.744	0.717	0.909	0.841	0.563	0.971	0.740	0.477	0.283	0.599	0.424	0.727	0.478	0.853	0.603
250	0.741	0.892	0.893	1.078	1.045	0.656	1.202	0.884	0.594	0.340	0.747	0.515	0.903	0.579	1.060	0.733
300	0.851	1.082	1.024	1.309	1.200	0.797	1.384	1.094	0.684	0.457	0.857	0.611	1.038	0.731	1.216	0.861
	3.114	3.875	3.755	4.703	4.410	2.924	5.084	3.899	2.499	1.532	3.140	2.232	3.814	2.510	4.472	3.138
A		0.039		0.041		0.258		0.093		0.398		0.166		0.270		0.181
B		0.2246		0.2351		1.5338		0.6158		2.6275		0.9889		1.9756		1.1681
C		0.113		0.176		0.438		0.269		0.176		0.162		0.307		0.337

Run 7 – C Error = 28.167

	Test case: 7_03_8e3_150e4															
	X dir - DIC															
Time	1 (54)		2 (56)		3 (64)		4 (66)		5 (74)		6 (77)		7 (79)		8 (84)	
	Exp Disp	FE Displ	Exp Disp	FE Displ	Exp Disp	FE Displ	Exp Disp	FE Displ	Exp Disp	FE Displ	Exp Disp	FE Displ	Exp Disp	FE Displ	Exp Disp	FE Displ
50	0.121	-0.049	0.079	0.000	0.037	0.001	-0.005	0.047	0.080	0.091	-0.039	0.050	0.000	0.131	-0.043	0.091
100	0.240	-0.116	0.159	0.007	0.076	0.002	0.000	0.109	0.162	0.199	0.083	0.116	0.000	0.279	-0.078	0.199
150	0.373	-0.160	0.249	0.015	0.121	0.019	-0.002	0.159	0.253	0.307	0.130	0.169	0.002	0.435	-0.119	0.303
200	0.525	-0.140	0.351	0.015	0.172	-0.014	0.001	0.144	0.358	0.401	0.185	0.163	0.008	0.575	-0.163	0.404
250	0.699	-0.154	0.465	0.032	0.227	-0.009	0.002	0.155	0.476	0.552	0.247	0.236	0.010	0.713	-0.214	0.549
300	0.902	-0.590	0.609	-0.250	0.305	-0.041	0.014	0.322	0.605	0.910	0.244	0.043	0.020	1.195	-0.266	0.852
	2.861	-1.209	1.912	-0.182	0.938	-0.042	0.010	0.937	1.934	2.461	0.849	0.776	0.039	3.328	-0.883	2.398
A		11.337		132.769		544.35		0.979		0.046		0.009		0.977		1.872
B		92.136		656687		3593.9		6.1269		0.2235		24.856		5.9078		11.686
C		3.709		1.100		0.222		0.168		0.104		0.050		2.402		2.349

	Y dir - DIC															
Time	1 (54)		2 (56)		3 (64)		4 (66)		5 (74)		6 (77)		7 (79)		8 (84)	
	Exp Disp	FE Displ	Exp Disp	FE Displ	Exp Disp	FE Displ	Exp Disp	FE Displ	Exp Disp	FE Displ	Exp Disp	FE Displ	Exp Disp	FE Displ	Exp Disp	FE Displ
50	0.242	0.280	0.276	0.322	0.312	0.239	0.352	0.280	0.203	0.161	0.239	0.200	0.276	0.201	0.315	0.242
100	0.446	0.559	0.504	0.648	0.574	0.477	0.727	0.568	0.375	0.324	0.440	0.401	0.474	0.405	0.576	0.488
150	0.652	0.821	0.744	0.962	0.841	0.716	0.946	0.849	0.551	0.490	0.645	0.603	0.739	0.610	0.839	0.738
200	0.859	1.031	0.980	1.194	1.111	0.899	1.253	1.060	0.726	0.610	0.849	0.753	0.973	0.755	1.108	0.926
250	1.067	1.132	1.215	1.320	1.370	0.992	1.540	1.162	0.903	0.676	1.056	0.828	1.205	0.835	1.365	1.015
300	1.227	1.906	1.399	1.969	1.580	1.659	1.773	1.666	1.037	1.022	1.210	1.410	1.387	1.052	1.572	1.301
	4.493	5.729	5.117	6.415	5.789	4.982	6.592	5.584	3.795	3.283	4.439	4.195	5.054	3.857	5.776	4.710
A		0.047		0.041		0.026		0.033		0.024		0.003		0.096		0.051
B		0.260		0.244		0.369		0.301		0.259		0.164		0.595		0.344
C		0.524		0.432		0.215		0.207		0.070		0.104		0.319		0.245

Run 7 (Cont.)

	Test case: 7_03_8e3_150e4															
	X dir - DIC															
Time	9 (91)		10 (93)		11 (98)		12 (104)		13 (107)		14 (109)		15 (114)		16 (118)	
	Exp Disp	Exp Displ	Exp Disp	Exp Displ	Exp Disp	Exp Displ	Exp Disp	Exp Displ	Exp Disp	Exp Displ	Exp Disp	Exp Displ	Exp Disp	Exp Displ	Exp Disp	Exp Displ
50	0.038	-0.131	-0.004	-0.091	-0.047	-0.091	-0.086	-0.048	-0.004	0.000	-0.046	-0.046	-0.092	0.050	-0.131	-0.003
100	0.079	-0.281	-0.001	-0.200	-0.083	-0.200	-0.161	-0.105	-0.004	-0.012	-0.083	-0.102	-0.169	0.119	-0.245	-0.021
150	0.124	-0.444	-0.001	-0.289	-0.126	-0.294	-0.248	-0.153	-0.004	-0.007	-0.128	-0.153	-0.257	0.171	-0.375	-0.048
200	0.174	-0.779	0.001	-0.462	-0.173	-0.388	-0.342	-0.230	-0.002	-0.015	-0.173	-0.288	-0.351	0.236	-0.519	-0.134
250	0.230	-0.788	0.001	-0.499	-0.230	-0.417	-0.455	-0.252	-0.004	0.056	-0.230	-0.287	-0.467	0.378	-0.691	-0.137
300	0.291	-1.314	0.002	-0.768	-0.292	-0.607	-0.581	-0.427	-0.008	-0.109	-0.294	-0.364	-0.599	0.318	-0.884	0.019
	0.936	-3.736	-0.002	-2.309	-0.951	-1.996	-1.874	-1.214	-0.027	-0.087	-0.955	-1.241	-1.934	1.270	-2.846	-0.324
A		1.564		0.998		0.274		0.295		0.483		0.053		6.363		60.510
B		9.605		5.909		1.6784		2.3308		117.02		0.2973		39.743		4483.9
C		4.870		1.148		0.210		0.088		0.014		0.022		2.100		1.395

	Y dir - DIC															
Time	9 (91)		10 (93)		11 (98)		12 (104)		13 (107)		14 (109)		15 (114)		16 (118)	
	Exp Disp	FE Displ	Exp Disp	FE Displ	Exp Disp	FE Displ	Exp Disp	FE Displ	Exp Disp	FE Displ	Exp Disp	FE Displ	Exp Disp	FE Displ	Exp Disp	FE Displ
50	0.167	0.197	0.203	0.237	0.241	0.156	0.279	0.197	0.133	0.076	0.168	0.117	0.209	0.118	0.245	0.159
100	0.307	0.391	0.373	0.474	0.441	0.308	0.509	0.396	0.247	0.150	0.311	0.228	0.381	0.240	0.447	0.315
150	0.454	0.570	0.545	0.697	0.641	0.444	0.739	0.587	0.365	0.226	0.458	0.336	0.556	0.365	0.651	0.467
200	0.595	0.720	0.717	0.876	0.841	0.561	0.971	0.725	0.477	0.286	0.599	0.425	0.727	0.452	0.853	0.585
250	0.741	0.791	0.893	0.960	1.045	0.612	1.202	0.800	0.594	0.313	0.747	0.463	0.903	0.505	1.060	0.640
300	0.851	1.769	1.024	1.897	1.200	1.700	1.384	1.802	0.684	1.856	0.857	1.702	1.038	1.514	1.216	1.736
	3.114	4.438	3.755	5.142	4.410	3.782	5.084	4.508	2.499	2.907	3.140	3.272	3.814	3.193	4.472	3.902
A		0.089		0.073		0.028		0.016		0.020		0.002		0.038		0.021
B		0.414		0.364		1.515		0.740		3.003		1.243		2.305		1.357
C		0.877		0.816		0.562		0.427		1.510		0.843		0.506		0.560

Run 8 – C Error = 24.216

	Test case: 8_06_2e3_150e4															
	X dir - DIC															
Time	1 (54)		2 (56)		3 (64)		4 (66)		5 (74)		6 (77)		7 (79)		8 (84)	
	Exp Disp	FE Displ	Exp Disp	FE Displ	Exp Disp	FE Displ	Exp Disp	FE Displ	Exp Disp	FE Displ	Exp Disp	FE Displ	Exp Disp	FE Displ	Exp Disp	FE Displ
50	0.121	-0.045	0.079	-0.001	0.037	-0.002	-0.005	0.041	0.080	0.085	-0.039	0.044	0.000	0.127	-0.043	0.085
100	0.240	-0.101	0.159	0.003	0.076	-0.003	0.000	0.100	0.162	0.192	0.083	0.111	0.000	0.279	-0.078	0.182
150	0.373	-0.155	0.249	-0.006	0.121	0.037	-0.002	0.163	0.253	0.308	0.130	0.182	0.002	0.453	-0.119	0.295
200	0.525	-0.215	0.351	-0.006	0.172	0.085	0.001	0.259	0.358	0.460	0.185	0.270	0.008	0.708	-0.163	0.429
250	0.699	-0.288	0.465	-0.007	0.227	0.191	0.002	0.431	0.476	0.673	0.247	0.427	0.010	1.092	-0.214	0.622
300	0.902	-0.443	0.609	0.000	0.305	0.261	0.014	0.510	0.605	0.837	0.244	0.585	0.020	1.250	-0.266	0.826
	2.861	-1.247	1.912	-0.017	0.938	0.569	0.010	1.503	1.934	2.555	0.849	1.619	0.039	3.909	-0.883	2.441
A		10.853		######		0.422		0.987		0.059		0.226		0.980		1.855
B		69.502		2E+06		1172.2		6.2114		0.2719		4.3422		5.9241		11.745
C		3.638		0.793		0.019		0.525		0.106		0.166		3.396		2.431

	Y dir - DIC															
Time	1 (54)		2 (56)		3 (64)		4 (66)		5 (74)		6 (77)		7 (79)		8 (84)	
	Exp Disp	FE Displ	Exp Disp	FE Displ	Exp Disp	FE Displ	Exp Disp	FE Displ	Exp Disp	FE Displ	Exp Disp	FE Displ	Exp Disp	FE Displ	Exp Disp	FE Displ
50	0.242	0.279	0.276	0.321	0.312	0.239	0.352	0.280	0.203	0.162	0.239	0.201	0.276	0.201	0.315	0.242
100	0.446	0.559	0.504	0.644	0.574	0.480	0.727	0.570	0.375	0.330	0.440	0.411	0.474	0.411	0.576	0.494
150	0.652	0.833	0.744	0.963	0.841	0.740	0.946	0.868	0.551	0.493	0.645	0.621	0.739	0.620	0.839	0.752
200	0.859	1.104	0.980	1.289	1.111	0.999	1.253	1.166	0.726	0.668	0.849	0.837	0.973	0.837	1.108	1.017
250	1.067	1.348	1.215	1.594	1.370	1.263	1.540	1.479	0.903	0.842	1.056	1.062	1.205	1.049	1.365	1.299
300	1.227	1.602	1.399	1.916	1.580	1.496	1.773	1.728	1.037	0.998	1.210	1.270	1.387	1.205	1.572	1.527
	4.493	5.725	5.117	6.726	5.789	5.217	6.592	6.090	3.795	3.494	4.439	4.402	5.054	4.323	5.776	5.330
A		0.046		0.057		0.012		0.007		0.007		0.000		0.029		0.007
B		0.2535		0.3056		0.173		0.1584		0.1098		0.0444		0.2694		0.1441
C		0.313		0.557		0.047		0.025		0.014		0.006		0.096		0.028

Run 8 (Cont.)

	Test case: 8_06_2e3_150e4															
	X dir - DIC															
Time	9 (91)		10 (93)		11 (98)		12 (104)		13 (107)		14 (109)		15 (114)		16 (118)	
	Exp Disp	Exp Displ	Exp Disp	Exp Displ	Exp Disp	Exp Displ	Exp Disp	Exp Displ	Exp Disp	Exp Displ	Exp Disp	Exp Displ	Exp Disp	Exp Displ	Exp Disp	Exp Displ
50	0.038	-0.127	-0.004	-0.088	-0.047	-0.086	-0.086	-0.044	-0.004	0.000	-0.046	-0.043	-0.092	0.042	-0.131	-0.003
100	0.079	-0.279	-0.001	-0.189	-0.083	-0.195	-0.161	-0.093	-0.004	0.004	-0.083	-0.099	-0.169	0.095	-0.245	-0.004
150	0.124	-0.458	-0.001	-0.294	-0.126	-0.312	-0.248	-0.142	-0.004	0.014	-0.128	-0.150	-0.257	0.155	-0.375	-0.013
200	0.174	-0.682	0.001	-0.433	-0.173	-0.485	-0.342	-0.210	-0.002	0.021	-0.173	-0.237	-0.351	0.217	-0.519	-0.028
250	0.230	-1.012	0.001	-0.581	-0.230	-0.700	-0.455	-0.295	-0.004	0.052	-0.230	-0.403	-0.467	0.271	-0.691	-0.081
300	0.291	-1.220	0.002	-0.754	-0.292	-0.899	-0.581	-0.304	-0.008	0.060	-0.294	-0.460	-0.599	0.337	-0.884	-0.049
	0.936	-3.778	-0.002	-2.339	-0.951	-2.678	-1.874	-1.088	-0.027	0.152	-0.955	-1.393	-1.934	1.116	-2.846	-0.179
A		1.557		0.998		0.416		0.522		1.381		0.099		7.465		222.859
B		9.5662		5.9055		2.2151		3.5599		403.51		0.4396		47.022		6368.8
C		4.923		1.191		0.723		0.133		0.009		0.062		1.929		1.458

	Y dir - DIC															
Time	9 (91)		10 (93)		11 (98)		12 (104)		13 (107)		14 (109)		15 (114)		16 (118)	
	Exp Disp	FE Displ	Exp Disp	FE Displ	Exp Disp	FE Displ	Exp Disp	FE Displ	Exp Disp	FE Displ	Exp Disp	FE Displ	Exp Disp	FE Displ	Exp Disp	FE Displ
50	0.167	0.199	0.203	0.238	0.241	0.159	0.279	0.198	0.133	0.080	0.168	0.118	0.209	0.120	0.245	0.158
100	0.307	0.392	0.373	0.472	0.441	0.311	0.509	0.394	0.247	0.157	0.311	0.227	0.381	0.248	0.447	0.319
150	0.454	0.578	0.545	0.699	0.641	0.447	0.739	0.593	0.365	0.232	0.458	0.334	0.556	0.374	0.651	0.479
200	0.595	0.762	0.717	0.924	0.841	0.572	0.971	0.787	0.477	0.317	0.599	0.436	0.727	0.512	0.853	0.640
250	0.741	0.935	0.893	1.141	1.045	0.698	1.202	0.981	0.594	0.404	0.747	0.514	0.903	0.646	1.060	0.797
300	0.851	1.127	1.024	1.355	1.200	0.863	1.384	1.179	0.684	0.479	0.857	0.619	1.038	0.766	1.216	0.947
	3.114	3.994	3.755	4.829	4.410	3.051	5.084	4.132	2.499	1.669	3.140	2.248	3.814	2.666	4.472	3.341
A		0.049		0.049		0.199		0.053		0.247		0.157		0.185		0.115
B		0.2707		0.2712		1.2513		0.4502		1.7512		0.953		1.5325		0.8933
C		0.159		0.239		0.351		0.153		0.124		0.155		0.227		0.224